ANTAL KERPELY DOCTORAL SCHOOL OF

MATERIAL SCIENCE AND TECHNOLOGY

The recovery of pure Zn from spent pickling liquor by combining electrowinning and anion-exchange separation process

A dissertation submitted in partial fulfilment of the requirements for

the degree of Doctor of Philosophy in Chemical Metallurgy as a part of

Stipendium Hungaricum Scholarship in

Material Science and Technology

By

Hanna Zakiyya

Supervisor:

Prof. Dr. Tamás Kékesi, DSc.

Head of the Doctoral School:

Prof. Dr. Valéria Mertinger

Institute of Chemical Metallurgy and Foundry Engineering
Faculty of Materials and Chemical Engineering
University of Miskolc
Miskolc, Hungary

2024

Supervisor recommendation

Having supervised the research work of the applicant over the past four years, I have become convinced that she worked with full dedication, ardent enthusiasm and conscience. Although the field of hydro-electrometallurgy had initially posed special challenges for her, she has acquired the necessary new knowledge and skills to become efficient in carrying out the tasks in the laboratory and processing, also interpreting, the results. She has become capable of designing her way to explore the depths of the scientific proposals. During this procedure she has successfully fulfilled also her curricular tasks, and developed her publication skills starting from the domestic journals and conferences towards the prestigious international level.

The elaborated subject is based on an important industrial technology producing a large quantity of hazardous waste liquor, containing however, valuable metal, like zinc. The recovery of this value has never been considered really economic as the approaches have always considered just the environmental aspects or a convenient handling of the residues. With the devised complex method – implying anion-exchange separations in the adjusted chloride aqueous medium followed by a practically implementable electrowinning technique, however, could offer the realistic target of obtaining zinc of a higher than ordinary grade. For this purpose, a thorough investigation of the chloro-complex formation and anion-exchange separation characteristics of Zn, Fe and some practical impurities have been investigated. The devised separation procedure could result in a pure chloride solution. Economy and workability was even enhanced by substituting NaCl whenever possible for HCl as the source of free Cl^- ions. The fine tuning of the electrowinning conditions were based on the potentiodynamic study of the cathodic processes, expanding our understanding of the interfering reactions. The optimised procedure, tested under longer term galvanostatic conditions, could justify the expectations, and a practically feasible procedure has finally been demonstrated.

With her strenuous effort invested, the applicant is **considered eligible and recommendable** for the aspired scientific grade, after publicly defending her results.

…….

ACKNOWLEDGEMENT

I am very grateful to my supervisor, Prof. Dr. Tamás Kékesi, DSc., for his time and continuous guidance, and effective co-operation in this PhD research. With his patience and support, I could complete this doctoral course. I learned a lot from his vast experience in the research and teaching field. He also taught me extensive knowledge besides the PhD work. All that was based on his expertise in the research subject, language, laboratory work, dedication, and persistence. On the first day I met him, he told me his time would always be available for his students, and it was true. He guided me from scratch in every step of my study and was ready to answer any question at any time. It would have been impossible to carry out this work without his advising and mentoring. He was so helpful also in and providing me with complete guidance to survive in Hungary, which is not my home country.

I would also like to thank Istvan Illés, my colleague and doctoral fellow, for his valuable contribution to my laboratory work and to my understanding of the special aspects of practical chemistry. Not only did he teach me in the laboratory, but he also showed me how to be a dedicated researcher and enjoy laboratory life.

To my kind reviewer, Prof. Dr. Tamás Török, I wish to express my gratitude for his advice on various points in my research work. His support and trust during the review of my work gave me self-confidence during my study period. His positive opinions helped me find my self-encouragement to do this challenging PhD work from the beginning of the completion of the whole research process.

Many thanks to my colleagues in the Kerpely Antal Doctoral School of the Faculty of Materials Science and Engineering (now Materials and Chemical Engineering) for helping me with the whole process during the PhD process, especially for Ms. Ágnes Solczi and Dr. Mária Svéda. Also the Institute of Chemical Metallurgy and Foundry Engineering for providing me with a comfortable workspace and a laboratory.

I would also like to thank the State University of Surabaya and all my colleagues back in my home country for supporting me in extending my higher education.

Eventually, these achievements and success would be impossible without the support, blessings, and understanding of my dear my parent's, husband and child.

Statement

I, the undersigned, Hanna Zakiyya (Neptun Code: JGW88S, born: 3rd September 1989, in Bukittinggi, Indonesia) certify and declare under my criminal responsibility by law that this dissertation is my own work.

Dater: Miskolc,

_____

Hanna Zakiyya, Student

The statement was taken over.

Date: Miskolc,

_____

Prof. Dr. Tamás Kékesi, DSc., Supervisor

Table of Contents

List of figures

List of tables

List of Abbreviations

AIEX = anion-exchange

AAS = atomic absorption spectrometry

BAT = Best Available Technology

BV = bed volume

CEM = cation exchange membranes

CER = chloride evolution reaction

c.d. = current density

c.e. = current efficiencies

DSA = dimensionally stable anodes

HDG = hot dip galvanizing

HER = hydrogen evolution reaction

OER = oxygen evolution reaction

SCE = saturated calomel reference electrode

SHE = standard hydrogen electrode

SPL = spent pickling liquor

UDP = under-potential deposition

1. Introduction

Preventing corrosion on the surface of metals is a modern requirement in the production of metal structures. One of the most common corrosion control methods is coating the steel surface with a passivating layer, like in the case of hot dip galvanizing (HDG), where a thick zinc coating protects the surface of the steel objects. The most commonly used version of this method is the batch operation by the dry HDG technology. The forming of the Zn coating could be thought as a simple procedure, where the metals are immersed in a molten zinc bath at approximately 430-460 ^{o}C temperature. Zinc coating protects the metal by two effects: (i) it provides a barrier, and (ii) it acts as a sacrificial anode if the substrate surface is exposed to the corrosive environment because it has a more negative electrode potential than the protected metal. However, the steel surface usually exhibits scaling and corrosion, making direct Zn coating impossible. Surface cleaning is an important preparatory procedure. Thus, HDG technology, as illustrated by Fig. 1.1, may produce numerous wastes too and cause severe environmental hazards [1] [2] [3].

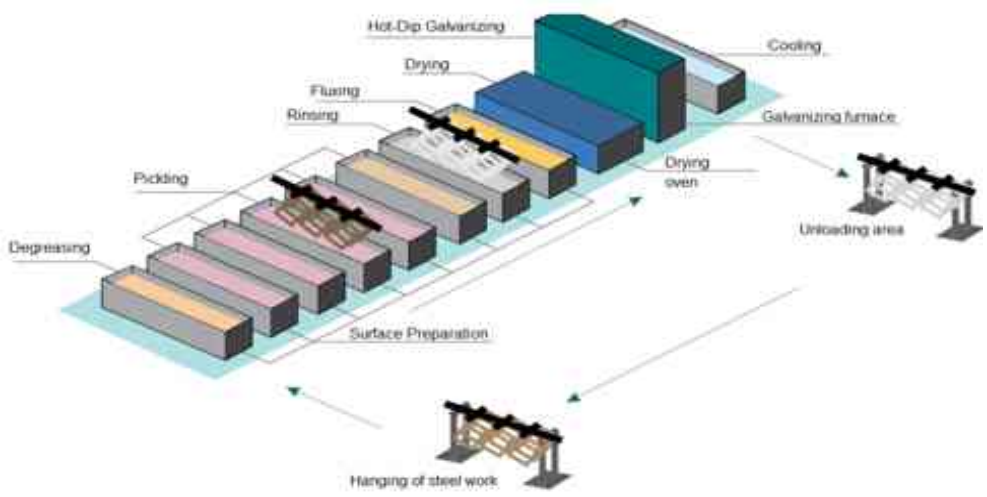

Fig. 1.1 The main units of hot dip galvanizing plants using the dry batch technology [4].

The raw objects intended to be galvanized are subjected to a complex chemical pre-treatment to achieve a pure metallic surface combined with its activation. Figure 1.2 illustrates the chemical pre-treatment sequences. The parts are first degreased and then pickled. Pickling removes rust, scales, the corrosion products and possibly other soluble impurities from the surface. However, before the all-important pickling step, it is also necessary to remove the grease from the surface as it would affect the wetting properties of the pickling liquor. The most common reagent used for degreasing is

alkaline media, such as caustic soda and potassium phosphate. However, acidic degreasing, using a mixture of surfactants with either HCl, H_2SO_4 or HNO_3, is becoming popular because no heating and extensive rinsing is required.

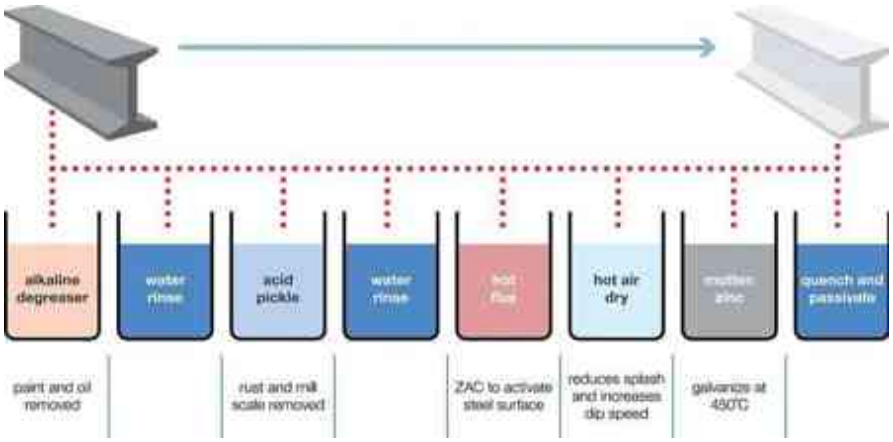

Fig. 1.2 Chemical pre-treatment sequence of dry batch HDG technology [5].

The pickling step is also used to remove faulty Zn coatings from the recycled objects. Generally, acidic media are applied. The object is immersed or end-to-end passed through a hydrochloric (HCl) or sulphuric (H_2SO_4) acid solution in which magnetite, hematite, wustite, minor oxide constituents, or recycled Zn layers react with hydrogen ions in the bath [6]. In practice, quite a large proportion of the products with faulty zinc coatings are returned to this step, either mixed with raw materials or separately. This practice results in the enrichment of the pickling liquor in zinc while the concentrations of iron and the acid decrease simultaneously. The amount of Zn in spent pickling liquor (SPL) highly depends on how they are processed. If the faulty zinc layer is removed in a separate "stripping" line, like in most modern technologies, usually a special SPL (stripping solution) of remarkably high Zn concentration arises associated with considerably lower iron content. In other cases, the SPL carries the whole of the stripped zinc beside the dissolved iron. Some part of the Zn concentration is also found in the SPL because of the use of hooks, cages, and baskets during immersion.

Known for its superiority in maintaining the adherence of the galvanic coating and lowering the possibility of localized corrosion, HCl is preferably used as the pickling agent [7] [8]. Furthermore, it offers faster pickling, easier cleaning, lower acid and heat consumption, and less liquid waste. As shown in Fig. 1.3, pickling can effectively dissolve the oxides and the faulty Zn-coat into the bath.

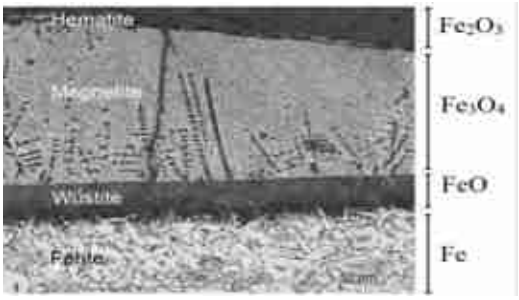

$$Fe_2O_3 + Fe + 6HCl \rightarrow 3FeCl_2 + 3H_2O \quad (1.1)$$

$$Fe_3O_4 + Fe + 8HCl \rightarrow 4FeCl_2 + 4H_2O \quad (1.2)$$

$$FeO + 2\,HCl \rightarrow FeCl_2 + H_2O \quad (1.3)$$

$$Fe + 2HCl \rightarrow FeCl_2 + H_2 \quad (1.4)$$

Fig. 1.3 Scale layer on the surface of steel structure and its reaction with HCl [9].

On the other hand, in the pre-treatment of faulty Zn-coated structures in the Zn stripping line, the main reaction is Zn dissolution by the reaction with HCl:

$$Zn + 2HCl \rightarrow ZnCl_2 + H_2 \quad (1.5)$$

However, the reaction of iron with the pickling media cannot be hindered either. Thus, $FeCl_2$ may accumulate in the SPL, although at a relatively low concentration.

The reagent loses its efficiency after decreasing its initial HCl concentration by 75-85% [6] [10]. The dominant components of the spent chloride acid solution are $ZnCl_2$, $FeCl_2$, and HCl, in this molar order if it arises from the stripping line. In this case, the exhausted solution would be highly rich in zinc in the range of 80–230 g/dm^3, and low in Fe (about 5–20 g/dm^3) along with the remaining active HCl of about 5–30 g/dm^3 concentration. If however the spent liquor comes from the main production line treating basically the previously uncoated metal, the composition may vary as 100–160 g/dm^3 of Fe, 5–20 g/dm^3 of Zn and 20–50 g/dm^3 of HCl [11] [12] [13]. Therefore, this research is oriented mainly towards the former type of SPL, coming from the stripping lines of modern galvanizing plants. As impurities, this solution may also contain trace amounts of other metals such as manganese, lead, aluminium, chromium, cadmium, nickel, copper, and cobalt, totalling in the range below 1 g/dm^3 [14] [15].

Given the contained heavy metals and the corrosive nature, the SPL is categorized as a complex hazardous waste by the EU Waste Framework [7] [16] [17] [18]. With the tightening laws and regulations on the release of residual materials containing acids and heavy metals, as well as the increased emphasis on required regeneration, recycling, or reuse of industrial waste, this effluent must be treated to satisfy the “near zero discharge” concept [19]. In addition, according to the circular economic strategies, SPL can be considered as a secondary source of Zn, and also Fe. The recovery of these metallic values may be economical even without the legal encouragement if the purity of the recycled metal reaches levels beyond the ordinary

technical grades. Due to the environmental protection regulations, the processes of Zn recovery from various industrial wastes are becoming progressively more attractive lately. If the metals can be extracted at a high purity level, the processing of the waste material may offer some extra economic benefit [6]. It is mentioned in the 2015 European Union action plan for a circular economy as "… the value of products, materials, and resources must be maintained in the economy for as long as possible, and the generation of waste is minimized to develop a resource-efficient, and competitive economy…" [14] [20]. Thus recycling SPL may be directly in line with the relevant EU regulations and also with economic aspirations if an efficient procedure is devised producing pure Zn as the main product. Additionally, the Bureau of International Recycling mentioned that producing Zn and Fe from secondary raw materials may affect CO_2 saving by great ratios [20]. If however the SPL is not recycled, just neutralized and a heterogeneous waste mass is disposed of, the allowed concentration of metals and chloride ions is strictly regulated in Europe, and similarly elsewhere [21]. Not neglecting the legal incentives that generally promote hazardous waste recycling, the economic feasibility of Zn recovery from the SPL depends strongly on the value of the recovered product. As with all metals, the price of zinc strongly depends on purity. For example, the 99.999% (5N) purity zinc (available as a special material) may cost almost 4000 times more than the common commodity at the metal markets [22]. High pure zinc can be used for producing semiconductor compounds, such as CdZnTe for detectors, ZnSe for blue light emitting diodes, ZnTe for thermo-electric cooling devices and doping semiconductors to make p-type [23]. Even though nanomaterials/powders production from secondary resources has gained considerable attention, the research for this production from spent pickling liquor is still limited to iron nanomaterial. Preparing ZnO nanoparticles from ultra-pure Zn metal is also extensively popular as it has excellent optical, electrical, and electrochemical super capacitor, thermal properties, and catalytic activities and is economically favourable [24]. In addition, using pure zinc in preparing biodegradable material, mainly in bone and blood vessels, has increased significant interest [25]. Therefore, reaching a high purity in the recovered is the main goal of the envisaged research challenge.

2. Major approaches to the SPL treatment

2.1. The conventional approach to treat SPL

A conventional treatment of this waste solution is just neutralisation, producing a harmful sludge as by-product to be disposed of at high expenses. In this process, the liquid waste from the pickling step is reacted with a 10 to 15% lime suspension or NaOH/KOH, resulting in metal hydroxides [26] [11]. Neutralization is widely used to treat SPL because of its simple technique. It has been reported by developed European steel companies that approximately 300 000 m^3 of spent pickling liquor is produced every year [27] [11]. This stream is neutralised to produce 150 000 t/y of wet sludge, which is stored under special provisions [28]. The properties of the neutralization product depend on the composition of the SPL, which varies according to the plant of origin. Beyond the simplicity, neutralization may offer low operating costs, but there are several disadvantages, such as no metal recovery, extensive use of chemicals, expensive sludge storage, hazardous precipitates, and no acid is recovered in the plant, and an increased need for the landfill for sludge storage [29] [30] [26]. After neutralisation, European standards state that the metal and chloride ion contents must not exceed 2 mg/dm^3 Zn, 10 mg/dm^3 Fe and 1 g/ dm^3 Cl^- [1] [31]. Thus, the effluent usually must be treated to meet these regulations.

Another traditional treatment widely used in the HDG industries is spray roasting, in which the HCl-based SPL is heated up to 500-800 ^oC producing iron oxide granules, followed by the condensation of the vapour to produce HCl of 200 g/dm^3. Although this process can recover 99% of iron oxide, it may be contaminated by zinc [11] [30] [32]. In addition, this process produces gas emissions and is highly energy-consuming; thus, it is impractical for the small HDG industries. The methods of treatment are continually under development. Several options combine existing technologies, such as ion exchange [33] [12], solvent extraction [8] [34] and pyro-hydrolysis or evaporation, and anion exchange [28] [35] [26] [36] [37] with acid retardation [11] [28]. However only a few research studies have discussed the possibility of producing pure metal from SPL. A combination of anion exchange and electrowinning [26] appears promising due to its potential for recovering both metal and regenerating HCl.

As a straightforward approach, direct electrowinning has also been studied to recover the metals, especially zinc, from SPL. However, the loss of Zn during the cathodic

deposition has been observed under all experimental conditions, affected by the chlorine gas production at the anode and the co-existence of Fe in the electrolyte especially when the electrolysis duration was prolonged [26]. If the aqueous solution contains a significantly high concentration of HCl, the direct electrowinning of the metal content results in mixed electrode processes, implying chlorine generation at the anode and hydrogen evolution at the cathode. The current efficiency is impaired and chlorine emission may require special provisions. To avert these difficulties, membrane-based electrochemical reactors have been devised and tested [26] [38] [39] [40]. Using an anion and/or cation exchange membrane in a two- or three-compartment electrochemical cell, the harmful effects of chlorine can be safely avoided, Zn can be electrodeposited, and HCl can be regenerated. However, the application of membranes strongly increases the system resistance, while the separate compartments results in long cathode-anode distances, producing high energy consumptions [40] [41]. A direct recovery of Zn metal from SPL by electrodeposition would require a thorough preliminary electrolyte purification.

2.2. Special approaches to purify SPL

2.2.1 The characteristics of separation techniques

Even minor concentrations of impurities may harmfully influence the characteristics of Zn electrodeposition [42]. The purity of the zinc cathode can be assured only by a thorough preliminary purification of the solution. It is possible by the physicochemical differences of the elements in the SPL. Several techniques can be used for this purpose, as mentioned in Table 2.1.

Table 2.1 Classification of methods applied for impurity elimination [43]

No.	Nature of separation	Property utilized	Method of separation
1	Chemical	Reactivity	Selective reaction
2	Chemical	Solubility	Selective precipitation
3	Chemical	Electrode potential	Cementation
4	Chemical	Distribution of dissolved ions between phases	Ion exchange, solvent extraction
5	Electrochemical	Electrode potential	Electrowinning, electrorefining
6	Physical	Distribution of atoms between solid and liquid phase	Zone melting, fractional crystalization
7	Physical	Vapor pressure	Distillation, sublimation
8	Physical	Ion mobility	Electrotransport

In order to purify the Zn-bearing SPL, it is possible to apply various standard procedures [11] [26] [28] [44] [45] [46]. Iron, and other contaminants can be eliminated by precipitation, solvent extraction, and ion exchange [11] [47]. Precipitation is one of the simplest techniques to separate Zn and Fe from acidic solutions. However, it leads to a large consumption of chemicals that cannot be recovered or reused. Furthermore, it needs expensive handling of a hazardous final sludge [26] [48]. Solvent extraction is an efficient technique, but it also implies many processing steps and it needs expensive and dangerous reagents. Another drawback is that some organic impurities might be found in the purified aqueous phase [11] [49] [50], causing interference in the cathodic deposition mechanism. These organic impurities may even change the reactivity of the metal complex and redox potential, which is essential for an efficient electrowinning of Zn.

Besides the recovery of metallic values, the regeneration and recycling of hydrochloric acid from an exhausted pickling bath is recommended to reduce the use of fresh chemicals and to minimize the Cl_2 gas emission. The most generally considered modern techniques of aqueous separation are based on the ion exchange processes, either in the forms of conventional resins or their membrane versions. Other methods, such as solvent extraction and direct conversion to metal salts, are also available.

Ion-exchange methods and membrane techniques, conforming to the Best Available Technology (BAT) standards for waste treatment [11] are becoming more applicable. This way, the metal ions and acid regeneration recovery can be combined. The benefits offered are high efficiency, no chemical addition, low energy consumption, suitability for small industrial enterprises, and providing for the regeneration of mixed liquors.

Several membrane techniques can be applied, such as membrane distillation, diffusion dialysis, electro-dialysis, electrolysis with anion or cation-exchange membranes, and non-dispersive solvent extraction [11]. Although membrane techniques share some advantages, several drawbacks are also there, such as metal leakage, membrane fouling, extended operation, high investment costs – especially for specific membranes – as well as poor metal ion separation, gas formation during electrochemical reactions along with current efficiency issues. However, in some cases, membrane technologies are still considered and installed to replace the conventional precipitation/neutralisation method. According to a review by Regel-Rosacka [11], membrane distillation offers the highest efficiency of iron salt recovery

(approximately 95% - 99.9 %) in the form of $FeCl_3$. Membrane distillation is a liquid/vapour separation process in which aqueous solutions with different compositions are separated due to boiling temperature and partial pressure differences on both hydrophobic membrane surfaces. Although promising for the recovery of HCl, this process can recover no pure metals and is characterized by a long-term operation, so far being only applied on a laboratory scale [51] [52] [53].

Diffusion dialysis, which offers the highest energy efficiency and a long membrane lifetime. The driving force of the process is a chemical activity difference on both membrane surfaces. However, the HCl produced by this technique is contaminated with Zn(II). A salt effect can occur because of complex reactions between the metal and the Cl^- ions. It has also been reported that in HCl + $ZnCl_2$ systems, both anionic and cationic complexes with Cl^- co-existed in forms of $ZnCl^+$, $ZnCl_3^-$ and $ZnCl_4^{2-}$ resulting in highly difficult separations [54]. In this case, electro-dialysis can be used in which the ion-exchange membranes remove certain ionic species in combination with an electric potential difference. However, some unwanted chlorine gas may be formed in this process, destroying the membrane.

2.2.2. Separation methods based on liquid or solid ion-exchange materials

Solvent extraction, applying liquid organic reagents, is generally recommended due to its high ability to produce relatively pure products while handling large amounts of solutions and not producing any intermittent waste liquors during the procedure. Some researchers argued that solvent extraction is among the best for liquid waste treatment. However, the technique requires handling sometimes unpleasant, dangerous, and expensive organic reagents and diluents. Various extractants are introduced, including Alamine 336, Cyanex, DBBP, TEHA, TiOA, LIX, Kelex, etc. At the end of the first step, Zn(II) and Fe(II) are extracted in the organic phase, and in a subsequent step, they are re-extracted at the stripping stage [55]. Selectivity in either step of the procedure can be ensured by developing a proper organic reagent dissolved in an organic solvent and by setting proper kinetic conditions [56].

According to a study by Rosocka et al. [5], it is known that solvent extraction can be used for Zn ion recovery with an extraction efficiency of more than ~80% - in some cases reaching even ~ 100% - by Cyanex 923 (30 % solution). Some extractants (such as acidic DEHPA (30%) with n-paraffin diluents and DEHPA (40%) with kerosene

diluents) are currently applied in the industry. It is stated that the required criteria of an extractant for SPL are (i) good phase disengagement after extraction and stripping, (ii) high selectivity, especially for zinc and iron, (iii) and easy metal stripping. The difficulty is usually due to (micro-)emulsion formation in strongly acidic solutions. Membrane-based solvent extraction might be favoured [11]. It is better to eliminate the problem of phase-separation by immobilising the organic phase in membrane pores.

Sinha et al. [57] investigated the separation of zinc and iron from actual SPL (90 g/dm^3 HCl, 117 g/dm^3 Zn and 30 g/dm^3 Fe) and similar model solutions by solvent extraction using a tertiary amine (tri-iso-octyl amin. TiOA) or triethylhexyl amine (TEHA) in the absence or presence of di-(2-ethylhexyl) phosphoric acid (HDEHP) as a synergist additive. Kerosene was used – as usual – to dilute the organic phase, with 10% dodecanol added to avoid the formation of a third phase, and the organic/aqueous (O/A) phase ratio was set to 1. These amines were assumed to offer Zn/Fe separation as they can extract Zn-chloro-complex species from HCl solutions. A strong capability of the examined tertiary amines was found to extract HCl:

$$R_3N_{org} + HCl_{aq} \leftrightarrow R_3N^+H \cdot Cl_{org}^- \qquad (2.1)$$

Although solvent extraction can process the SPL, recovering zinc from secondary resources, does not seem economically suitable because of its complicated technology and the expensive and dangerous materials involved.

Ion exchange resins are polymer beads having a diameter between 0.3-1.2 mm in aqueous suspension, able to retain metal ions, which can be easily rinsed out with other eluent solutions [58] [59]. The application of ion exchange has been proven to be the simplest way to affect the separation of Fe ions from other metal species in HCl solutions. Thus, by a suitable design it can produce either pure Fe chloride or Zn chloride solutions while the hydrochloric acid is regenerated. In addition, ion exchange seems promising because of the inherent ecological safety. However, if arranged in a chromatographic column, this process may produce some transient waste solutions if many steps are included where the feed (in loading, multiple rinsing, and eluting steps) has to be different. These fractional solutions – accompanying the primary effluent – may need to be concentrated before further utilization. Another problem of ion exchange is its relatively low volumetric capacity and approaching the

equilibrium conditions requires considerable durations because of the relatively slow kinetic nature. Both shortcomings can be technically overcome at the expense of investment costs.

Kekesi et al. [60] found that – at a laboratory scale - all the impurities, including zinc and cobalt, can be virtually separated from the solution of iron chloride by anion exchange with proper control of the HCl concentration and volumes of the loading, rinsing and eluting steps. The separation scheme is based on the equilibrium distribution functions [35]. The separation and purification of transient metals in HCl media are facilitated by the formation of chloro-complex species of resultant charges, which also depend on the HCl concentration. However, controlling the redox conditions is also needed, especially for iron. They have also shown [59], that Zn could be efficiently separated from Fe and some other transient metals in HCl solutions by a procedure based on the different equilibrium distribution coefficients (*D*) of the elements in the noted oxidation states as functions of the HCl concentration (Fig. 2.1).

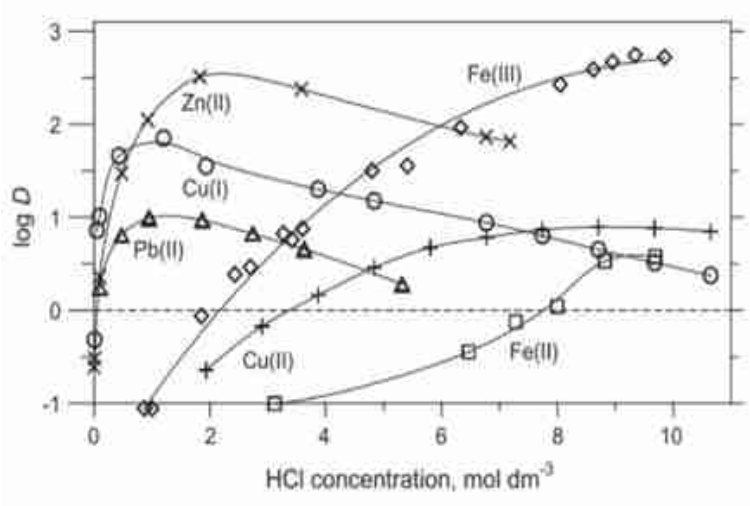

Fig. 2.1 Anion exchange distribution function of certain elements [35].

An efficient anion-exchange separation process has been suggested and proved by experimental results [35] for the purification of zinc. The elimination of these impurity elements is possible by standard [11] [26] [44] [45] [46] [28] methods. However, benefiting from the flexibility of forming complex ions of different resulting charges in chloride solutions, the purification of the targeted SPL may be carried out by applying the anion-exchange separations [37]. The decisive requirement is the elimination of Fe, the main impurity accompanying Zn [26].

In the case of purifying the HCl-based SPL, anion-exchange separation offers an efficient direct separation of Zn from the primary contaminants - Fe(II), Ni(II), Al(III), Mn(II) - which do not tend to form chloro-complex species at moderate (< ~ 3 M) Cl^- ion concentrations in the solution. On the other hand, in solutions of even relatively low (~ 1 M) Cl^- ion concentration, stable anionic zinc-chloro-complex species may arise [61]. The optimum condition of the separation process needs further investigation to prevent unnecessary dilution. For minor impurities that tend to form chloro-complexes, Cl^- ion concentration in the rinsing solution may be the critical separation parameter. Due to its environmentally friendly nature and the easy availability, NaCl is a potential chemical as the source of Cl^- to be investigated. Based on the understanding of the cathodic processes, the electrowinning process can be optimised to obtain a Zn metal of high purity and of acceptable physical morphology. If high purification is targeted, the chromatographic anion-exchange technique of serious practical disadvantages is greatly superior to the simple batch method, where the organic and the aqueous phases are contacted in repeated steps by stirring, followed by filtering. Although the principles of the necessary anion-exchange (AIEX) separations are well established, specific experiments are required to optimise a suitably devised procedure. Furthermore, the solution treatment has to include minimum dilution to keep the volumes low and the concentration of Zn sufficiently high for an efficient recovery. In addition, applying an eco-friendly addition of chloride ions where necessary in the form of NaCl instead of HCl is a new approach, corresponding to safer and more sustainable operation. Especially, because in the previously devised anion-exchange method the main goal was the preparation of an ultra-high purity iron or Zinc product [62], from solutions of initially low impurity concentrations. Also, in purifying Zn chloride solutions, the effect of a high iron background was not considered. This was later complemented by further research targeting specifically the SPL [26].

Equilibrium studies pointed out – applying the Varion AT-660 quaternary ammine type strongly basic anion-exchange resin - that a high $FeCl_2$ background may even partially substitute the effect of HCl in allowing the formation and the preferential anion-exchange sorption of Zn chloro complex species. This effect was also investigated by anion-exchange equilibrium experiments where the chloride ion concentration was set

by applying HCl and/or $FeCl_2$ in the tested solutions [63]. The relevant results, comparing the effects of chloride ions from different sources, are shown in Fig. 2.2.

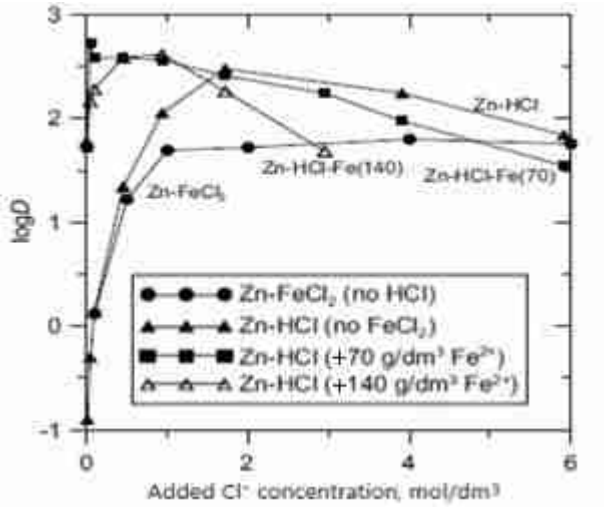

Fig. 2.2 Anion-exchange distribution of Zn in chloride solutions providing Cl^- ions from added HCl or $FeCl_2$ sources [63].

Despite the promising equilibrium results, the actual Fe/Zn ion chromatographic separation can be far from complete, evidently due to the slow reaction mechanism of Zn ion-exchange. In order to improve the separation, Csicsovszki et al. [63] introduced a strongly reduced, 1 bed volume/h (1 BV/h) feeding rate of the chromatographic column. Although it proved successful, further improvement was made by inserting a preliminary anion-exchange separation to remove the bulk of the Zn content of the SPL in a batch operation. A batch anion exchange in multiple steps, similarly to the solvent extraction technique, might be an alternative to the chromatographic process. Kononova et al. [36] suggested using Purolite S985, Purolite A500, and AM-2B anion-exchange resins to recover zinc from chloride solutions. The results show that both strong and weak basic resins can offer high sorption in a wide HCl range, where industrial acceptability is ensured by a zinc recovery of 75-80 %.

2.3. The electrolytic recovery of Zn from SPL solutions

2.3.1. The challenging electrode processes in pure $ZnCl_2$-HCl solutions

Zinc recovery from the purified SPL through electrodeposition faces severe challenges. The primary difficulty is caused by the possible reduction of H^+ ions as Zn is electrodeposited at the cathode. The two competing charge-transfer reactions are:

$$Zn^{2+} + 2e^- \rightleftharpoons Zn \qquad E^o = -0.763\ V_{/SHE} \qquad (2.2)$$

$$2H^+ + 2e^- \rightleftharpoons H_2 \qquad (SHE) \qquad (2.3)$$

This rivalry may severely decrease the current efficiency of Zn deposition and increase the specific energy consumption. The value of the Zn standard potential changes with the Zn-ion activity and the temperature according to the well-known Nernst-equation, as well with the existence of the complex ligands. Due to the readily formed zinc-chloro-complex species [64] [35], the metal deposition must be preceded by the dissociation of the complex structure, liberating the electroactive Zn^{2+} cation:

$$[ZnCl_x]^{(2-x)-} = Zn^{2+} + xCl^- \tag{2.4}$$

The relatively strong tendency of Zn to form chloro-complex species – which can be used to advantage in the separation schemes – may considerably modify the mechanism of the ionic transformation in the electrified interface. Thereby the ion supply to the cathode surface is influenced. This phenomenon has also been found important at the electrodeposition of tin from HCl media [65]. The ion supply to the active sites of electro-crystallization may not only change the actual deposition potential, but also affects the physical structure of the obtained cathodic deposit.

As practice has also confirmed, Zn can be deposited even from slightly acidic solutions of sufficiently high Zn-concentration because of the significant overpotential of hydrogen on zinc. The overpotential of hydrogen evolution on zinc is fortunately highly negative, -0.94 V in the alkaline [66] [67], and -0.8 V in acidic [68] solutions if the rate of reaction is at a considerable (~ 10 A/m^2) level. However, due to a local drop of zinc concentration at the cathode surface, the simultaneous reduction of hydrogen is often significant. Beyond decreasing the current efficiency, it affects also deposit morphology and solution stability.

Carrillo-Abad et al. [38] developed a special electrochemical reactor to recover zinc from SPL by a potential-controlled method. It was observed that zinc deposition started from a potential value more negative than -0.99V (vs. SHE). The applied potential values ranged between -1 V and -1.75 V. In the iron-free solution, polarization of the cathode enhances Zn deposition directly and indirectly, due to the increasing electrode surface roughness and the promoting action of the turbulence caused by the evolution of H_2 bubbles massively detaching from the cathode surface. Specific energy consumption decreases during the initial fast deposition of zinc, but cathodic potential may further drop due to the hydrogen evolution reaction (HER).

If the pH is increased near the cathode, Zn hydrolysis may generate some complex compounds at the cathode surface, appearing as stable corrosion products, as seen in Fig. 2.3. This passivation may result in a sudden drop of the current efficiency and a shift towards the rivalling H^+ ion reduction causing.

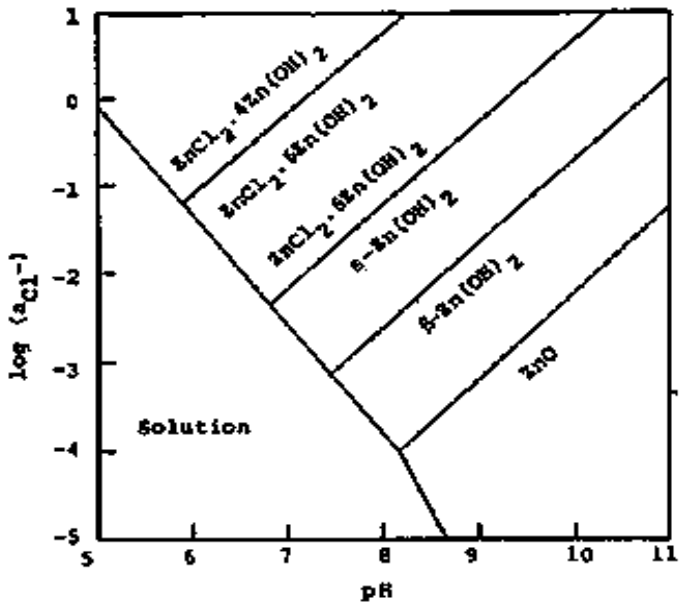

Fig. 2.3 Equilibrium diagram for zinc corrosion products in a chloride environment [69].

The mixed cathodic reaction has further consequences affecting the cathodic process. The generated H_2 bubbles initially adhere to the cathode surface, thus may interfere with the current distribution and intensifying the changes of ionic compositions [70]. Under extreme conditions, large zinc dendrites may appear as a result of inhomogeneous nucleation and crystal growth [71]. Low (<100 A/m^2) current densities are generally preferred to avoid excessive hydrogen evolution and the rough deposit quality [72], which seems rather low for an efficient production.

The depletion of the active cathodic sites in the electroactive Zn^{2+} ions, combined with a fast charge transfer process, may impose the growth of irregular and often dendritic crystals. These 3D morphologies in turn lead to inhomogeneous potential distribution as well, facilitating the further dendritic growth patterns. The obviously better ion supply from the volume of the electrolyte surrounding the cathode edge causes preferential peripheral deposition. This effect is coupled with a denser current distribution attributed to the tendency of the flow of electrons propelled to the sides and surfaces of metallic conductors. Additionally, the reduced distance of the projected surface to the counter electrode implies lower resistance, enhancing the inhomogeneity of the current density across the cell.

Kashida et al. [73] found that the deposition of Zn was depolarized with increasing chloride ion concentration in a low range (~ 300 mg/dm^3), indicating that chloride ions may promote charge-transfer processes. Furthermore, the study shows that the polarization resistance decreased with increasing chloride concentration, while the capacity of the electric double layer increased with increasing chloride concentration; however, from 3 to 6 g/dm^3, the capacity decreased and approached that obtained from a chloride ion-free solution.

The exchange current density of the reaction rises with increasing polarizability of the anion in solution. The polarizability of chloride ions (8.9 cm^3/mol) is greater than that of sulphate ions (3.9 cm^3/mol); thus, the exchange current density for Zn deposition in a sulphate solution is 3.10^{-5} A/cm^2, whereas it is 3.10^{-4} A/cm^2 in chloride solutions [73] [74] [75] [76]. Taking use of this effect, Thomas and Fray [77] [78] performed electrolysis in high concentrations (18~35 wt%) of zinc chloride with high current densities (220~250 mA/cm^2), obtaining ~ 90% current efficiencies (CE).

The overpotential for a cathode reaction is diminished by a drop in the potential at the inner Helmholtz plane caused by selective adsorption of chloro-anions at the cathode [79]. By increasing the polarizability – thereby the absorbability - of the complex ions, they are more capable to combine with metal ions increases. The depolarization of the Zn deposition potential observed in the presence of chloride ions is possibly caused by a this effect based on the formation of weak complexes or reaction intermediates involving chloride and Zn^{2+} ions [73].

As stated by Fukushima and Ishikawa [80], the electrodeposition process of Zn-iron-group metals involves a multi-step reduction mechanism. These metals do not initiate deposition at their equilibrium potentials. Instead, they proceed through a transient intermediate that contains hydroxyl groups. Chloride ions catalyse the deposition of Zn-iron-group metals as they modify the composition of the intermediate. Chloride ions act as catalysts to reduce the minimum overpotential of several metals, such as Ni, Fe, Cu, In and Zn [75] [81] [82].

Hurlen and Fischer [83] studied the kinetics of Zn deposition in acidified potassium chloride solution. They mentioned that Cl^- activity influences the reactions of the Zn(II)/Zn electrode rather than pH (pH = 0,5-5) in the solutions. The charge-transfer process occurs between $ZnCl_2(H_2O)_y^-/ZnCl_2(H_2O)_y$.

The anode reaction may vary from the chloride evolution reaction (CER) or oxygen evolution reaction (OER) depending on the pH of the electrolyte:

$$2Cl^- \rightleftharpoons Cl_2 + 2e^- \qquad E^0 = 1.396\ V_{/SHE} \tag{5.4}$$

$$2H_2O \rightleftharpoons O_2 + 4H^+ + 4e^- \qquad E^0 = 1.229\ V_{/SHE} \tag{5.5}$$

At high Cl^- ion concentrations, the evolution of chlorine may occur besides oxygen. at the anode. However, at elevated pH levels, the CER is impeded due to the increased stability of the produced hypochlorite ion.

Observing the current efficiency of Zn deposition at 500 A/m^2 for 6 hours in solutions containing various amounts of chloride ions, Kashida et al. found that the current efficiency is increasing as the function of Cl^- concentration and ~ 95% CE was reached with 6000 mg/dm^3 Cl^- [73]. The current efficiency improved by 1.1% upon adding 300 mg/ dm^3 of chloride ions and increased with increasing chloride ion concentration above 300 mg/dm^3. Chloride solutions offer higher rates of zinc deposition on the cathode surface than sulphate systems. However, the fast reaction and the slow transfer of the electroactive ions together make it difficult to obtain smooth and compact deposits.

The ionic diffusion coefficient and mobility determine the ion transport characteristics in stationary solutions. However, the formation of complexes also affects the ionic mobility of zinc. It is generally lower in complex form due to the large hydration shells. The values of the ionic equivalent conductance and diffusion coefficients of Zn^{2+} in infinite dilution at 25 ºC are 53 $\Omega^{-1}cm^2$/equivalent and 0.71×10^{-5} cm^2/s, respectively, while for Cl^-, these values are 76.34 $\Omega^{-1}cm^2$/equivalent, and the diffusion coefficient is 2.032×10^{-5} [84]. The diffusion coefficient of Zn^{2+} in 0.05M $ZnCl_2$ + 1M KCl solution is 0.89 x 10^{-5} cm^2/s [85]. In general, for zinc salt with a cation transport number smaller than the Cl^- anion transport number, the transport number of the central ion will decrease as the concentration increases. As a result, the conductivity of a zinc salt solution increases significantly with concentration but declines at high concentrations due to increasing viscosity. The conductivity as a function of zinc chloride concentration is depicted in Fig. 2.4.

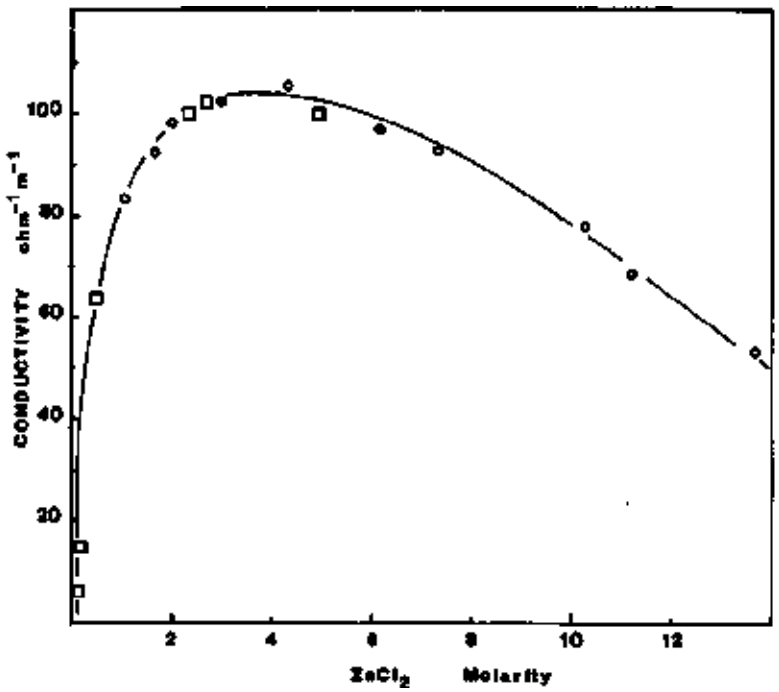

Fig. 2.4 Conductivity of aqueous zinc chloride [77].

It was reported [77] that conductivity increases to a peak at 3.7 M zinc chloride and subsequently falls when the concentration of complex ions, such as and $ZnCl_4(H_2O)_2^{2-}$ increases.

The form of the zinc deposit has been found and reported dependent upon several factors, including the current density, deposition period, and hydrodynamic circumstances [86]. When the Zn concentration is low, the resulting deposit generally exhibits a finer surface texture. Kim and Jorne [85] investigated the kinetics, mass transfer, and surface roughness of the Zn deposit in a chloride solution. The effects above were observed by consistently maintaining the current at several levels: beyond, nearby, and below the limiting current. The surface roughness depends upon the micro-throwing power while operating significantly below the limiting current [85]. However, the roughness of the surface was found to exhibit a direct relationship with the ratio to the limiting current, and the surface becomes extremely rough when the limiting current is surpassed. Zinc dendrites are shown to originate at the periphery of a revolving disc, where the local current density is significantly elevated. Dendritic development is subject to diffusion limitations and is notably affected by fluid dynamics, particularly at lower concentrations. The interaction between dendrites and the flow occurs because the protrusions also have a baffling effect. A detailed study of the effects exerted by the zinc and HCl concentration, current density and temperature

on the deposit quality has also been conducted [40] [86]. Fine-grained deposits were obtained with only 10 g/dm^3 of Zn in the electrolyte at current densities lower than 300 A m^{-2}, while at higher currents, dendritic and sponge-like deposits evolved. In the highest examined current densities (~1000 A/m^2), dense deposits occurred with a slight acidification (0.5 g/dm^3 HCl). The addition of more acid (to 50 g/dm^3 HCl) shifted the dendrite formation to higher current densities [72]. It may be in correlation with the build-up of highly coordinated, anionic chloro-complex species of Zn. It was also stated that increasing zinc concentration could produce more compact deposits, but the actual current efficiencies related to these results were not specified.

Kashida et al. [73] also investigated the impact of different chloride ion concentrations on the surface morphology of Zn deposits (Fig. 2.5) deposited with a current density of 500 A/m^2 for 6 hours. Spherical concavities were found on the surface of deposited zinc, which can be attributed to the adhering H_2 gas undergoing evolutionary processes. The dimensions of the spherical concavities exhibited a positive correlation with the concentration of chloride ions.

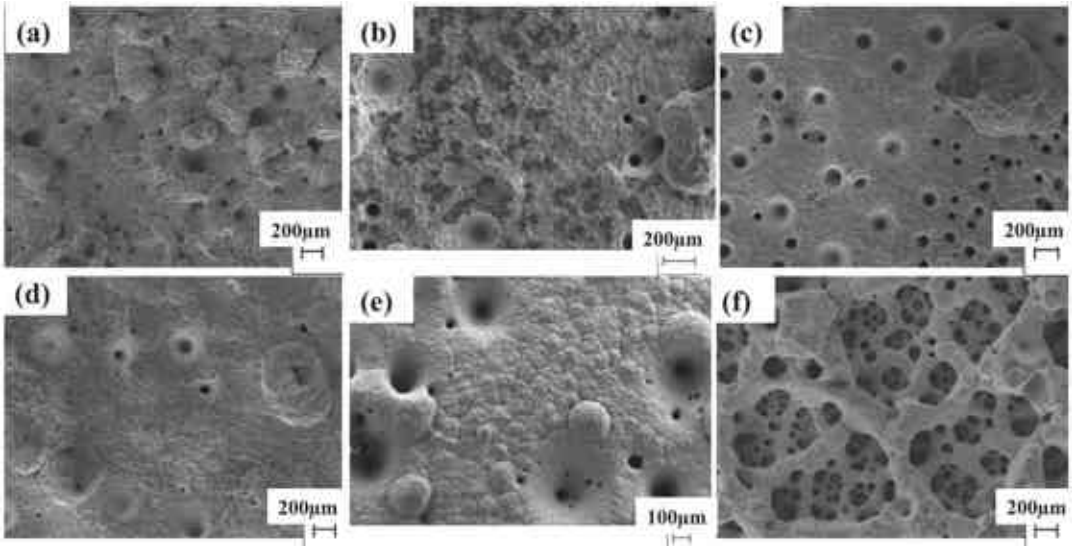

Fig. 2.5 Surface morphology of Zn deposited at 500 A/m^2 for 6 hours in solutions containing chloride ions of (a) 0, (b) 300, (c) 600, (d) 1200, (e) 3000, (f) 6000 mg/dm^3) [73].

The observed trend indicates a decrease in hydrogen evolution as the concentration of chloride ions increases, concurrently with the rise in the current efficiency of Zn deposition. It corroborates the assumed enhancing effect of the Cl^- ions on the main charge transfer process, as discussed above. The growth of the concavities indicates a decline in the ability of H_2 bubbles to be released from the Zn deposit, probably in

correlation with the increasing roughness of Zn crystal development as the concentration of chloride ions increases.

Anderson [87] investigated the formation of long striations and evaluated the kinetic parameters associated with the zinc chloride system. Deposition was carried out from a solution of 1M zinc chloride onto several substrates, including glassy carbon, graphite-loaded polymer, synthetic graphite, and platinum. The exchange-current density was found to be around 1 mA/cm^2. The densities of nodules exhibited a general rise in correlation with current density, spanning a range of 200 to 1000 nodules per square millimetre. The potential transient reached its peak within the initial milliseconds. Furthermore, it was observed that the amplitude of this transient was inversely proportional to the quantity of nucleation sites present.

2.3.2. The effect impurities on the cathodic process

The presence of iron in the solution may decrease the current efficiency by the Fe^{2+}/Fe^{3+} side-reaction. Iron as a major impurity may promote the reduction of hydrogen ions at the cathode because the hydrogen overpotential on iron is lower (by ~ 400 mV) than on a pure zinc surface [64]. Besides decreasing the efficiency of Zn deposition, iron as the main impurity metal, severely impacts the purity and the morphology of the cathode deposit. By enhancing the HER iron causes an escalation of the local pH at the cathode.

It has been found in general practice, that zinc electrodeposition might be possible even at lower potentials. As the optimum value, a -1.75 V cathode potential has even been proposed, which allowed relatively high current efficiencies [40]. The zinc deposition rate was found to increase by higher initial pH, yet the re-dissolution of zinc remained a problem. Oxygen evolution reaction was enhanced over chlorine evolution by the pH control, and above pH 3, the formation of stable hypochlorite was found to replace chlorine evolution. Dissolved chlorine gas in the electrolyte may corrode the electrode material; thus, some experiments applied simple physical barriers (diaphragms) between the two electrodes to prevent most of the chlorine gas from reaching the cathode. An ion-exchange membrane can act as a perfect barrier for the chlorine gas, thus prevents zinc re-dissolution, and it can also retain the generated hydrogen ions in the anode compartment [88]. However, iron may still co-deposit. Thus, researchers also tried to apply cation exchange membranes (CEM), like

NAFION-117. Zinc passes through the CEM, even preferentially over iron. However, a higher energy consumption occurred due to a high ohmic drop [88]. Thus the application of membranes to separate the two compartments were impractical and disadvantageous to economy. The specific energy consumption strongly increased. On the other hand, the transport of H^+ ions generated at the anode could be prevented efficiently by a proton-blocking membrane separation [63]. The application of both cationic and anionic membranes and a middle compartment to collect the regenerated acid [89] would result in even higher potential drops. The high cell voltage could be successfully reduced by applying a hydrogen diffusion anode instead of the inert material, offering also the generation of H^+ ions at the anode [63], however this system is rather delicate and the application of H_2 gas for the anode reaction is quite expensive. Thus the separation of the anodic and cathodic compartments by ion-exchange membranes, and the application of hydrogen diffusion anodes seem impractical to economy.

A practical improvement to be applied for diminishing the iron co-deposition is introducing some initial zinc before the electrochemical deposition, which depresses iron deposition [90]. It has also been observed that the co-deposition of iron is accompanied by a pH increase. It can even be put to some use in depressing the iron concentration in the electrolyte. Inducing iron hydroxide precipitation by increasing the OH^- concentration may be helpful in avoiding co-deposition. However, a close to 10% iron deposition ratio is still hindered the production of pure zinc deposits [40].

In support of the theory of “anomalous” Zn deposition, some researchers even argued that zinc undergoes “under-potential” deposition (UDP), in which it occurs at less negative potentials compared to its equilibrium reduction potential [91] [92]. This may accompany the inhibition effect of zinc-to-iron deposition discussed above. As a justification, the voltammograms were reported [39] to be similar to those of iron-free solutions at low Fe(II)/Zn(II) ratios, as can be seen in Fig. 2.6.

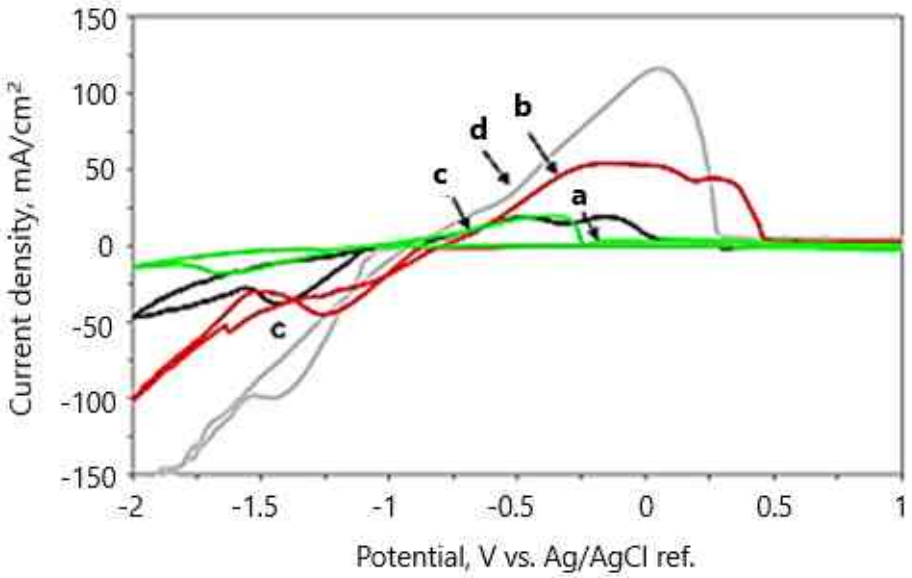

Fig. 2.6 Cyclic voltammograms obtained with different solutions: a) 0.055M $ZnCl_2$; b) 0.125M $FeCl_2$; c) 0.11M $FeCl_2$ and 0.055M $ZnCl_2$; d) 0.495M $FeCl_2$ and 0.055M $ZnCl_2$ [39].

The inhibition of iron deposition can be seen for the Fe(II)/Zn(II) ratio of 2:1, where the cyclic test produces relatively similar graphs to that of iron-free solutions, confirming the anomalous electrodeposition of zinc. However, if the ratio Fe(II)/Zn(II) is strongly increased, the iron deposition can become dominant. Further investigations have also reported the anomalous preferential deposition of zinc against the iron-group metals, although with delicate sensitivity to the electrolysis conditions. Decreasing the relative concentrations of Zn in the chloride solution, the mixed deposition becomes characteristic [93]. For more negative overpotentials, simultaneous hydrogen evolution is essential. Consequently, the local pH varies during the deposition and iron hydroxides can precipitate. This fact explains the shape of the voltammetric curves recorded when the scan was reversed at more negative limits. Under these conditions, the positive-going sweep shows a greater difficulty of iron oxidation when hydroxides are present. A strong decrease in the negative potential limit overcomes this inhibition, as reflected in the current curve by the appearance of a pure-iron oxidation peak. [94] The potentiostatic transients recorded under stationary conditions show an initial monotonic increase in the current, leading to the formation of zinc-rich deposits, followed by a sudden increase in current, from which iron-rich deposits may form.

A research of a special technology was performed by Diaz et al. [95], also addressing the co-deposition of zinc and iron in an acid solution. It is reported that the anomalous co-deposition process does not match any thermodynamic data; instead, it can be described by a kinetic argument.

A series of experiments was performed by Mackinnon et al. [72] to assess the effects of different metallic impurities on the current efficiency of Zn deposition from a 0.15M $ZnCl_2$ - HCl electrolyte and tetrabutylammonium chloride additions, utilising a diaphragm cell equipped with dimensionally stable anodes (DSA) and aluminium cathodes. The observed maximum current efficiency was ~ 96%, though the co-deposition of cadmium and lead with zinc was observed. The presence of antimony and copper has been seen to result in a reduction of polarisation, leading to a drop in current efficiency of Zn recovery. The introduction of cobalt and iron resulted in a shift towards a more basally oriented deposition structure, accompanied by a reduction in current efficiency. The inclusion of germanium resulted in a reduction in the overpotential associated with zinc deposition. However, it also led to significant dissolution of the deposited material, resulting in a commensurate fall in current efficiency. This effect was observed even at relatively low germanium concentrations, as low as 0.1 mg/l. The adverse effect of contaminants on the current efficiency of zinc electrowinning might be ranked as Sb > Ge > Cu > Pb > Cd > Ni > Fe > Co.

Some spent pickling liquors may contain other electropositive metals such as Ni, Pb, Co, Cr, and Cu [11]. The more noble practical impurities (especially Cu and Ni), which are more likely to be deposited, could significantly threaten the purity. Also, the promotion of hydrogen evolution may have a disturbing effect [94].

A suitable deposition of Zn at the cathode mainly depends on the composition of the electrolyte solution, in which the complexing agents (in this case, the abundance of chloride ions) influence the deposition process. In chloride solutions, it is hard to obtain a smooth, compact deposit [96] [88]. In a detailed study of the basic effects [86], it was observed that at 10 g/dm^3 Zn concentration, a fine-grained Zn deposit could arise at current densities lower than 300 A m^{-2}, while at higher currents, dendritic or sponge-like deposits were also formed, however dense deposits could also occur with a slight acidification (0.5 g/ dm^3 HCl). Further, acidification to 50 g/dm^3 HCl produced a honey-combed Zn deposit at the cathode surface.

2.3.3. Iron electrodeposition from pure chloride solutions

On the other hand, $FeCl_2$-HCl solutions – modelling the case when Zn had been removed from the purified SPL – were used in studying the iron deposition under various conditions by Csicsovszki et al. [63]. Iron could be practically deposited with

acceptable efficiency from solutions containing more Fe(II) than ~ 60 – 80 g/dm^3 and less HCl than ~ 0.1 – 0.2 mol/dm^3. Increased temperatures may enhance the iron deposition but also the unwanted side processes, such as re-dissolution. Thus it is deemed not beneficial for energy consumption, and finally room temperature was considered the optimum. These results also indicate the cathodic deposition of Zn, which element has even a lower electrode standard potential, implying even more difficulties. The potentiodynamic experiments in the prepared $FeCl_2$-HCl solutions carried out by the same authors [58] helped the general interpretation of the relevant cathodic polarization curves obtained. The slopes and the positions of the local peaks and steps in the plots were associated with the probable partial electrode processes. The main results referring to the cathodic deposition of iron from solutions of different original Fe(II) concentrations and 0.08 mol/dm^3 HCl content are illustrated in Fig. 2.7.

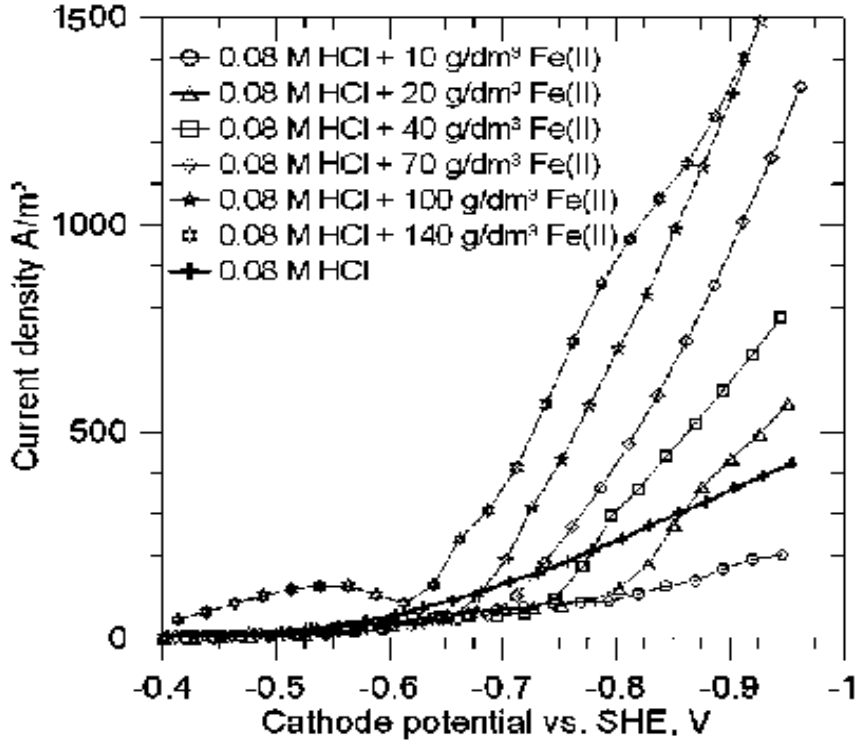

Fig. 2.7 Polarization curves measured with copper cathodes for solutions containing different Fe(II) concentrations at 0.08 M HCl, 20°C, 5s period and no stirring [87].

The apparent cathodic current densities (referring to the original geometric area of the electrode) are plotted against the cathode potential. Initially, the Fe(III)/Fe(II) reduction could be detected at lower cathodic (less negative) potentials, while there was no appreciable current in this range from the blank HCl solution. Subsequently, a local decrease can be observed in the cathodic current, which is attributable to the limited supply of Fe(III) ions, regenerated by the aerial contact of the basically Fe(II)

solution. At higher cathodic potentials, the curves started to rise again, which is related, to both the evolution of hydrogen and to the deposition of iron by the Fe(II)/Fe cathodic reaction. According to the tendencies observed, the efficiency of iron deposition may notably decrease if the Fe(II) content is lower. An iron concentration of 20 g/dm^3 still shows the characteristics of Fe(II) reduction, while at 10 g/dm^3, the slope of the polarization curve corresponds to the one of H_2 evolution. This type of potentiodynamic examination is a valid purpose to follow in zinc chloride solutions.

It can be seen that even though the purification of the zinc solution is developed to a comprehensively efficient level, several major issues remain to be tackled. Just to mention the most important ones: co-deposition of Fe and other impurity metals, Cl_2 and H_2 gas evolution, low current efficiencies, and rough – even dendritic - electro-crystallization instead of compact layers. These major problems currently hinder any industrial application. Thus, further research must be done to develop this process.

3. The application of anion-exchange to the purification of SPL

3.1. Principles of the planned separation

A novel, highly efficient anion-exchange chromatographic method [37] has been proposed to produce high purity electrolytes from SPL by relying on the differences in the formation and sorption characteristics of the main metals contained. The critical separation factor is the difference in the formation of chloro-complex ions and their distribution between the solution and resin phases. In chloride-based SPL, many positively charged ions form complex anions except for alkali, alkaline earth and the element in the first two rows of the p-block periodic table. These non-complexing species can be easily removed from the Zn solution while Zn is fixed into a strongly basic (quaternary ammine functional type) anion-exchange resin. Although there will be some impurity ions co-sorbed, the separation will be possible by suitably adjusting the Cl^- concentrations in subsequently applied rinsing and eluting solutions. Table 3.1 summarizes the classification of the practically important or characteristic impurities serving as the basis for devising the purification of the SPL.

Table 3.1 Classification of the potential elements in the SPL

Sorbability in strongly basic anion-exchange resins from 0.1 ≤ 8 M HCl	
Cr(III), Mn(II), Fe(II), Ni(II), Al(III)	Negligible/weak
Fe(II), Fe(III), Cu(II), Pb(II)	Variable
Cd(II), Zn(II), Cu(I)	Strong

Setting the Cl^- ion concentration as required for certain separations, the main impurities can be separated from Zn [43]. The procedure can be devised according to the established anion-exchange distribution coefficients (D), most accurately determined by equilibration in batch experiments:

$$D = \frac{c_{\mathrm{e,resin}}}{c_{\mathrm{e,solution}}} = \frac{V_{\mathrm{solution}}\left(c_{\mathrm{s,solution}} - c_{\mathrm{e,solution}}\right)}{V_{\mathrm{resin}} c_{\mathrm{e,solution}}} \tag{3.1}$$

where "e" and "s" at the index level refer to the equilibrium and the starting concentrations. Equilibrium distribution coefficients of metals in various oxidation states, determined by this technique [60], are shown as a function of the Cl^- ion concentration in Fig. 3.1.

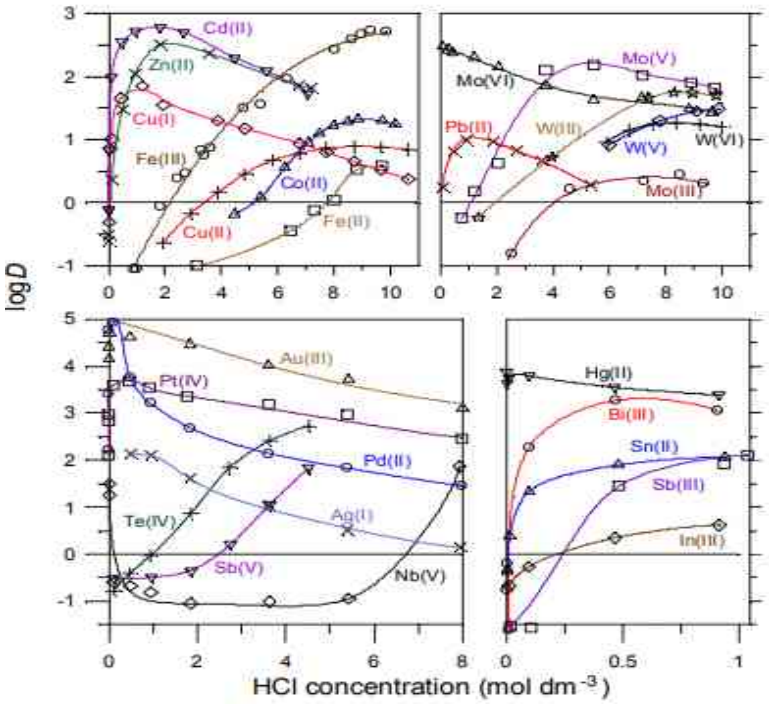

Fig. 3.1 Anion exchange distribution functions determined by batch equilibration [60].

According to the differences in the equilibrium distribution functions, Zn(II) can be separated from either Fe(III) or Fe(II) by means of properly setting the HCl concentration. An overlay of the most important distribution functions from different sources is shown in Fig. 3.2, where the cases of Mn and Ni are also marked despite the negligible/non-existing anion-exchange sorption in their cases.

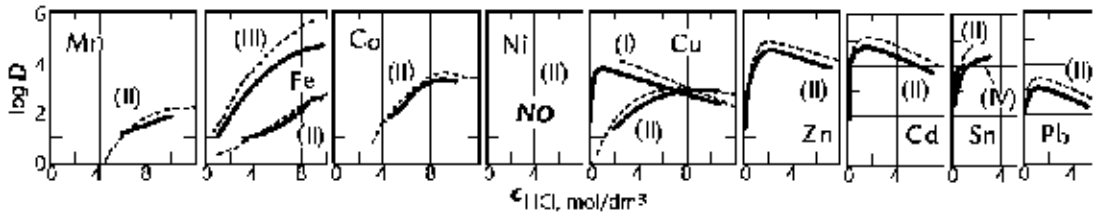

Fig. 3.2 Sorption of elements from HCl on strong base anion exchange resins (solid lines represent batch equilibrium results) [43] [97].

It is quite fortunate that Ni(II) and Mn(II) species do not show any appreciable anion-exchange sorption in the examined Cl^- ion concentration range. However, Zn0 and some other elements are capable of forming negatively charged chloro-complex species:

$$p\mathrm{Me}^{\nu+} + px\mathrm{Cl}^- \Leftrightarrow \left[\mathrm{Me}_p\mathrm{Cl}_{px}\right]^{p(\nu-x)} \tag{3.2}$$

where ν is the valence of the cation, x is the coordination number and p is the degree of polymerization of the complex structure of $p(\nu\text{-}x)$ resulting charge, which needs to be negative ($\nu\text{-}x = -z$) to be exchanged for the chloride counter ions in the resin:

$$\left[\mathrm{Me}_p\mathrm{Cl}_{pn}\right]^{pz-} + pz\left\{\mathrm{Cl}^-\right\} \Leftrightarrow \left\{\left[\mathrm{Me}_p\mathrm{Cl}_{pn}\right]^{pz-}\right\} + pz\mathrm{Cl}^- \tag{3.3}$$

The former transformation in Eq. (8) is the reason behind the rising section of the distribution functions in Figs. 2.1 and 2.2, and the decline is caused by the mass action effect in the exchange process, expressed by the equilibrium constant (K) derived [43] from Eq. (3.3):

$$\mathbf{K} = \frac{a_{\left\{\left[\mathrm{Me}_p\mathrm{Cl}_{pn}\right]^{pz-}\right\}} \cdot a_{Cl^-}^{pz}}{a_{\left[\mathrm{Me}_p\mathrm{Cl}_{pn}\right]^{pz-}} \cdot a_{\left\{\mathrm{Cl}^-\right\}}^{pz}} = \frac{c_{\left\{\left[\mathrm{Me}_p\mathrm{Cl}_{pn}\right]^{pz-}\right\}}}{c_{\left[\mathrm{Me}_p\mathrm{Cl}_{pn}\right]^{pz-}}} \cdot \frac{\gamma_{\{\pm\}}}{\gamma_{\pm}} \cdot \frac{a_{\mathrm{Cl}^-}^{pz}}{a_{\left\{\mathrm{Cl}^-\right\}}^{pz}} \tag{3.4}$$

where $\gamma_{\pm}$ is the mean activity coefficient, and the $\{\}$ braces indicate the resin phase. The effects can be distinctly seen after a convenient rearrangement:

$$\log D = \log\left(pK \frac{c_{\left[\mathrm{Me}_p\mathrm{Cl}_{pn}\right]^{pz-}}}{c_{\mathrm{Me}}}\right) + \log\left(\frac{\gamma_{\pm}}{\gamma_{\{\pm\}}}\right) - pz\log\left(\frac{a_{\mathrm{Cl}^-}}{a_{\left\{\mathrm{Cl}^-\right\}}}\right) \tag{3.5}$$

This expression helps understand the characteristic shapes of the determined distribution functions, with the first tag corresponding to initial steep rise, and the

decreasing activity coefficient ratio [61] and the increasing Cl^- ion concentration in the aqueous phase resulting in the later decline of the distribution coefficient. It has been shown by Kekesi et al. [61] that this relationship can even be used for the determination of the average charges of the chloro-complex species [43]. As suggested by the published equilibrium data, Zn may be retained in the resin bed while a number of practically important impurities can be removed with the drained solution at a relatively low concentration of HCl. The behaviour patterns of Fe(III) and of Fe(II) are distinctly different. While Fe(III) is gradually sorbed and reaches a high distribution as the HCl concentration is increased, Fe(II) remains rejected by the resin.

Ion exchange has also been mentioned by the Joint Research Centre of the EU in 2021 as one of the best techniques for Zn removal from SPL [98]. Anion exchange has also been examined, pointing out similarly strong retention of Zn in different types of strongly basic anion exchange resins (e.g. Lewatit MP-500 and Lewatit M504) [99]. They examined the sorption and elution of Zn and Fe(III) oxidised by hydrogen peroxide, pointing out differences in the behaviour patterns. Still, the separation efficiency achieved with a single anion exchange unit could not be considered satisfactory for preparing a pure Zn electrolyte. Also, the oxidation of iron to the trivalent state makes the process more expensive, while the Zn/Fe separation is not improved. Zinc can be most efficiently separated from Fe, if it is removed in the reduced Fe(II) state [26]. Reduction to the Fe(II) state can be assured by vigorously stirring iron granules in the solution, to cause the com-proportionation reaction:

$$2Fe(III) + Fe = 3Fe(II) \tag{3.6}$$

The standard electrode potential of the Fe^{3+}/Fe^{2+} couple is + 0.741 V, whereas that for the Fe^{2+}/Fe is -0.42, which definitely dictates the reaction in Eq. (3.6), however the chloro-complexation equilibria slightly modify the resulting ratio of the Fe(II)/Fe(III) species. Applying the ROCC computer software, developed for the simulation of the relative concentrations (c_i) in the chloride solutions [43] and the known constants of chloro-complex stabilities [100], Fig. 3.3 shows that the predominance of the Fe(II) species can be assured even if the solution is in contact not only with the Fe granules, but also with air.

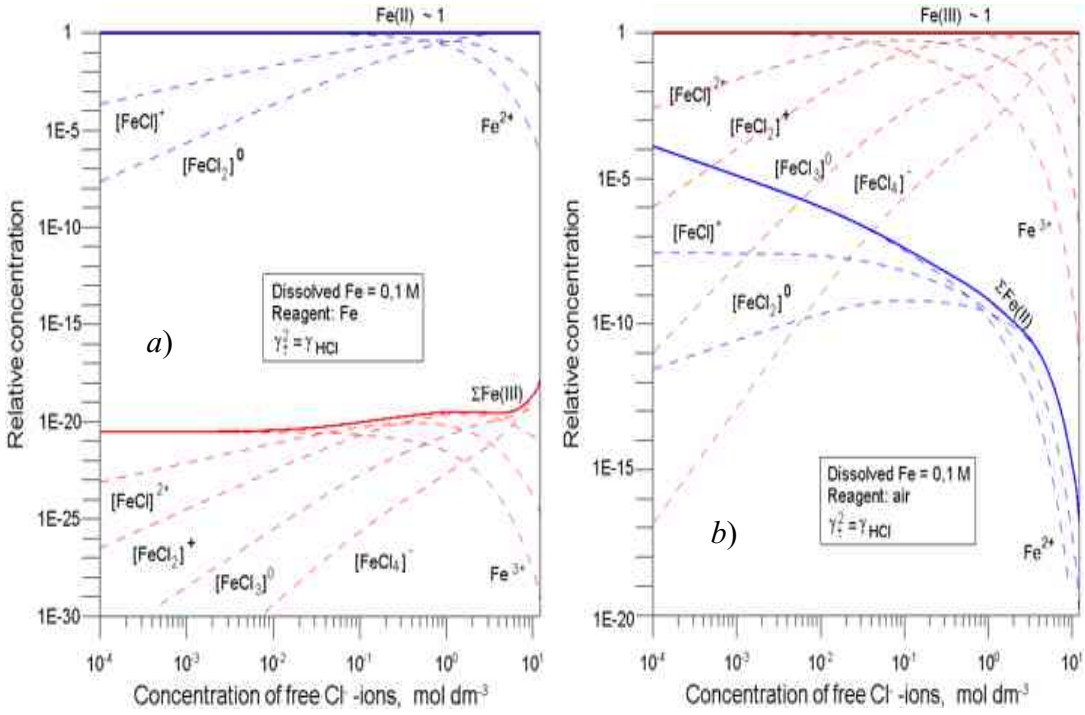

Fig. 3.3 The distribution of Fe in HCl solutions in contact with Fe powder (a) or air (b).

The majority of the iron in SPL is contained in the Fe(II) state in the SPL if it is in contact with the iron sludge – as in the collecting vessels – also produced in the pickling process. Stirring in some Fe powder serves the virtually complete reduction of the Fe(III) species formed by the contact with air.

Fixing Zn primarily in the column (at lower than 4 M HCl) and applying sufficient rinsing with a blank HCl solution of the same molarity is essential to eliminate the non-complexing elements such as Ni, Mn, Al in their common oxidation states, and Fe(II). Elements of variable distribution characteristics in this HCl range, like Co(II), require a careful setting of the initial Cl^- ion concentration. It is also required for economic and environmental reasons to considered also how NaCl can substitute free HCl to supply the needed free Cl^- ions. Figure 3.4 describes the general major step of SPL purification by chromatographic anion-exchange separation.

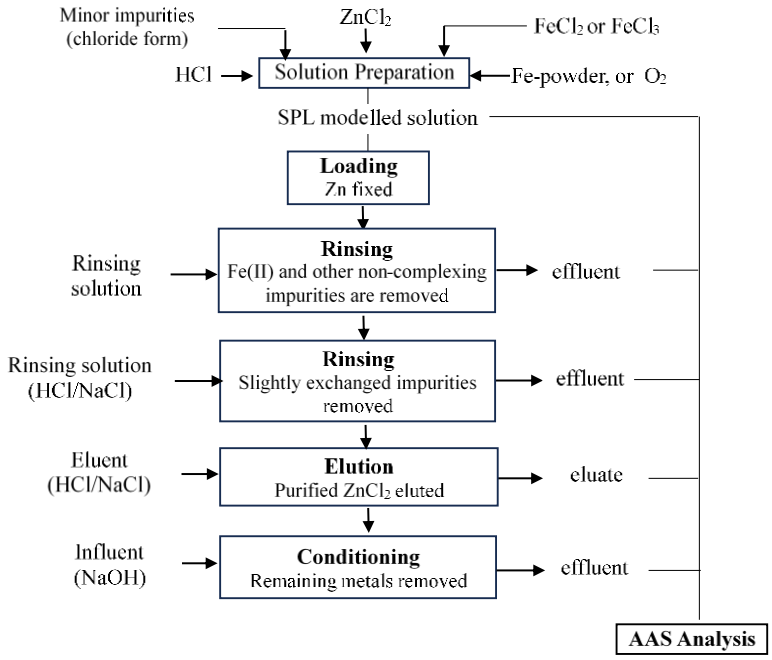

Fig. 3.4 The conceptual scheme of anion exchange purification of a SPL model solution.

Cadmium, which has similar ion exchange distribution functions to Zn, can be treated by cementation or a pre-deposition step before electrowinning. The remaining impurity (Sn) can be retained in the resin during Zn elution.

3.2. Experimental investigation of the anion-exchange purification

Commercially available, strongly basic anion-exchange resins (Varion AD, or a practically corresponding Varion AT660 type Nitrokémia Co., Hungary) were used, which followed the common international standards (e.g. Dowex-1, DIAION SA10A, etc.). It was based on a polystyrene matrix, cross-linked with the appropriate amount of divinylbenzene, and the functional groups were quaternary ammonium attached.

3.2.1. Equilibrium anion-exchange examinations in NaCl solutions

To devise a reliable anion-exchange separation for preparing a pure $ZnCl_2$ electrolyte from SPL, the characteristics of the equilibrium distribution of Zn, Fe and the practically important impurities must be known as functions of the Cl^- concentration. It is of economic and environmental relevance to apply NaCl in the possible steps of the procedure instead of HCl. The NaCl background is anyway inevitable in the purified solution prepared for the electrowinning of Zn, as setting the controlled pH would require a preliminary hydrolytic precipitation by neutralization, applying NaOH. The difference in the physico-chemical properties of the salt solution from those of the HCl background influences the anion-exchange distribution

characteristics of Zn. It has been suggested by earlier results presented in Figs. 3.2 and 3.3. Although the behaviour patterns were the same, the HCl background provided appreciably higher anion-exchange sorption as compared to the salt ($FeCl_2$) background. Therefore, determining the anion-exchange distribution in NaCl solutions required additional experimentation for the most important cases (Zn and Fe) in the 0 – 5M NaCl solutions, physically compatible with the anion-exchange chromatography. Higher salt concentrations would cause difficulties due to the high density and viscosity of the solution fed into the resin bed. A significant difference is still expected in Zn and Fe behaviour patterns. The new distribution functions were determined by using the batch equilibration method, generally accepted as the most accurate. According to the known distribution functions in HCl (Fig. 3.1) [60] [97], and the thermodynamic simulation results (Fig. 3.3), Fe(II) is not capable of forming anionic chloro-complexes in the practical range of chloride concentration. However, imperfect preliminary reduction or subsequent oxidation may cause the presence of ferric species, which would interfere with the separation of Zn devised for Fe(II) in HCl solutions. Actually, the contact with air is highly likely to turn the equilibrium in favour of the Fe(III) species, as shown by the thermodynamic simulation results in Fig. 3.3.*b*. Therefore, the establishment of the anion-exchange behaviour for Fe(III) in the NaCl solutions has been of considerable interest. Further, if the presence of Fe(III) cannot be avoided anyway, a different approach to the Zn/Fe separation would be also possible with a scheme of separation focusing on the Fe(III) state in the solution, thereby omitting the cumbersome preliminary reduction and the sealing of the system to exclude ambient air. A procedure under air contact is always more practical. The scheme previously outlined in Fig. 3.4 allows both approach.

The Zn and Fe chloride salts were dissolved to prepare the stock solution of 2000 mg/dm^3 Zn and Fe concentrations. A few drops of HCl were added to avoid hydrolytic precipitation. Aliquots of 10 cm^3 from the stock solution were filled up with distilled water to 100 cm^3 to prepare 200 mg/dm^3 concentrations of the examined element, and crystalline NaCl was added as required to set the required free Cl^- ion concentrations (e.g. 0; 0.5; 1; 2; 4; 5 M). Samples of 10 cm^3 resin and 25 cm^3 of the prepared solution were contacted for 1 hour. A horizontal shaking machine was used at the suitable frequency to thoroughly mix the two phases. After equilibration, the solution was quickly filtered and diluted for atomic absorption spectrometry (AAS). The

equilibrium distribution coefficients (D) were computed from the analytical results as described in Eq. (3.1). Figure 3.5. shows the equipment used for the determination.

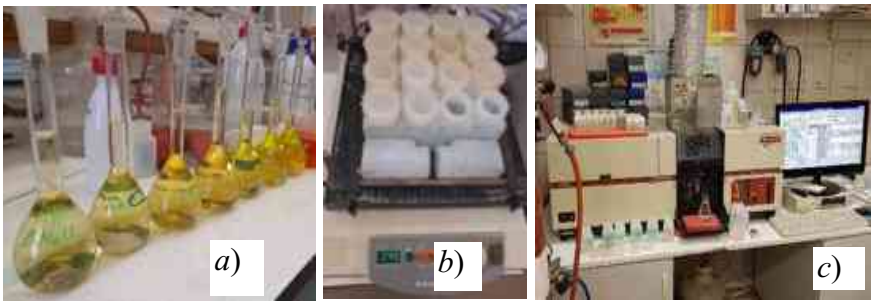

Fig. 3.5 The equipment used for the distribution studies with (a) flasks of varied solution concentrations, (b) mechanical shaker, and (c) AAS instrument.

The fundamental distribution data referring to the practically important elements as functions of the free HCl concentration, shown in Fig. 1, can be applied for devising the anion-exchange separation procedures. Further investigation was justified by the possible difference if the HCl background is changed for NaCl. It may have importance in the cases where distribution coefficients are not negligible. Therefore, the anion-exchange distribution of Zn and the major impurity in the Fe(III) state have been determined as functions of the added NaCl concentration, shown in Fig. 3.6.

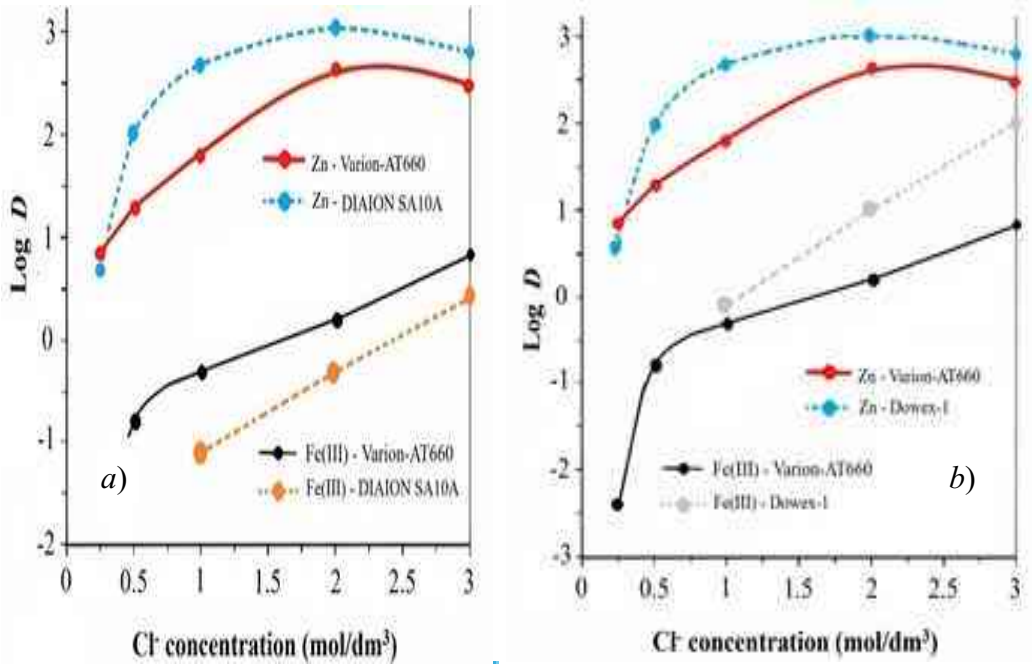

Fig. 3.6 The anion-exchange distribution functions determined for Zn and Fe(III) in NaCl solutions (solid lines) with Varion AT660 resin, and earlier results [60] [97] in HCl solutions with Diaion SA10A (a) and Dowex-1 (b) resins (dashed lines).

The results obtained with NaCl are consistent with those obtained in the HCl solutions, however, the higher activity coefficients in the HCl medium enhances the anion exchange by promoting the formation of the chloro-complex species. Even though there is only a weak sorption for Fe(III) at the Cl^- ion concentration where the Zn sorption is strong (~ 1.5 M Cl^-), the separation can hardly be perfect. A level of log$D$ = 0, still means an equal distribution of Fe among the two phases, and the Fe(III) distribution function rises rapidly with further increasing the Cl^- concentration. The conditions of separation can be improved by reducing the iron content to Fe(II). As seen in Figs. 3.2 and 3.3, the divalent iron may only start to be sorbed appreciably in the resin at approximately 8 M Cl^- concentration. The reduced state is more suitable for direct purification of the SPL. However, even as low a distribution as log$D$ of -1, would mean ~ 10 % of the Fe(II) still be retained in the resin. Thus, a perfect separation, allowing the production of a virtually Fe-free solution can only be achieved by the chromatographic technique.

3.2.2. Determining the actual exchange capacity

The targeted strongly basic anion-exchange was the Hungarian made Varion AT660 type, available also in hour laboratory. The strongly basic (salt-splitting) capacity of the fresh resin in the chloride form was measured by determining the amount of NaOH liberated after complete regeneration. The prepared resin of 10 cm^3 was fed into the test ion-exchange column and transformed into the hydroxide form with 750 cm^3 of 2M NaOH, applying a high flow rate that the column could allow (approx. 30 bed-volumes/hour – 30 BV/h). The procedure was followed by rinsing with 1000 cm^3 of water and 250 cm^3 of 5% NaCl, from which 250 cm^3 effluent was collected. Subsequently, three times 50 cm^3 of the collected eluate was accurately taken to be titrated with 0.1 M HCl to determine the amount of the eluted OH^- ions. Methyl red was applied as an indicator. The neutral salt-splitting capacity (NSSC) was then calculated according to the equation below:

$$\text{NSSC} = \frac{\text{titre of 0.1 N HCl} \cdot (\text{factor of HCl}) \cdot 0.1 \cdot \frac{250}{50}}{10} \tag{3.7}$$

The apparatus set up for this experiment can be seen in Fig. 3.7.

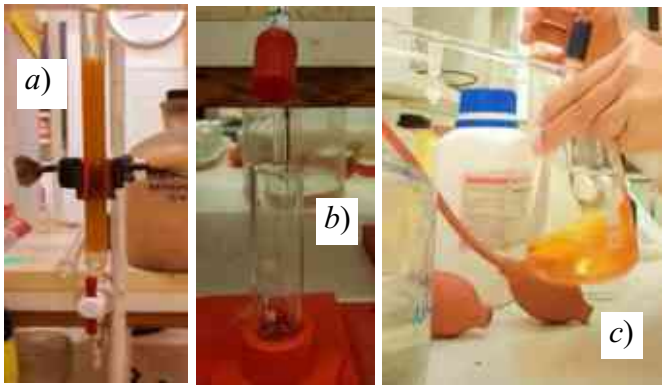

Fig. 3.7 Simple setup for the determination of the exchange capacity with the AIEX column (a), measuring flask (b), and the titration tools (c).

The strongly basic exchange capacity (C) of the resin was found as 1.39 mmol/cm^3, referring to the wet volume. To have a desired degree of saturation (S) in the resin bed, the volume of the starting solution V_s should be:

$$V_s = \frac{S\ C\ V_r}{z\ c_{Zn}} \tag{3.8}$$

where $c_{Zn}$is the zinc concentration in the loaded solution, V_r is the volume of the resin bed, and z is the average charge of the anionic complex species. It can be derived from the slope analysis of the distribution function of Zn [61]. In the separation experiments, basically the oxidized conditions determined by the air contact and the stable Fe(III) state was applied. The reduced Fe(II) state would mean a more efficient Zn/Fe separation, but also a technically more complicated system to use.

3.2.3. The first scheme of anion-exchange chromatographic separation

In order to examine a practical separation by anion-exchange chromatography, a model solution containing 300 mg/dm^3 of the studied metals Fe, Zn, Sn each in 2.5 M NaCl was applied, where a strong sorption of Zn is expected. The solution was slightly acidified to avoid any danger of hydrolytic precipitation. The necessary amount of a strongly basic anion-exchange resin was first physically purified and then conditioned to assure the chloride form. A portion of this resin was used for the actual determination of the fundamental anion exchange capacity, as described above.

The prepared resin in the chloride form was fed into the glass column with an inner diameter of 2.5 cm to a height of approx. 25 cm, thus providing a resin bed of ~ 110 cm^3 of volume. The chromatographic setup of continuous procedure is shown in Fig. 3.8.*a*, as opposed to a simple mixed reactor in Fig. 3.8.*b*, used for batch operation.

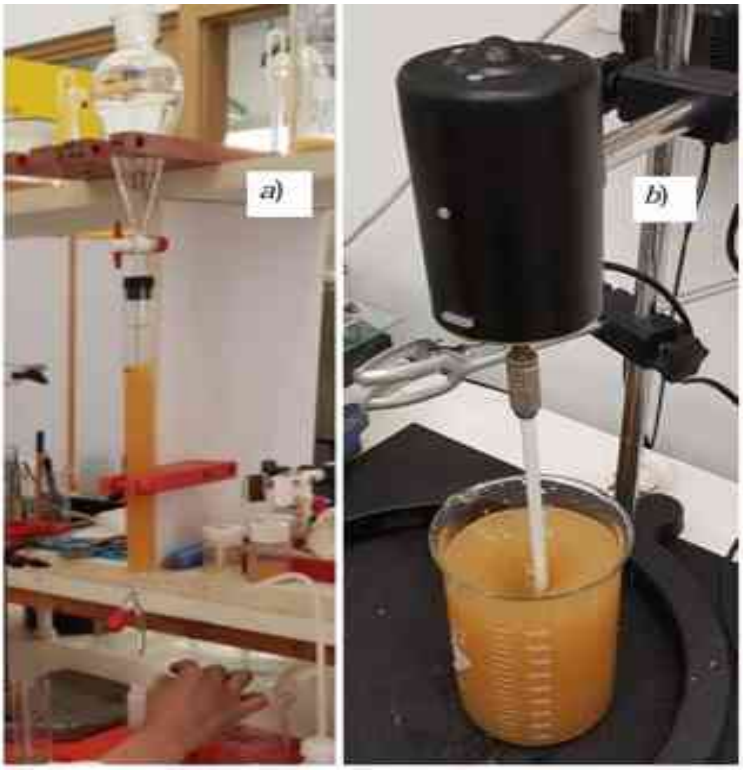

Fig. 3.8 The anion-exchange equipment used for chromatographic method (a), as compared to a simple batch (b) arrangement.

All the air was forced out from the part of the column below the glass frit filter serving as the bottom of the bed. After a short backwash, the column was gently tapped to assist in the formation of a stable, densely packed resin bed. The flow rate was set lower than the practically applied 1-3 bed volumes per hour (BV) speed to achieve better separation but still technically acceptable productivity. The preferred value was ~ 1.7 BV during the most delicate phases of the procedure, and at the latter parts of the rinsing steps, it was raised to 2 ~ 2.5 BV.

The procedure was started by loading 250 cm^3 blank solution of pH 1, and 2.25 M NaCl to the column to set the chloride ion concentration to the starting value in the void fraction of the bed and equilibrate the conditions of the resin. It was followed by loading the prepared solution (250 cm^3) of the same NaCl concentration but containing the examined metals, too. The subsequent rinsing step was divided into two segments, Rinsing-I and rinsing-II. First, 150 cm^3 of 2.25 NaCl was used to finish the removal of Fe(II) from the column. It was followed by feeding 150 cm^3 of 0.75 HCl consecutively. The second rinsing served checking purposes, showing if any Fe(III) had been in the resin retarded by the previously applied relatively high chloride concentrations. To remove Zn, elution-I was carried out with 250 cm^3 of 0.05 HCl,

followed by elution-II with 150 cm^3 of 2 NaOH. The second elution was included for checking if zinc and tin remained in the resin after the relatively short first elution step. The rinsing with NaOH, as the final step, also served to condition the resin, after which the column can be used again for another batch of the SPL to be purified. Effluent solution samples (10 cm^3 each) were collected regularly at set intervals to be analysed by AAS. Figure 3.9 shows the flow chart of the anion exchange process.

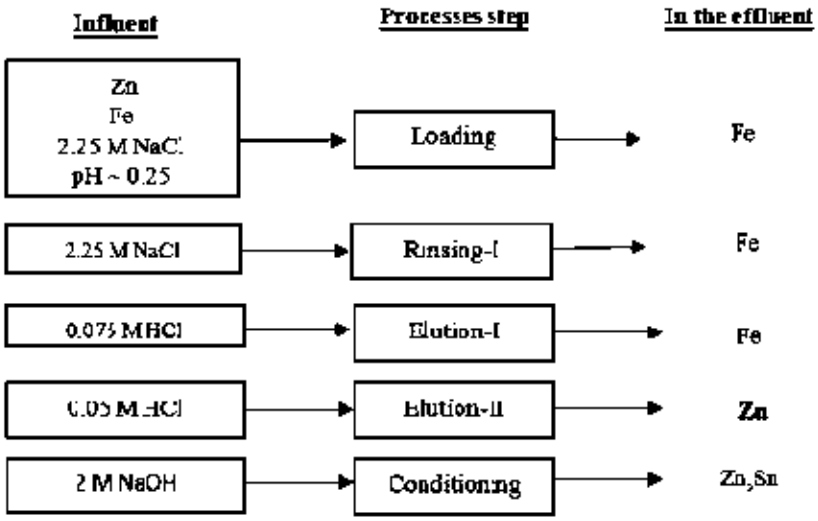

Fig. 3.9 The basic anion exchange separation in the SPL with NaCl-HCl solutions effecting the separation of Fe and the practically important minor impurities.

Iron, being in the oxidised Fe(III) state was not completely removed in this first approach before zinc was eluted, and the Zn-elution was inefficient, offering a relatively low recovery and leaving too much of the targeted element behind for the conditioning step. Therefore, the procedure needed improvement, and nickel had to be included in the model solution, to represent, on the one hand a practical impurity and, on the other, an element of reliably rejected by the resin at this low Cl- ion concentration in the background.

3.2.4. The second scheme of anion-exchange chromatographic separation

The resin was physically purified and then conditioned in the chloride form, then fed into the glass column as described above and the procedure started according to the scheme shown in Fig. 3.10. The flow rate was set at 1.5 ~ 1.7 bed volumes per hour (BV), lower than the 3 BV usually applied value in practice, to enhance separation but still allow a technically acceptable productivity.

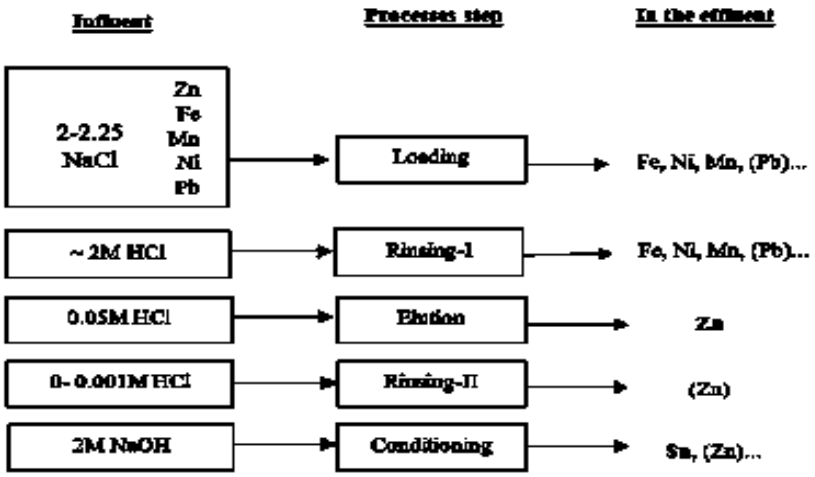

Fig. 3.10 A possible method for the anion exchange purification of Zn in HCl solutions effecting the separation of Fe and the practically important minor impurities.

As a major difference, the loading solution in this case contained HCl to provide the free Cl^- ions for the necessary chloro-complexes of Zn to be formed. The preliminary treatment of the fresh resin was also carried out with the corresponding HCl solution. After the delicate steps, the rinsing flow rate was raised to ~ 3 BV. Effluent samples (10 cm^3 each) were collected regularly during the procedure.

3.2.5. The experimental setup of chromatographic separations

The liquid level in the chromatographic columns – of the dimensions given above - was kept at approx. 3 cm higher than the resin bed. It prevented any disturbance of the top layer as the influent solution was fed drop-by-drop from the overhead vessel, avoiding also any accidental inclusion of air bubbles. Glass beads were placed on the top of the resin, separated by a layer of glass wool to prevent the floating of the resin when denser solutions were fed. Operating conditions can be seen in Fig. 3.11.

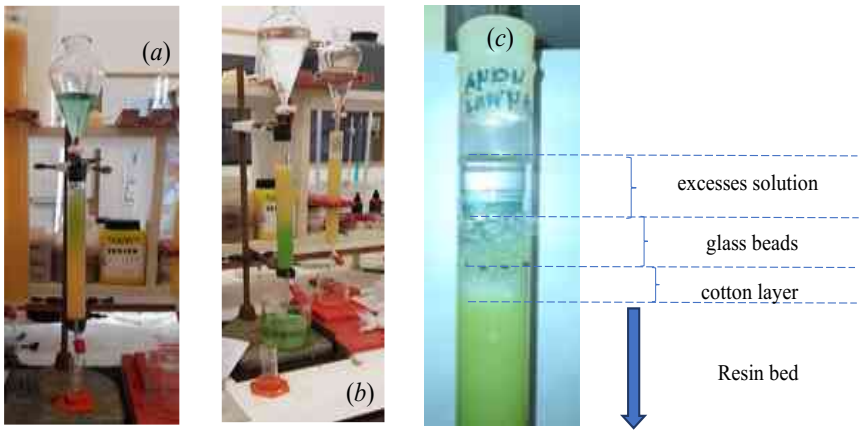

Fig. 3.11 The loading (a) and the rinsing (b) stages of a chromatographic separation process, and the arrangement of the upper part of the resin bed in the column(c).

During the critical phases of the procedure, the flow was can be set lower than usually applied to achieve a better separation but still maintain a technically acceptable productivity. The lowest value was ~ 1 BV/h during the most delicate phases of some experiments, but even then, it was raised to the normal ~ 3 BV/h for the later parts of the rinsing steps. The composition of model solutions containing Zn, Fe, and other impurity elements was as specified in Table 3.2.

Table 3.2 Composition of the loaded solutions

Cl^- (M)	Zn (g/dm^3)	Fe(II) (g/dm^3)	Other impurity elements (mg/dm^3)						
			Mn	Ni	Sn	Cu	Al	Pb	Co
6.5	25	140	~ 500	~ 500	~ 500	~ 500	~ 500	~ 500	~ 500

The procedure was started by loading 100 cm^3, 2 M HCl blank solution to the column to set the Cl^- ion concentration to the starting value in the void fraction of the bed. It was followed by loading the prepared solution (100 cm^3) of the same free Cl^- ion concentration but containing the metals too. In the rinsing step, 200 cm^3 2M of NaCl was applied to remove all the Fe(II) from the column. Elution of Zn was carried out by slightly acidified solutions, containing low concentration (0.05 – 0.2 M) HCl. The conditioning step was devised to remove the residual strongly sorbed elements with 300 cm^3 of 2M NaOH. Effluent solution samples (10 cm^3 each) were collected regularly at fixed intervals to be analysed by AAS.

3.2.6. The experimental setup of the batch anion-exchange separation

In order to simplify the procedure and to avoid the intermittent waste solutions of transient compositions, the batch anion exchange technique has also been examined. The process was carried out in a 250 cm^3 glass beaker and with the same loading solution but here only of 100 cm^3 volume as used in the chromatographic approach. The prepared resin batch was of 75 cm^3, and the stirring speed was adjusted to homogenize the slurry, but not breaking the resin beads. The five consecutive process steps used in the chromatographic procedure were also included in the batch process. In the loading and Elution-I stage, 1 cm^3 of solution samples were taken every 10 minutes and diluted with 10 ml distilled water prepared for the AAS test. After each process step, the resin was decanted and rinsed. The first rinsing process was completed with 2 M HCl after one-hour loading, followed by elution with 0.02 HCl and distilled water rinsing process consecutively. In the final stage, 2M NaOH was added to the decanted resin to check the remaining metals in the resin.

3.2.7 Examining the breakthrough volumes in the chromatographic setup

Since the main objective was to obtain a pure Zn electrolyte with an efficient recovery rate, the determination of the breakthrough volume (BTV) was essential. It shows the maximum volume of the influent solution with which the resin bed can still retain the specific ions. It essentially depends on the capacity of the resin bed and the average charge of the sorbed species. However, the flow rate of the solution should allow sufficient time for the exchange reaction to take place. The BTV for the non-sorbed Fe(II) species may occur when the effluent volume reaches the sum of the void space in the resin bed (usually ~ 40%) and the - ideally negligible - extra "dome volume" under the bottom of the bed. In this case it indicates an efficient rejection by the resin bed. The practical break-through properties have been determined with various Cl^- concentrations and flow rates (BV/h) of the loaded solution. the results can be used for adjusting the practical parameters of the purification process. The model SPL solution was prepared by dissolving the relevant chlorides in water and adding some HCl for hydrolytic stability. Further, NaCl was added to set the Cl^- ion concentration in the loaded solution. The added Fe was reduced to the Fe(II) state to provide a wider gap relative to the distribution function of Zn. The composition of the basic model solution containing Zn, Fe, and some minor impurities are specified in Table 3.3.

Table 3.3 Composition of the stock solution used for the break-through experiments.

Cl^-	Zn	Fe	Other contaminants (mg/dm^3)					
(M)	(g/dm^3)	(g/dm^3)	Mn	Ni	Sn	Cu	Al	Pb
7	30	150	~ 500	~ 500	~ 500	~ 500	~ 500	~ 500

The resin in the chloride form was filled into the column used for all the chromatographic separation experiments. A test solution of 100 cm^3 volume and pH 0.24 M was loaded into the column continuously. After every 10 cm^3 outflow, 1 cm^3 of effluent was collected periodically for analysis. This procedure was repeated for the solution with an extra 2M HCl included or neutralized. The same method was applied for various flow rates (2, 4, 8 BV/h) and Zn concentrations of 40 and 80 g/dm^3. Table 3.4. summarized the examined variable during the determination of breakthrough volume.

Table 3.4 The settings for the determination of breakthrough volumes

Loaded volumes	Composition modifications	BV/h
100 dm^3	-	1
	neutralized	1
	+ 2 M HCl	1
	-	2
	-	4
	40 g/dm^3 Zn	1
	80 g/dm^3 Zn	1 2 4 6 8
	20 g/dm^3 Zn	6 8
500 dm^3	40 g/dm^3 Zn	1 4

4. The optimization of the SPL purification by anion-exchange

4.1. The results of separating Zn and Fe by anion-exchange

4.1.1. Basic separation by chromatography

The anion-exchange procedure designed according to the equilibrium distribution functions could practically separate Zn and Fe directly at the loading stage. The method and the results of this purification process are shown in Fig. 4.1.

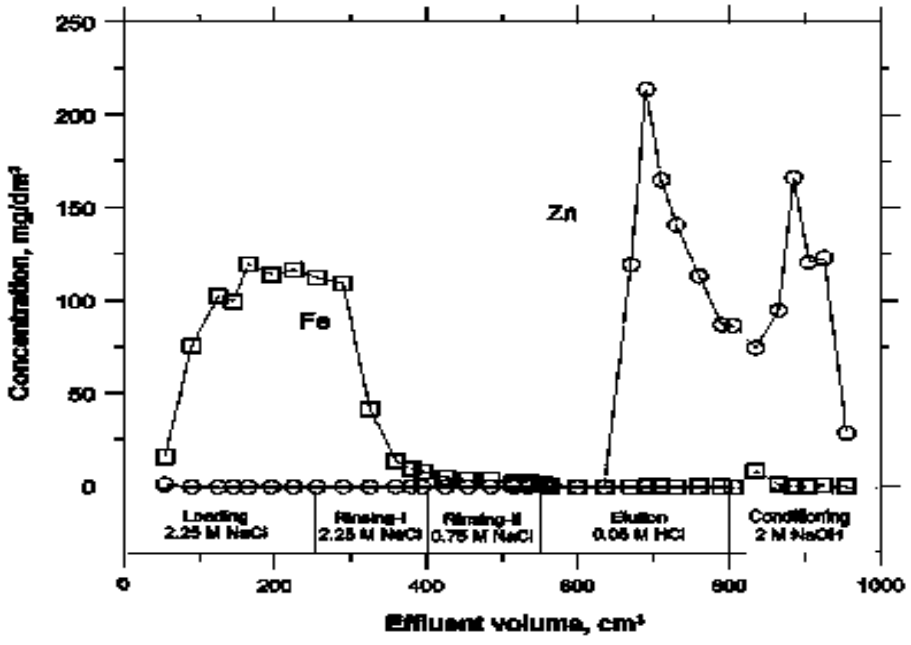

Fig. 4.1 The separation of Fe and Zn by anion exchange chromatography (3 BV/h).

This initial chromatographic experiment was carried out with only NaCl applied as the source of the free Cl^- ions. The loaded solution contained only the main elements (Zn and Fe), both at very low concentrations, so as to see the clear elution peaks certainly corresponding to the clean effects of the differences in the equilibrium distribution properties, not interfered by the practical effects f saturating the capacity of the resin bed.

Zinc was completely fixed in the resin from the 2.25 M NaCl-loaded solution. No leakage could be observed during the loading and neither during the subsequent rinsing steps, which continued with the same NaCl background. It indicated that this Cl^- ion concentration – provided by the NaCl background – was safely enough to stabilize the negatively charged chloro-complex zinc species, and not too high to cause a competition of the still free Cl^- ions for the active sites of the anion-exchange resin. Even a relatively high flow rate, as here and afterwards generally kept at ~3 bed volumes/hour (BV/h) could be applied for a visibly clean separation. The resin practically rejects iron in its divalent form at the Cl^- concentration applied. However, some tailing of the main Fe elution peak could be seen during the rinsing with the relatively high NaCl concentration in the influent. Therefore, a small portion of Fe was only removed from the column in the subsequent stages, causing a slight contamination of the Zn effluent. As suggested by the different distribution curves of iron in the different oxidation states (Fig. 3.3), this iron portion might be trivalent, which had not been fully reduced before the loading step or inadvertently oxidized during the solution preparation.

In case of a special need to eliminate the – still almost negligible - Fe-contamination, the preliminary reduction should be more complete and the first two stages of the separation should be carried out under a protective atmosphere (N_2) to exclude the formation of any Fe(III) species. Also, the first rinsing step can be extended. As no leakage of Zn was observed during the first two steps, applying a slightly lower initial Cl^- concentration may also be beneficial in this respect. An arrangement of a sealed anion-exchange chromatographic system excluding ambient air is schematically presented in Fig. 4.2.

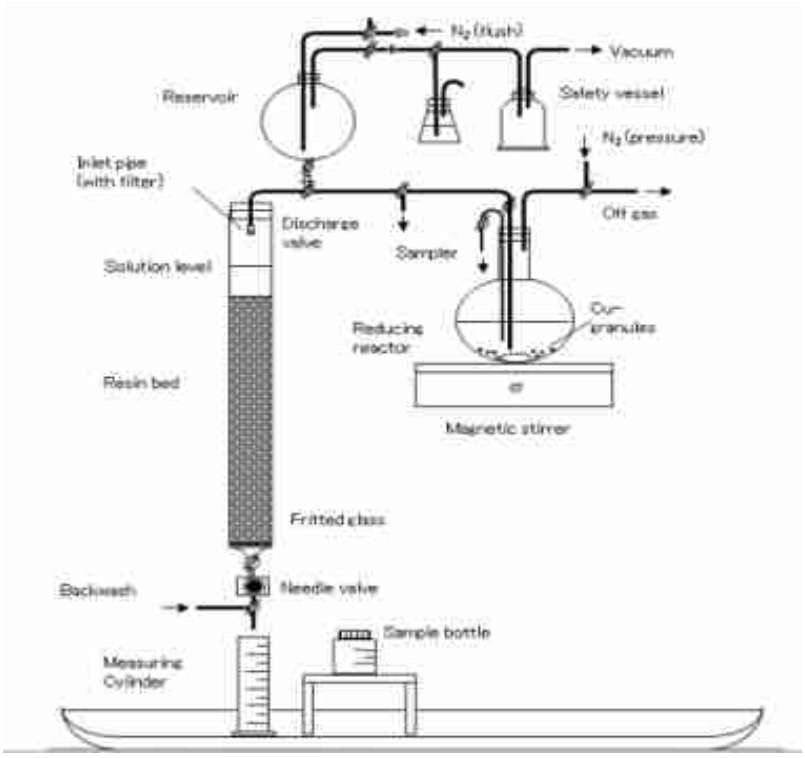

Fig. 4.2 A chromatographic system providing reduced conditions for the separations.

The elution of Zn was carried out by a solution of 0.05 HCl fed into the column. It could be expected by the relevant distribution curves plotted in Fig. 3.2 and 3.7 to be efficient in decomposing the chloro-complex anions of Zn. The addition of 0.05 M HCl served just to maintain a slight acidity thereby avoiding any hydrolytic precipitation. Although the elution peak of Zn appeared sharp, a significant tailing also occurred, and the removal was incomplete with applied eluent. Much of the zinc was probably still locked in the column because of still strong chloro-complexation or some starting hydrolytic precipitation in the resin bed.

4.1.2. Extended separations by chromatography

In a further separation experiment, high concentrations of the main elements (Zn and Fe) were used, and Mn, Ni were added as minor, but practical impurities. Also Pb was added to test the behaviour of a practically negligible impurity that has a similar anion-exchange tendency as Zn. Due to the almost missing formation of chloro-complex anions of Mn and Ni [100], these impurities are confirmed to be separated from Zn together with Fe during the loading and rinsing steps. The corresponding concentration points of these two minor impurities coincide in Fig. 4.3. On the other hand, due to the analogous anion-exchange distribution functions (Figs. 3.3), Pb cannot be separated from Zn by this method, despite the different maxima of the distribution

functions. The separation of Pb impurity – if ever it exists beyond the usually negligible level - would require different techniques, such as selective precipitation or selective solvent extraction [95]. Due to the high salt content by the main elements, in this separation the free Cl^- ions were provided by the added HCl instead of NaCl.

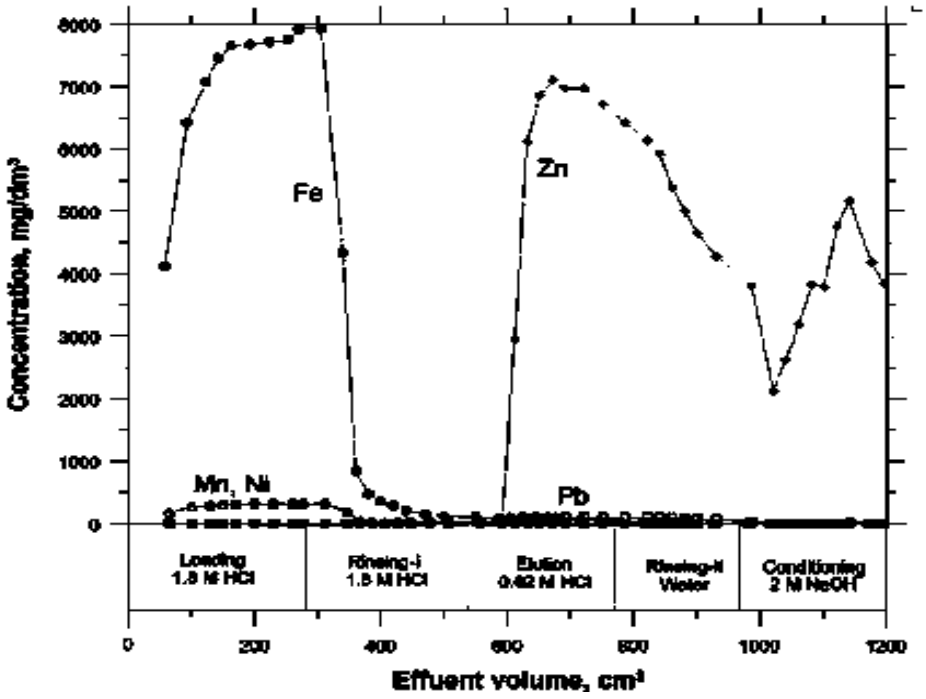

Fig. 4.3 Elution curves of the extended anion exchange chromatographic separation.

Despite decreasing the HCl concentration in the eluent, the elution peak of Zn became even wider, showing a broad declining section (a long tailing). It indicates the known preferential retention of HCl by the resin [61], causing a rise in the pH of the aqueous phase and some partial precipitation in the hydroxide form. Thereby a relatively dilute eluate can be obtained. Thus the lower HCl concentration in the eluent rather hindered the elution of Zn. As a confirming step, NaOH was also used to show that the portion of Zn entrapped physically as fine crystals in the resin bed is removed with the alkaline influent in the zincate form. The efficiency of a pure Zn elution can be improved by carefully adjusting the addition of acid (as HCl, to avoid different anions, especially sulphates for a clean electrowinning afterwards). Higher concentration than the tested 0.05 M level could not be either efficient because of the early start of the formation of the anionic Zn chloro-complex species (Fig. 3.2). The feasibility of an excellent cathodic deposition may require a minimum of 10 ~ 15 g/dm^3 Zn concentration in the chloride electrolyte [72]. Therefore, if the Zn elution cannot provide this level, evaporation of the eluate should also be included to provide a suitable electrolyte.

The chromatographic separations justified the feasibilities of the separation procedures devised according to the equilibrium distribution functions in solutions of free Cl^- ions provided by either HCl or NaCl. The distribution functions of Zn and the practically important impurities offered enough differences. However, the rinsing procedures produced relatively large partial volumes of effluents, and the elution of Zn ran into physical difficulties. In order to remedy these practical difficulties, a version of separation by the batch anion-exchange method has also been carried out. As a further advantage, the separation could be made simpler and faster. The two experimental setups can be seen compared in Fig. 3.9. The batch procedure includes the mixing of the solutions with the resin in a suitable vessel and decantation (or more precisely) a filtration to separate the two phases after the required time of contact in each step. It is quite similar to the solvent extraction technique, but in this case the separation of the aqueous and organic phases is far simpler, faster, and more accurate. Applying similar settings of free Cl^- ion concentrations – provided by the added HCl - as used in the optimized chromatographic procedure, Fig. 4.4 shows the concentration profiles obtained with the batch technique. In this case samples of the solution were taken periodically, thus the kinetics of the exchange process can be observed. It is clearly seen that Zn is retained in the resin quickly after the solution is in contact with the resin in the stirred vessel.

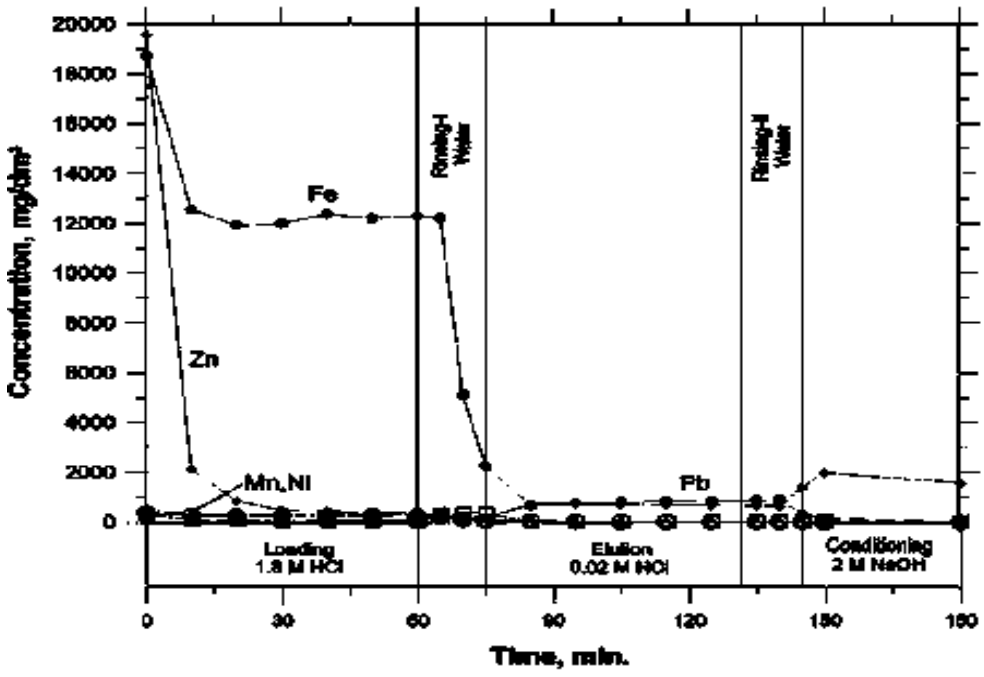

Fig. 4.4 Solution concentration changes during the batch anion exchange separation.

It can be seen that almost all the Zn is transferred to the resin from the solution in approx. 30 minutes. This kinetic condition also needs to be considered in setting the flow rate through the loading of the anion-exchange chromatographic column. This is the actual limitation of the production efficiency of the chromatographic, and also the batch ion-exchange procedures. Generally, the ion-exchange sorption of a species implies a multi-step process: (i) transport from the bulk solution, (ii) diffusion across the liquid film around the resin beads, (iii) diffusion in the liquid contained in the resin pore to the wall, (iv) transfer through the interface, and (v) chemisorption in the resin. In the case of vigorous mechanical stirring, usually, the first step has negligible influence on controlling the overall sorption rate. Desorption can follow the reverse order. As seen in Fig. 4.4, the ratio of sorbed Zn species rises rapidly with contact time. The decrease in the concentration of the sorbable species in the solution and the growing occupation of the active sites in the resin phase results in the slowing of the sorption process until equilibrium is reached. In the case of chromatographic operation, an early break-through of the sorbed species may appear in the effluent if this time is not provided for the species to stay in contact with the resin bed in the column, due to increased flow rates.

At the first glance, it may be surprising to see the iron concentration dropping in the reduced solution initially. However, it may be justified by the equilibrium distribution function of Fe(II) in Fig. 3.2, showing that at the applied free HCl concentration, the log$D$ ~ -1 value implies that the equilibrium iron concentration in the resin may reach a level of approximately a tenth of that in the solution. This Fe portion may be retained if the total exchange capacity of the resin allows it. There is no chromatographic effect of a mobile aqueous phase, displacing the weakly sorbed Fe species by the mobile Zn species arriving at the same site. In addition, the possible partial re-oxidation of Fe(II) in the unprotected stirred vessel may increase the total ratio of sorption in the Fe(III) state. Thus, the separation of iron cannot be so efficient with the batch technique as with the previously described ion chromatography. The average charge of the zinc chloro-complex anions can be approximated in the -1 to – 2 range according to published results [61]. It corresponds to the highest coordination number of 4, with a tetrahedral arrangement of the ligands. With more Zn in the solution than the capacity of the resin batch can sorb, the strongly sorbed Zn chloro-complex anions may displace virtually all the slightly sorbable Fe species. It implies a lower efficiency of

utilizing the Zn content in the prepared solution batch., but in return, the resin batch separated from the residual solution will only contain the strongly sorbed Zn species. After the elution step, a high purity of the Zn eluate can be expected.

In this experiment neutral water was used to rinse the resin after the loading solution was drained. It is interesting to see the previously sorbed iron quickly released from the resin, as shown by the first concentration point. Then, the analytical samples indicate a rapid decrease in its concentration, evidently due to hydrolytic precipitation. It also indicates that during the stirring in the open vessel, most of the Fe(II) is oxidised to the Fe(III) stat, which is prone to early hydrolysis. In the same way, however, the stronger sorbed species of Zn can also suffer precipitation even before being released from the resin phase. It may have consequences for their capability of eluting. The elution of Zn under the conditions presented in Fig. 4.4 clearly failed in the batch process. The sorbed Zn species were not removed by the eluent, acidified to 0.02 M HCl concentration. It should have initiated thee decomposition of the sorbed chloro-complex species, but the previous neutral water rinsing possibly converted them into a hydroxide precipitate even inside the micro-porous resin beads. The in situ precipitated Zn still in the resin could not react efficiently even to the NaOH solution applied in the end of the procedure.

This experience explains why the elution peak of the Zn in the chromatographic procedure showed increasing tailing by strongly decreasing the HCl concentration in the eluent. As higher HCl concentration would have been inefficient in the decomposition of the Zn chloro-complexes sorbed in the resin, a special eluent of different nature can be looked for. The best practice is to change the Zn into a cationic complex, resisting hydrolytic precipitation, rejected by the anion-exchange resin. It can be effected by applying another agent, e.g. ammonia [99]. In this case, applying close to neutral or slightly alkaline solutions would also keep the slight portion of initially sorbed Fe in the resin physically as a hydroxide precipitate.

4.2. Break-through analysis

The breakthrough volume (BTV) has been examined as a function of various factors to determine the possible ways of optimization. The Zn species at this free Cl^- ion concentration may form mostly the highest tetrahedral complex ions of $x = 4$ coordination [101]:

$$Zn^{2+} + xCl^{-} = [ZnCl_x]^{2-x} \quad (4.1)$$

which will result in approximately -2 molar value of the resulting charge. Besides, the sorption of the additional impurity species may consume some of the capacity. In this case, only Cd and Sn could be preferentially sorbed by the resin [97] relative to Zn, but these impurities are present only at negligible concentrations. Thus, they could occupy just a negligible fraction of the available capacity. The species characterised by no sorption should appear in the effluent after passing the volume approximately equal to the void space fraction of the resin bed, which can be approx. 40% [102].

The effect of Zn concentration on the BTV of the SPL model solution is shown in Fig. 4.5. The volume of the examined effluent was equal to that of the loaded solution, as only the front edges of the developing concentration profiles were targeted. Adding a 100 cm^3 of the 80 g/dm^3 (most concentrated) Zn solution of 7 M NaCl, no breakthrough of Zn appeared within the same volume of the effluent. Due to physical discrepancies, some erroneous leakage of even the strongly sorbed species can occur. According to the practically negligible Fe(II) distribution [60] at the Cl^- concentration 7 M, no iron sorption can interfere with the purification of Zn. The non-sorbed species appear in the effluent around the expected volume corresponding to the inactive void space in the resin bed - and below it - in the column. The breakthrough curves of Fe(II) at different Zn concentrations, however indicate a slight sorption of also Fe(II), which is displaced by the preferred Zn species. Zinc is efficiently retained in the resin at the applied low flow rate, which allowed sufficient time for the exchange reaction. Iron breaks through soon, as expected and it is even slightly pushed forward as the Zn concentration is higher.

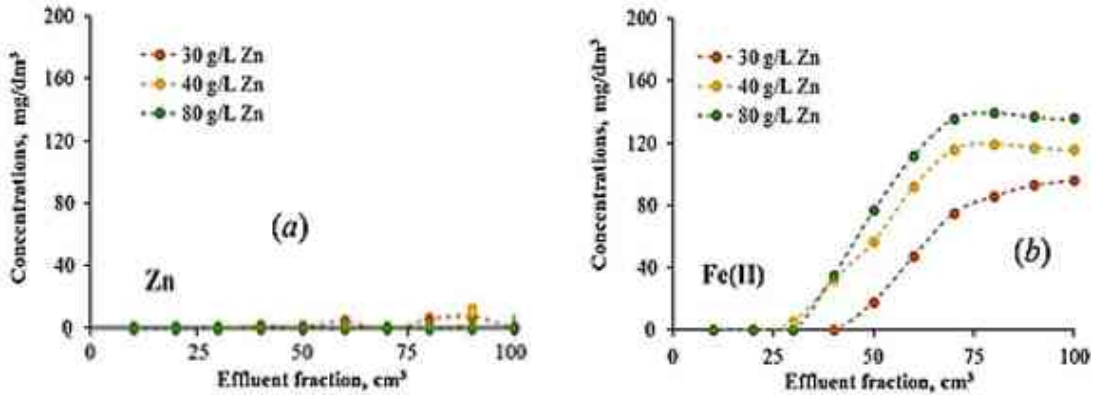

Fig. 4.5 The breakthrough curves of Zn (a) and Fe(II) (b) at varied Zn concentrations in the loaded solution (140 g/dm^3 Fe, 1 BV/h, pH 0.25, 7 M NaCl).

The flow rate of the mobile phase, expressed as bed volumes per hour (BV/h), is one of the factors affecting the separation process by ion-exchange chromatography. The flow rate determines the length of time the species in the solution can have a direct contact with the resin in the column. Some ions are faster, and others are slower exchanged, even if the equilibrium distribution coefficients are similar. Thus, the flow rate may affect the virtual exchange capacity and the separation of the elution peaks. Figure 4.6 shows the effect of various flow rates on the leakage characteristics of sorbed Zn species and the breakthrough curves of the non-sorbed Fe(II) species.

The internal diffusion in the pores and then in the material of the beads needs time before the species reach the exchange sites, and so do the Cl^- ions, which are liberated from the resin to the solution. A higher flow rate may spoil the separation, by not giving the species sufficient time to interact with the stationary resin phase. Higher flow rates may disperse the Zn sorption more towards the bottom of the column. The practically most important flow-rate tests were carried out at a relatively high (~ 80 g/dm^3) Zn concentration in the loaded solution. In this case, the added ~ 0.6 M HCl background and the included 2.5 M $FeCl_2$ salt supplied enough free Cl^- ions to form the anionic complex species of Zn, as Fe(II) is not forming chloride complexes unless the free Cl^- concentration is extremely high. Figure 4.6.*a* shows the leakage curve is sharper and appears earlier as the flow rate of the solution through the resin bed is increased.

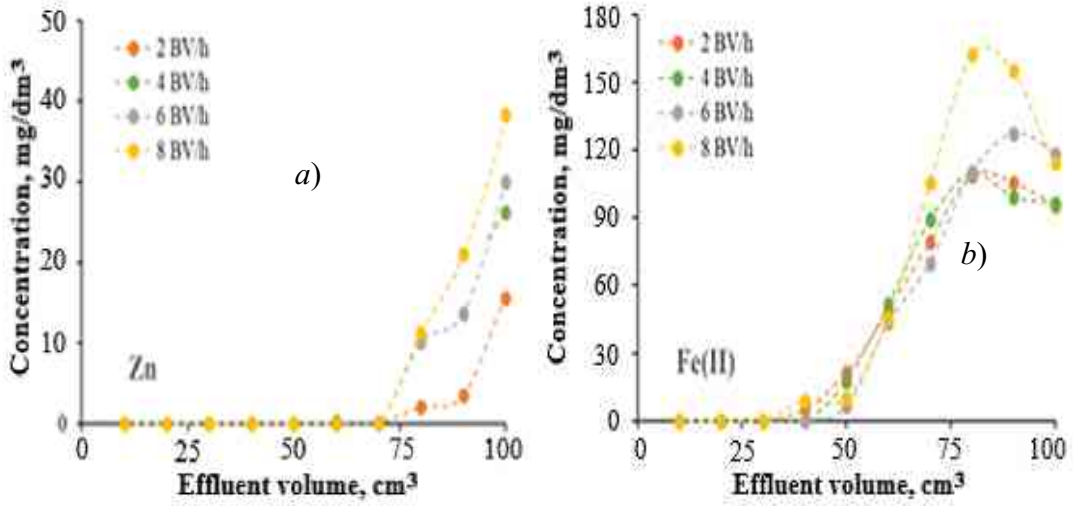

Fig. 4.6 Break-through of Zn and Fe(II) at varied flow rates (80 g/dm^3 Zn, pH 0.25, Fe 140 g/dm^3).

There was no break-through (or leakage) of Zn observed within this effluent range if the flow rate was set as low as 1 BV/h. The 110 cm^3 volume of the resin bed of the confirmed ~ 1.4 $mmol/cm^3$ specific exchange capacity, offering 154 mmol total capacity, could fix ~ 77 mmol Zn species of ~ -2 average charge, corresponding to 5 g Zn. This amount is carried by 63 cm^3 volume of the concentrated solution holding 80 g/dm^3 Zn. With the total inactive volume shown by the non-sorbed Fe(II) species of ~ 45 cm^3, shown in Fig. 4.7.*b*, the BTV of Zn could be expected only after collecting more than 100 cm^3 effluent. It could be so with the slowest (1 BV/h) flow rate, but, as shown in Fig. 4.7.*a*, the Zn leakage appeared earlier and sharper as higher flow rates were applied. Thus for a complete retention of the Zn during the loading step, the capacity of the resin and the average charge of the Zn species need to be respected, as shown above, and the flow rate should not be significantly higher than 1 BV/h. Higher flow rates would reduce the efficiency of Zn recovery, although, as suggested by Fig. 4.6.*b*, may enhance the removing of the practically non-sorbable impurities.

In some cases, the SPL does not contain more than 20 g/dm^3 Zn, which can be applied directly for the chromatographic anion-exchange purification. Figure 4.8 shows the breakthrough/leakage curves of Zn and Fe(II) obtained from experiments carried out with such a practical setting.

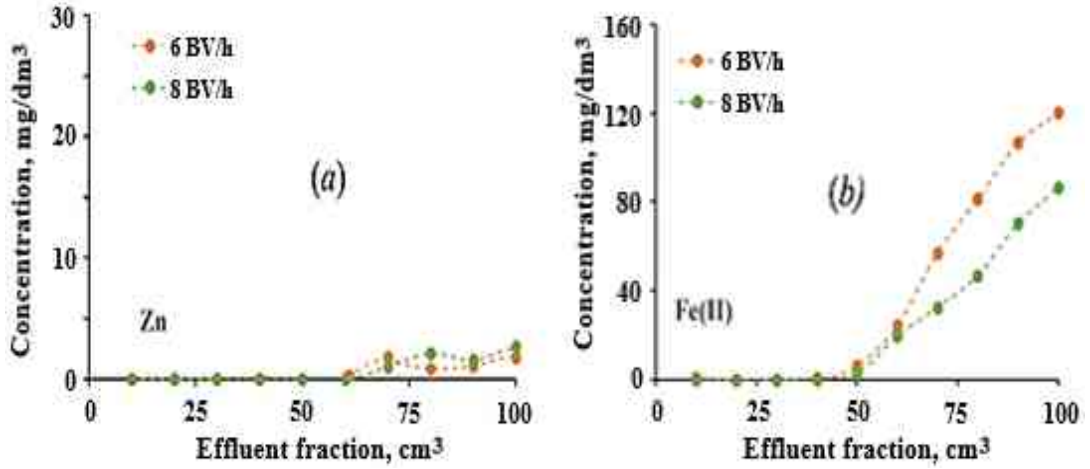

Fig. 4.7 The breakthrough/leakage of Zn (a) and of (Fe(II) (b) at different flow rates (20 g/dm^3 Zn, 140 $g/dm0^3$ Fe(II), pH 0.25).

The lower Zn concentration allows better Zn retention even at higher flow rates of loading. The actual capacity for Zn retention compared to the loaded amount of Zn was in large excess.

4.3. The optimised separation procedure and the complete results of separations

The model solution of the SPL loaded into the column was specified in Table 3.2. The major process steps, the fed influent solutions are described in Table 3.

4.3.1. The separation scheme

The most common concentration of Zn in the SPL can be used as the sampling concentration as well as the pH of common SPL. Figures 4.8 and 4.9 show the Zn and the impurities separation elution curves.

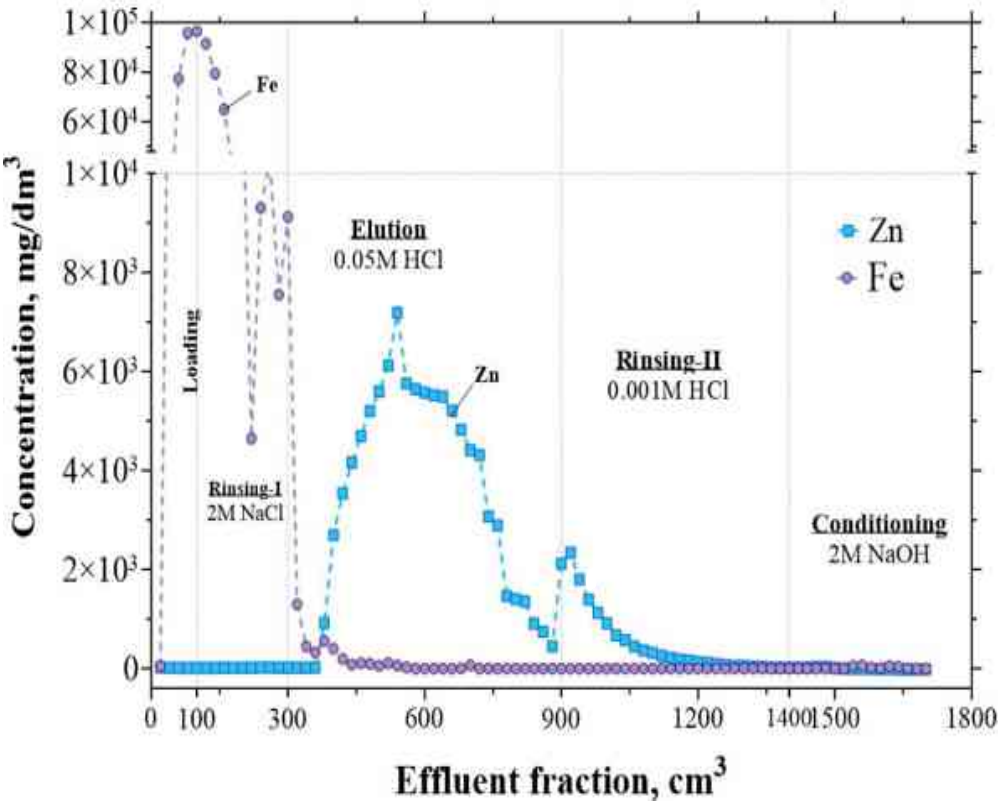

Fig. 4.8 The main elution curves of the SPL purification procedure (3 BV/h).

As also shown by the results of the initial chromatographic experiment, the loaded Zn was fully fixed in the resin from the loaded solution of 2M free NaCl. No leakage could be observed either during the subsequent rinsing step, continued with the same NaCl background. It indicated that this Cl^- ion concentration – provided by the NaCl background – was enough to stabilise the negatively charged chloro-complex zinc species. Meanwhile, virtually all the Fe passed through the column. The resin rejects iron in its divalent form in the relatively low Cl^- concentration applied. The elution process removed Zn by adding 0.05 HCl with more volume fraction. It could be expected to be efficient in decomposing the chloro-complex anions of Zn by the

distribution curve plotted in Fig. 3.7. Although a sharp elution peak of Zn appeared with the applied 0.05 M HCl eluent, a significant tailing also occurred, and the recovery – in the pure section of the eluate – needed some enhancement. Much zinc remained still locked in the column because of – probably - still strong chloro-complexation or some starting hydrolytic precipitation *in situ*. The broad peak of the elution curve for Zn inferred that a relatively dilute eluate could be obtained. Therefore, a second step of elution with 0.001 M HCl was added to push out the remaining Zn from the resin. Again, a sharp secondary peak followed by a broad tail curve, indicating that the reason of strong tailing in the first peak was the incomplete decomposition of the sorbable Zn chloro-complex species. Practically all the Zn can be removed with this enhanced elution step. The procedure was repeated by adding also the minor impurities in the loaded solution. Figure 4.9 shows the complete separation characteristics by the multiple elution peaks. The logarithmic scale of the concentration axis allows to see even the minor peaks clearly.

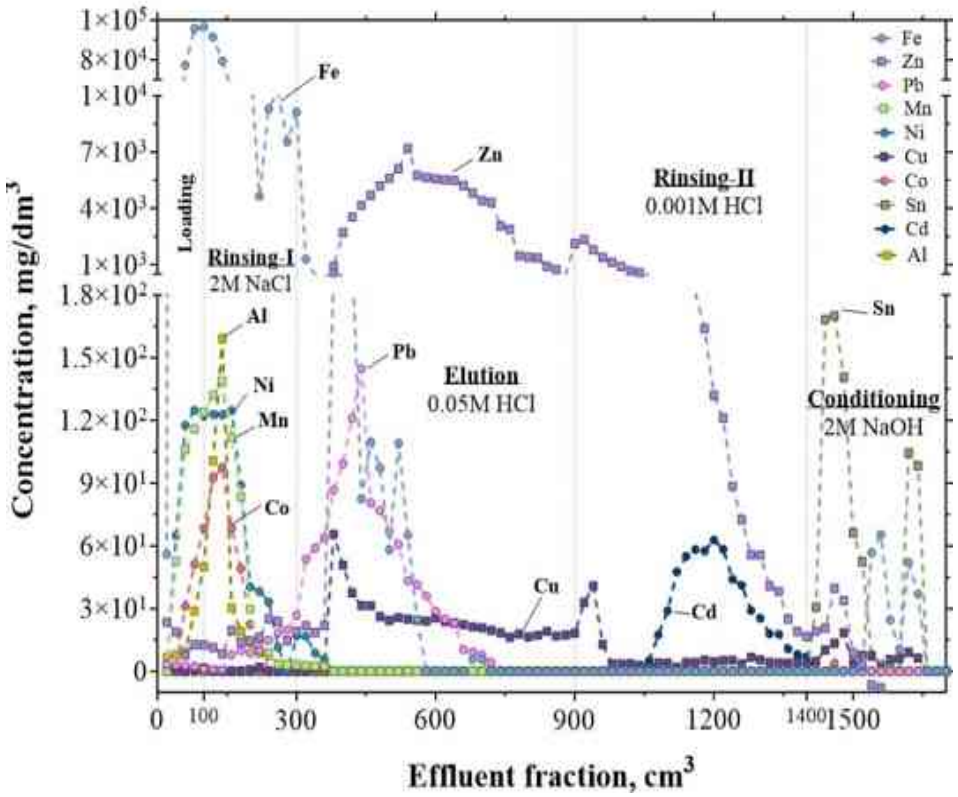

Fig. 4.9 Elution curves of complete SPL purification to produce pure Zn electrolyte.

According to the distribution functions of several practical or characteristic elements, a large number of potential impurities, like Al, Ni, showing no anion-exchange capability can be separated directly. The same applies to Fe(II), Co(II) and Mn(II),

which may form anionic chloro-complexes at very high Cl^- concentration (> 8 M). All the impurities mentioned above are out of the column before the elution of Zn occurs. Just a few impurities – of negligible importance – may have similar distribution functions to that of Zn. In the first elution curve, Pb(II) and Cu(II) appear in the eluate along with the Zn. Lead contamination, however, is almost excluded by the modern European standards of hot dip galvanising. Similar may be true for cadmium. Cadmium leakage could only be observed at the second elution step, and only at the last tail of the Zn elution curve, so this fraction can also be discarded. On the other hand, those impurities which remain strongly fixed in the resin during the elution of Zn, like Sn, will cause no contamination, eluted only at the subsequent conditioning step with – in this case - NaOH.

The conditioning step with NaOH was also used to confirm that there was no appreciable portion of Zn retaining in the resin, neither by possible hydrolytic precipitation. However, the produced dilute Zn solution might pose some challenge for a direct electrodeposition.

The feasibility of an efficient cathodic deposition may require a minimum of 10 ~ 15 g/dm^3 Zn concentration in the chloride electrolyte [72]. To reach even higher Zn concentrations, we tested the hydrolytic precipitation from the purified low-HCl eluate by slightly increasing the pH value, then re-dissolving the separated crystals at the lowest possible level of HCl added (approximately at pH 4~5). In this way, the concentration of the solution can be increased without the necessity of an energy-intensive and time consuming evaporation treatment.

4.3.2. Derived efficiency characteristics of the separation process

Separation efficiency can be expressed by the elimination ratio (R) [102]:

$$R = \frac{\frac{m_{\mathrm{Me}}^{\mathrm{load}}}{m_{\mathrm{Zn}}^{\mathrm{load}}}}{\frac{m_{\mathrm{Me}}^{\mathrm{elu}}}{m_{\mathrm{Zn}}^{\mathrm{elu}}}} = \frac{m_{\mathrm{Me}}^{\mathrm{load}} \int_{V_s}^{V_e} c_{\mathrm{Zn}} dV}{m_{\mathrm{Zn}}^{\mathrm{load}} \int_{V_s}^{V_e} c_{\mathrm{Me}} dV} \tag{4.2}$$

Where V_s, is the total effluent volume at the starting point of eluate collection and V_e is at the endpoint. While $m_{\mathrm{Me}}^{\mathrm{load}}$ is the total mass of the loaded and $m_{\mathrm{Me}}^{\mathrm{elu}}$ is the eluted amount of the examined metal, referring to the collected central fraction of the eluate. The analysed concentration (e.g. mg/dm^3) is denoted by c_{Zn} and c_{Me}, respectively. The standard value of the elimination ratio refers to the fraction of the effluent that

comprises the central section of the main elution peak of zinc, extending from the point at the half-height on the front (rinsing) side to that of the tail (declining) side.

As another efficiency indicator, the relative amount (m_{Zn}) of Zn recovered in the collected fraction of the eluate from the loaded mass can be expressed by the zinc elution ratio (or zinc yield):

$$E_{\mathrm{Zn}} = \frac{m_{\mathrm{Zn}}^{\mathrm{elu}}}{m_{\mathrm{Zn}}^{\mathrm{load}}} = \frac{\int_{V_s}^{V_e} c_{\mathrm{Zn}}\, dV}{m_{\mathrm{Zn}}^{\mathrm{load}}} \tag{4.3}$$

The standard efficiency parameters referring to the elution peaks in Fig. 4.10 are given in Table 4.1. The results were obtained by applying a computer program of smoothing the elution peaks by the running average method, followed by numerical integration of the concentration curves. The non-sorbable impurities are not included as their removal is considered complete. Most of the practically considerable (or possible) impurities (Al, Co, Ni, Mn, Fe, Cd) of SPL have an overall elimination ratio higher than 1000. This indicates an efficient separation process, producing a pure Zn solution. In contrast, some minor – and practically negligible - impurities (Pb, Cu) characterised by anion exchange distribution functions similar to that of zinc have low elimination ratios, but they are not expected to arise in modern HDG technologies. However, cementation or precipitation techniques can remove these impurities from the purified solution, in other cases.

Table 4.1 Characteristics of the Zn anion-exchange purification procedure shown in Fig. 4.9

Zn effluent fractions (cm^3)	Standard Zn Yield, E_{Zn}	Standard elimination ratio, R_{std} **$R_{std} > 1000$ for Al, Co, Ni, Mn and Fe**			
		Fe	Pb	Cu(I)	**Cd**
I. (380-880)	0.91	**> 1000**	3.9	3.14	**> 1000**
II. (500-880)	0.47	**> 1000**	7.7	2.9	**> 1000**

* The conditioning step is not considered (Sn was fully eluted in the conditioning step)

The section of the effluent in the 380 to 880 cm^3 range can be preferably used directly for electrowinning implying ~ 4 times dilution relative to the loading solution. However, the precipitation and re-dissolution treatment can be easily applied for concentration, even holding some potential for additional purification.

5. The examination of the electrode processes of zinc deposition

5.1 The effects of the electrolyte composition

In order to find feasible conditions in a simple open electrolysis system to produce pure Zn at high efficiency and in an acceptable physical state, the kinetic properties of the process of Zn deposition needs further investigations. As it has been discussed above, due to the inherent electrochemical properties, the occurrence of the hydrogen evolution cannot be excluded. It does not only decrease the current efficiency, but it is also associated with the generation of OH^- ions at the cathode through the breakdown of H_2O [70]. This may cause the precipitation of hydroxides in the immediate vicinity. The relevant conditions are described in the E-pCl diagram, also showing the effect of pH (Fig. 5.1.*a*) and the usual E-pH (Pourbaix) diagram of Fig. 5.1.*b*. Both diagrams have been constructed by applying the available equilibrium data [100].

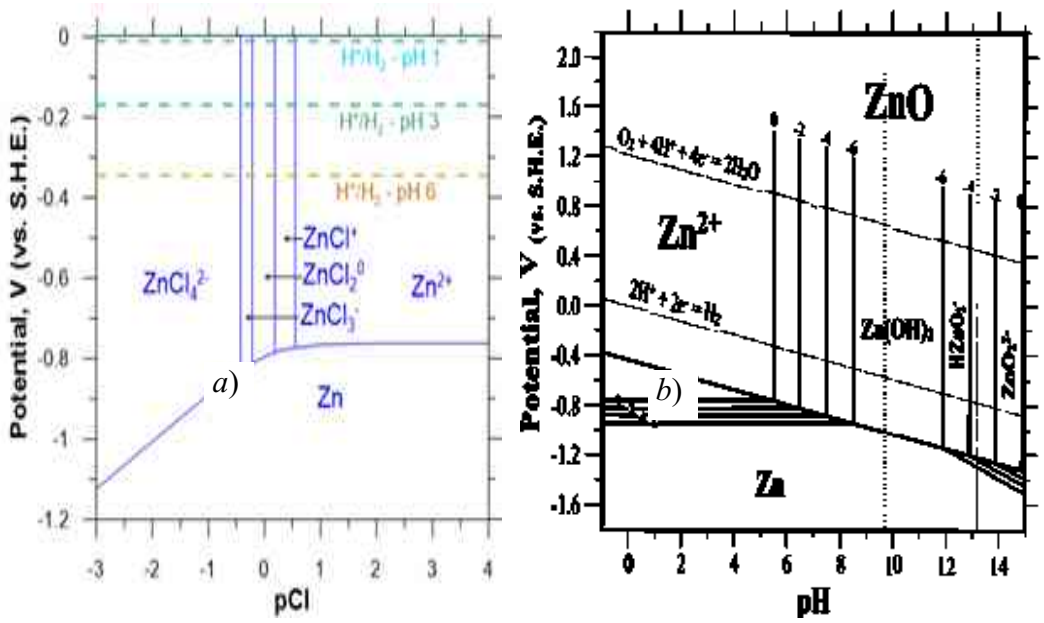

Fig. 5.1 The E-pCl diagram in the Zn-Cl^- (a) and the E-pH diagram in the Zn-H_2O (b) computed from the stability constants for the aqueous systems (25 °C).

Increasing the pH in $ZnCl_2$ solutions the hydrolytic processes may generate more even complex compounds (as has been shown in Fig. 2.3), blocking the surface and shifting the cathodic process towards excessive H_2 evolution.

A serious challenge in the electrodeposition of pure Zn is the interference of the cathodic process caused by the side reactions with the iron species. The redox potentials of the Fe^{2+}/Fe and the Fe^{3+}/Fe^{2+} couples are -0,44 and +0,74 V, respectively [64]. These potentials directly indicate the stability of the Fe^{2+} oxidation state if

metallic iron is present in the system, and oxidation by a strong agent (like oxygen in the ambient air) can be excluded. With its more negative standard electrode potential of the Zn^{2+}/Zn couple, zinc will also directly reduce the Fe(III) species if present. However, the oxidation by air or also by the anode can always generate the ferric species, which – in contact with the deposited metal – may cause cathode corrosion by a partial or complete reduction:

$$2Fe^{3+} + Zn = Zn^{2+} + 2Fe^{2+} \quad (5.1)$$

$$Fe^{2+} + Zn = Zn^{2+} + Fe_{(s)} \quad (5.2)$$

The latter step, results in contamination of the Zn cathode by the cementation of Fe. It is an indirect route beside the direct electrochemical reduction.

Although the formation of the respective chloro-complex species [64]:

$$Me^{z+} + xCl^{-} = [MeClx]^{z-x} \quad (5.3)$$

may influence the Me(Z)/Me formal potentials, where z is the charge of the aqua-ions and Z is the valence of the oxidation state, and x is the coordination number of the chloride ions in the complex species formed [87] [64].

The relative concentrations of the electroactive cations and the chloro-complex species in equilibrium with them can be represented by the results based on the computation applying the stability constants in the database of the ROCC [87] [64] software (developed for this purpose in the laboratory). An example of the system is given in Fig. 5.2. for the relative concentrations Zn species in equilibrium.

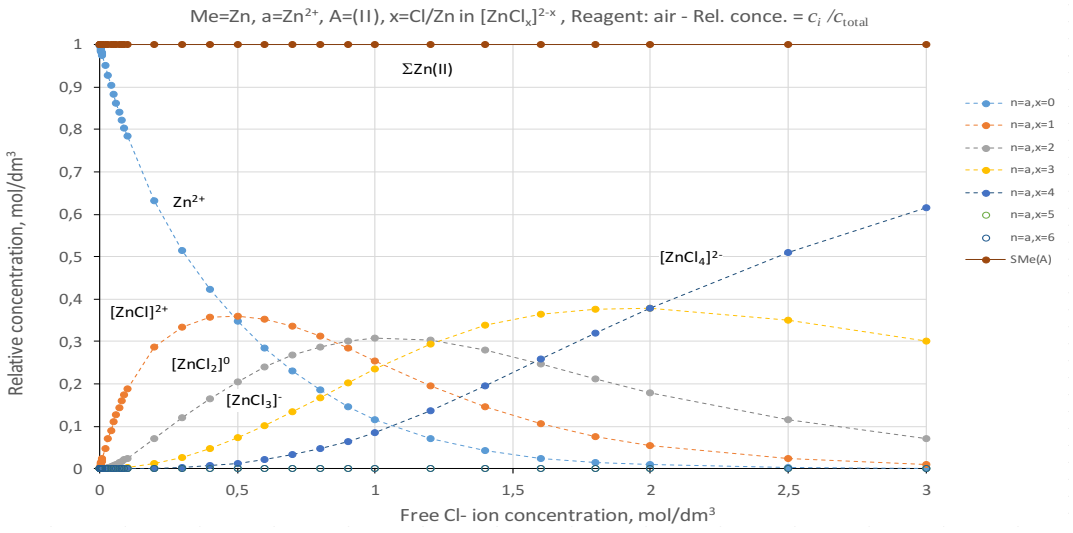

Fig. 5.2 Distribution of Zn among its species in chloride solutions in contact with air.

The computed distribution suggests that various chloro-complex species of Zn may dominate the equilibrium, with the anionic complexes becoming dominant above 1.5 M HCl concentrations. Similar relative concentrations have been computed as shown in Fig. 5.3 for the Fe(0), Fe(II) and Fe(III) species. The cementation of iron with metallic zinc by reaction (5.1) is thermodynamically driven throughout the whole Cl^- concentration range. It is even enhanced at higher concentrations of the Cl^- ions.

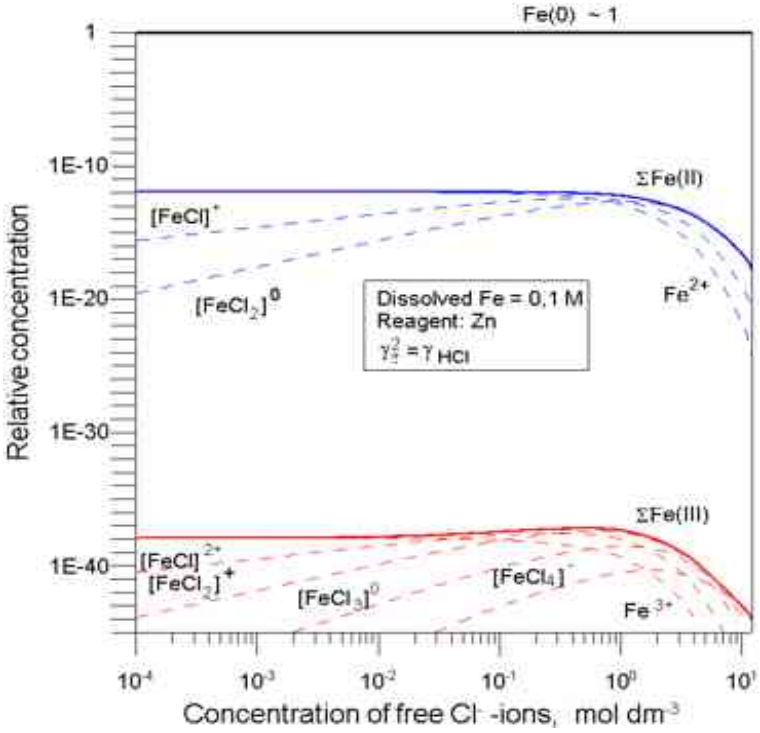

Fig. 5.3 Distribution of the total Fe among its species in chloride solutions in contact with metallic zinc (c).

However, the oxidation of the Fe(II) species by air, as described by the computed equilibrium distribution in Fig. 3.4.*b*, will continuously regenerate the Fe(III) species. The re-oxidation is even enhanced by applying stirring.

5.2. Potentiodynamic investigation

Despite the high equilibrium potential of $2H^+/H_2$ reaction, even at low acid concentration (pH ~ 2), Zn can be electrodeposited from HCl solutions, as the overpotential of the H^+ reduction on Zn hinders this harmful side-reaction. The cathodic reduction of zinc is characterised by a high exchange current density ($j_0 > 1.8$ −8.8 A/dm^2) [103]. In addition, chloride ions may exert a virtual depolarization effect [86] [104] [105]. Chloride solutions offer higher rates of zinc deposition on the cathode surface than sulphate systems. It is practically hard to obtain smooth and

compact deposits. The kinetic processes are to be revealed by the analysis of polarization curves from the potentiodynamic technique.

5.2.1. The experimental setup and method of potentiodynamic examinations

An electrolysis cell with the dimensions of 50×50×50 mm made of glass was used, giving 85 cm^3 volume of the electrolyte. The saturated calomel reference electrode (SCE) was connected to the surface of the cathode (working electrode) through a bridge tube ending in a Lugging-capillary tip (of ~ 1 mm diameter) and filled with the given electrolyte solution. The initial cathode was a copper plate with an active surface area of 2 cm^2, surrounded by polyethylene masking. The potentiodynamic set-up is shown in Fig. 5.4. A thin layer of Zn was pre-deposited on the active cathode surface, then polished with SiC sandpaper of 800 grit, rinsed with distilled water and acetone, and finally dried to create a uniform surface before installation into the cell.

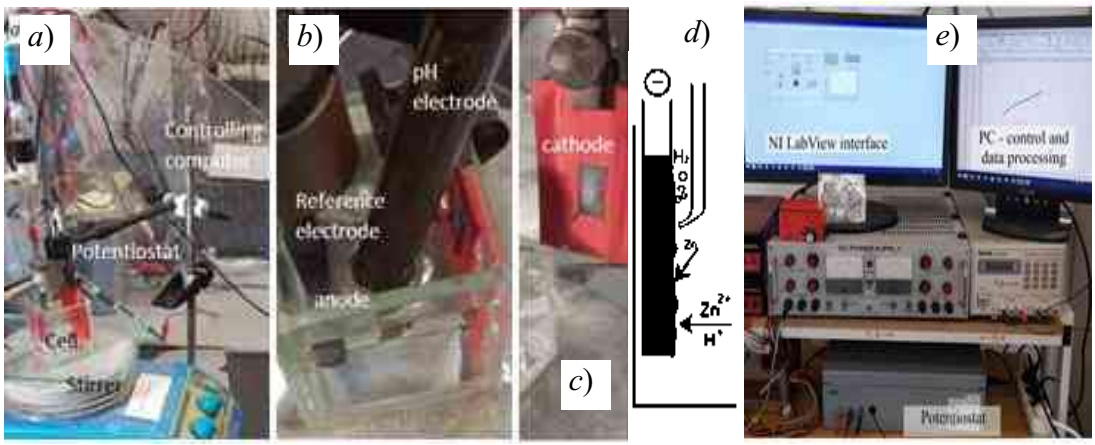

Fig. 5.4 Potentiodynamic experimental set-up (a – the test cell, b – electrode arrangement, c – removed cathode, d –the schematic of the electrode surface, e- potentiostat).

Avoiding changes in the conditions of the electrolyte, a pure Zn anode was used as the counter electrode in repeated cycles of the main experiments. However, to an inert anode made of graphite was used in the case of electrodeposition from the Ni, Fe, Zn-Fe, and Zn-Ni solutions. A magnetic stirrer and a rotating rod of 2 cm length at the bottom of the cell were used with rotation speeds from 0 to 800 r.p.m.

The cell was connected to a computer-controlled potentiostat, developed at our laboratory. It was capable of producing rapid increments of the current to investigate the cathodic processes under increasing surface of the working electrode caused by irregular zinc deposition. Due to the remarkable changes of the surface structure, the uncertain actual current densities could not be expressed. Therefore, the actual current

readings were recorded and plotted, without dividing with the initial (geometric) surface area. Because the potentiostat can only produce a total voltage of 10 V, the voltage drops necessary to drive the current through the main cell from the counter electrode (anode) to the work electrode may limit the polarization runs. If the resistivity of the complete electric circuit is high, the polarization curve can span only a limited current range. The specially developed software controlled the potentiostat and recorded the results using the NI LabView platform. The surface structures were photographed through the glass walls during the polarization process. The solutions were kept at room temperature with 40 mV/s continuous polarization speed – giving the broadest range of clear results - and with a 10/s potential sampling rate.

The model electrolyte solutions were prepared from analytical grade $ZnCl_2$ chlorides dissolved in slightly acidified water. The compositions are given in Table 5.1.

Table 5.1 Electrolyte compositions applied in the Potentiodynamic experiments

Pure Zn electrolyte

Zn concentration, g/dm^3	pH	Added impurity, g/dm^3	Agitation, rpm
30, 60, 90, 120, 150	1.5; 2; 3; 4.5	0	0, 50, 200, 350, 500

Zn + Fe electrolyte

Zn Concentration	pH	Fe concentration, g/dm^3	Agitation, rpm
90 g/dm^3	1~2	0.1, 0.25, 0.5, 0.75, 1, 2.5, 5, 5, 15, 30, 45, 60, 90, and 120	0, 50, 200, 500, 800

Zn + Ni electrolyte

Zn Concentration	pH	Ni concentration, g/dm^3	Agitation, rpm
90 g/dm^3	1~2	0.9, 0.45, 0.3, 0.225, 0.18, 0.09, 0.009	0, 50, 200, 500, 800

The total mass of the deposit was determined by weighing the rinsed and dried cathode before and after the potentiodynamic runs. Then, these electrodes were immersed into 1 M HCl + cc. HNO_3 to dissolve the deposit on its surface, followed by atomic adsorption spectrometric (AAS) analysis (Fig. 5.5). The reduction of the H^+ ions was also studied at various levels of acidity (pH 2 - 5) with blank HCl and the prepared model solutions. Results referring to the same pH were compared.

Fig. 5.5 The AAS analytical instrument.

5.2.2. Potentiodynamic characteristics of Zn deposition from chloride media

In the first series of experiments, the goal was to identify the dominant cathodic process in different ranges of the examined parameters. Zn deposition was investigated from pure Zn chloride solutions. The deposits were observed to form irregular growths of dendrites and loose crystals, as seen in Fig. 5.6.

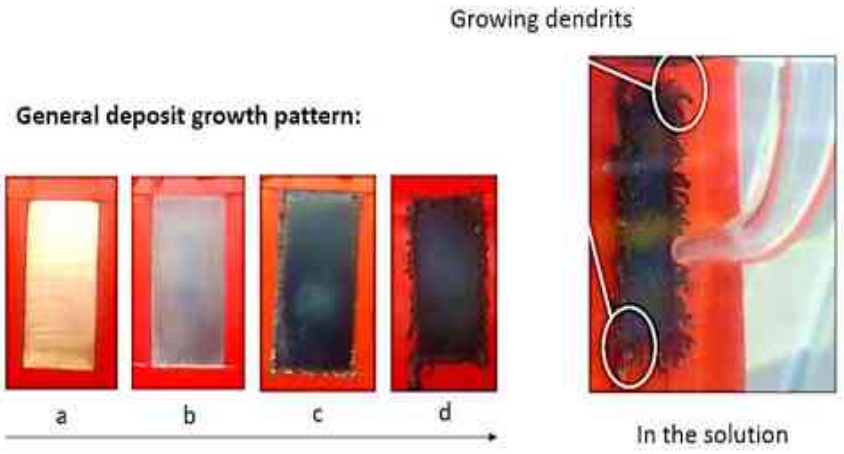

Fig. 5.6 The changes in the cathode surfaces during potentiodynamic runs showing (a) the Cu starting surface, (b) a uniform dense deposition, (c) a black spongy deposit and (d) a dendritic growth pattern. (1 min runs at 40 mV/s polarization speed).

The electrodeposition of Zn started with the uniform nucleation of Zn metal on the pre-Zn deposited cathode surface, inferring a uniform current distribution over the electrode surfaces. The deposit was visually observed to grow layer by layer over time and seemed uniform at the beginning of the electrodeposition. While after several seconds, the edge growth became apparent, confirming the general expectations discussed above. The protrusion growth - which then continues as dendrites - changed the electrical field distribution of the overall surface. Although overpotential may shift

the hydrogen reduction potential to be less noble, the co-existence of Zn deposition and hydrogen evolution is observed from the beginning. Furthermore, a local Zn concentration drop facilitates this side-reaction.

Regarding the development of the deposits at different pH levels, the photographs of the cathodes are compiled in Fig. 5.7, showing the surface structures developing in potentiodynamic runs applying 60 g/dm^3 Zn concentration in a stationary electrolyte.

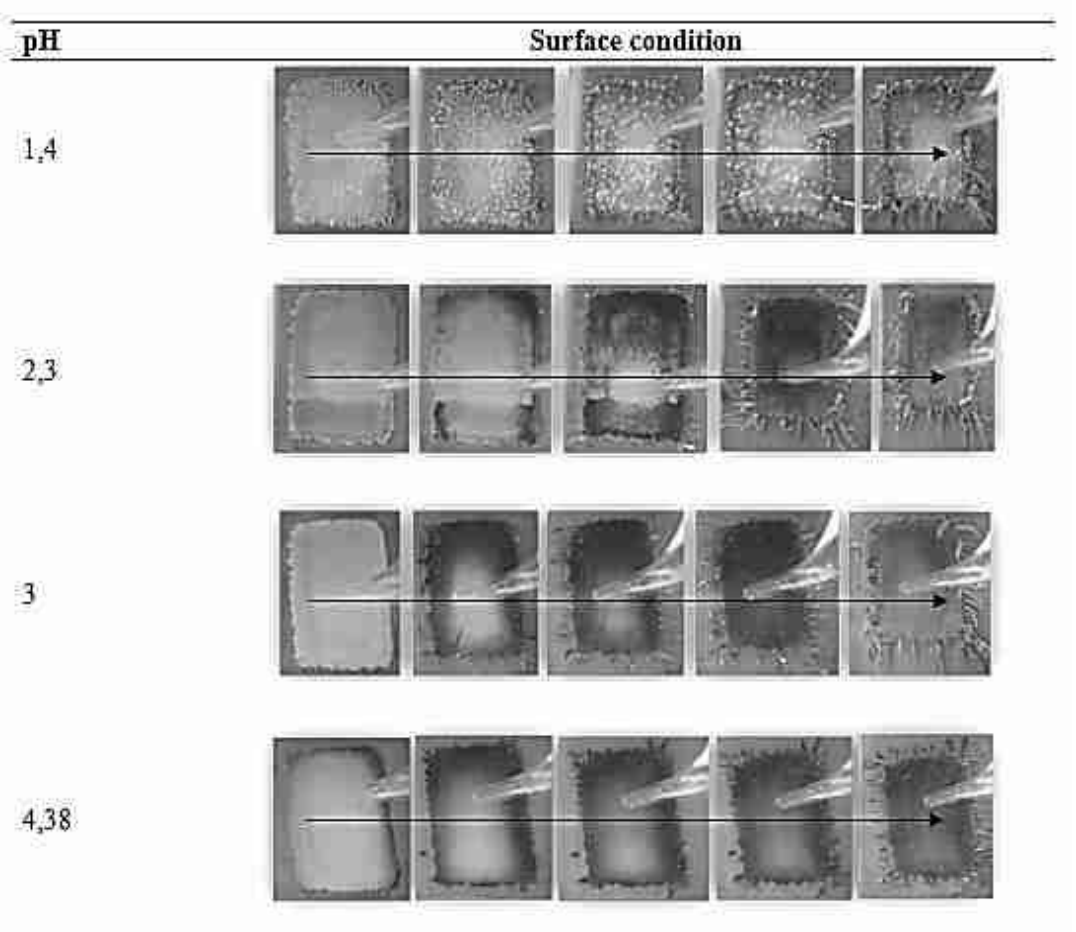

Fig. 5.7 Cathode surfaces during polarization at the indicated pH values of the stationary solution (60 g/dm^3 Zn) taken every 15 s at 40 mV/s polarization speed.

It is seen that in the pH range lower than 2, the hydrogen evolution constituted most of the cathodic reaction. However, zinc deposition started to take dominance as the pH was raised. With pH values higher than 2, the initial stage of zinc deposition formed a uniform zinc coating on the surface, followed by black spongy deposits, which later propagated the growth of dendrites at the edges of the active cathode surface. The appearance of the zinc deposits obtained from the electrolytes with a pH lower than 2 and those from the higher pH solutions are markedly different. Hydrogen evolution started early in the lowest pH range. At first, bubbles just accumulated, partially

blocking the active surface before being evolved. The process is reflected in the development of the current as the cathode is polarized. Since the actual surface of the working electrode may change during the run, the polarization curves are constructed with the directly measured current values. The initial (geometric) area can be used to calculate apparent current densities. The accumulation of the H_2 bubbles may even create a virtual limiting current for H_2 evolution while zinc may continue to deposit. To better interpret the observed phenomena, the surface photographs are fit into the cathodic polarization diagram of Fig. 5.8 referring to a low and a high pH setting in the electrolyte. At pH 1.5, there are enough H^+ ions present; therefore, H_2 evolution could develop easily at the cathode. The ratio of the two parallel currents of the main and the side reactions - belonging to either Zn^{2+} or H^+ reduction - expresses different tendencies at the two extreme pH settings.

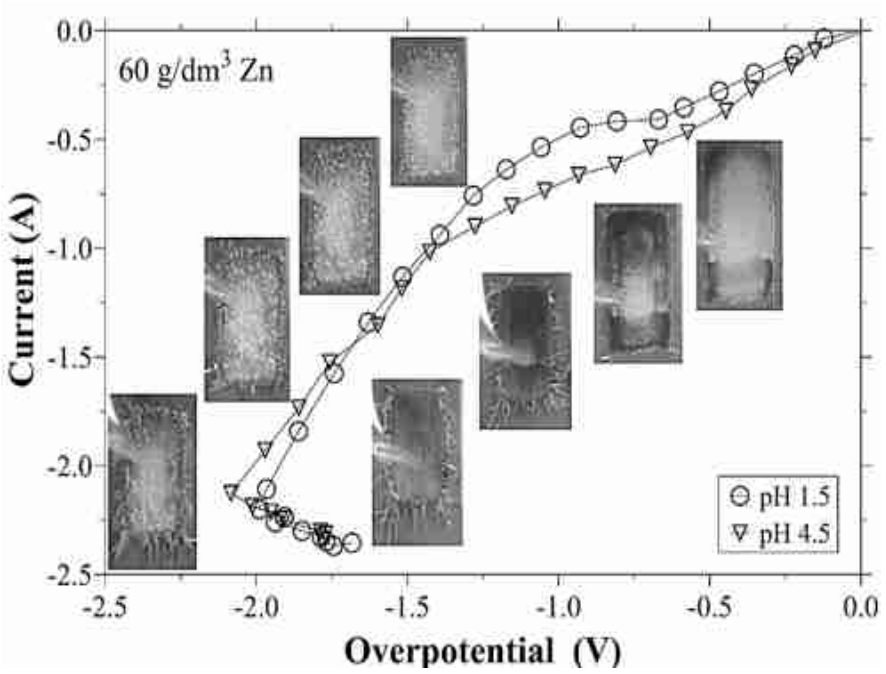

Fig. 5.8 Polarization curves of Zn (60 g/dm^3) electrodeposition from chloride media of different acid concentrations (pH 1.5 and 4.5).

Starting from the equilibrium (0 V overpotential) in the cathodic direction, the current plots lose their steady slope around -0.7 V, where a temporary limiting current density plateau appeared. The incomplete formation of a limiting current infers the beginning of a mixed mechanism. In the electrolyte of the higher H^+ concentration, the initial rise of the current plot can be dominated by the H^+ reduction, which, after the virtual limiting section changed for a more dominant Zn^{2+} reduction induced by the roughening of the deposit structure. The virtual plateau is mostly caused by the

blocking of the active surface, as the initially formed H_2 bubbles are still attached before growing to the size to be released. Thus the local overpotential is increased while the recorded current is not growing significantly. The series of the photographs on the left, next to this plot show the obvious formation and accumulation of the H_2 bubbles. On the other hand, the diagram and the series of photographs belonging to the conditions of pH 4.5 show hardly any effect of H_2 evolution. In this case the reduction of the Zn^{2+} ions is dominant all over the polarization range. Further on, the surface of the electrode gradually turned rougher. At the higher ranges of polarization Zn deposition could remain the dominant electrode process.

As the overpotential became more negative than -1 V, branchy fern-like dendrites were formed, increasing the actual surface area, thus allowing a faster current increase. Towards the final section of the polarization curve, the surface grew excessively, decreasing the real current density sharply. More current could be generated by even decreasing overpotentials. This "back-drop" in the potential occurs as the development of the dendritic structure explodes. Actually, the apparatus lost its ability to keep the current increasing as fast as to incur the voltage set by the program. The total current is increased while the actual current density drops, thus the overpotential is also dropping under such conditions. Actually the circuitry of the potentiostat cannot increase the current in such a pace as the surface gets rougher. The contribution of the tips of both primary and secondary dendrite branches to the electrodeposition process becomes pronounced as they protrude out from the limits of the diffusion layer.

Agitation helps homogenize the electrolyte by enhancing the ion transport to the active surface. The main results of applying various rotation speeds are shown in Fig. 5.9. Applying agitation in the 90 g/dm^3 Zn electrolyte could not eliminate the backdrop in the polarization curve (Fig. 5.9.*a*) at the extremely high overpotentials required from the potentiostat. The stronger increase of the current in the stationary electrolyte is caused by a more intensive H^+ reduction and a coincidentally rougher electrode surface. As the electrolyte is agitated the ion transport is faster, more compact cathode deposits arise. Therefore, the actual current density is higher, resulting in lower currents at a certain overpotential. However, it does not avoid the extra deposition at the electrode edges.

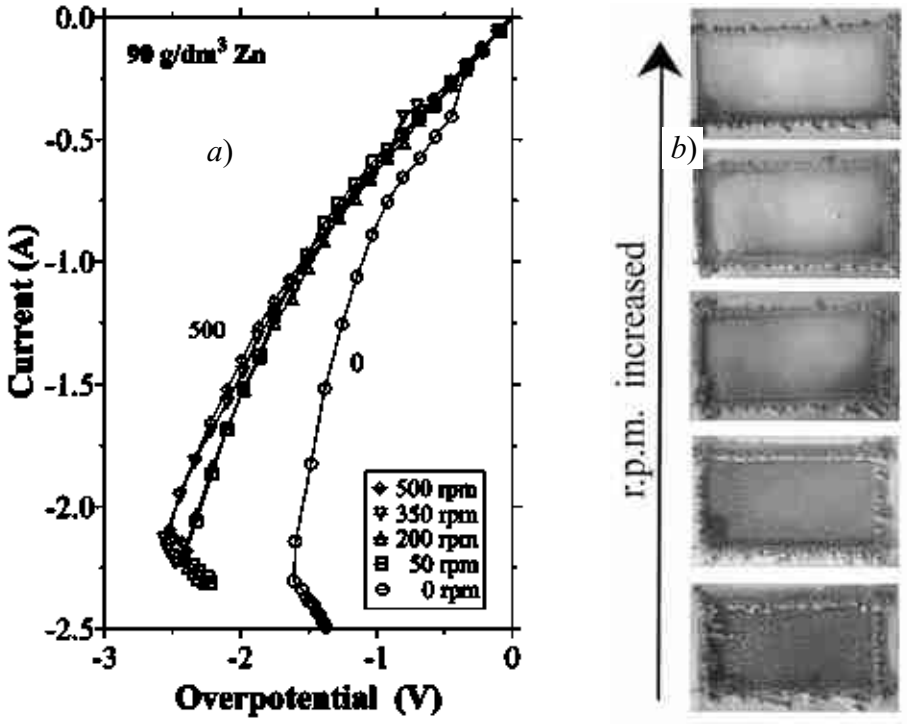

Fig. 5.9 Polarization curves as the functions of agitation intensity in chloride solutions of pH 2.5 and 90 g/dm^3 Zn concentration (a) and the final deposits (b).

Stirring minimizes the concentration gradient at the electrolyte-electrode interface, virtually increasing the effective concentration of the electroactive Zn species. Thereby it provides a more uniform deposition. In general, agitation is also related to the more efficient removal of hydrogen bubbles, liberating more active sites for Zn ions to be deposited with better current distribution.

It is also practically important to consider the effects of Zn concentration on the cathodic processes. At higher levels of Zn in the stationary electrolyte, the polarization curves showed more constant slopes, and the effects of the hydrogen side-reaction seemed to diminish. This phenomenon is demonstrated by the results shown in Fig. 5.10. The beneficial effect of increased Zn concentration was also confirmed by the visual observation of less hydrogen gas evolution. The steeper the slope, the more hydrogen reduction occurs. It is evident from the relevant surface photographs (Fig. 5.10.*b*) that the more concentrated Zn is in the solution, the more uniform is the metal deposit and less dendrites are grown at the cathode edges. Therefore, the mass transfer and concentration gradient play essential roles in the deposit macro-morphology. Also the hydrogen evolution reaction has a significant impact on the growth of the dendrites.

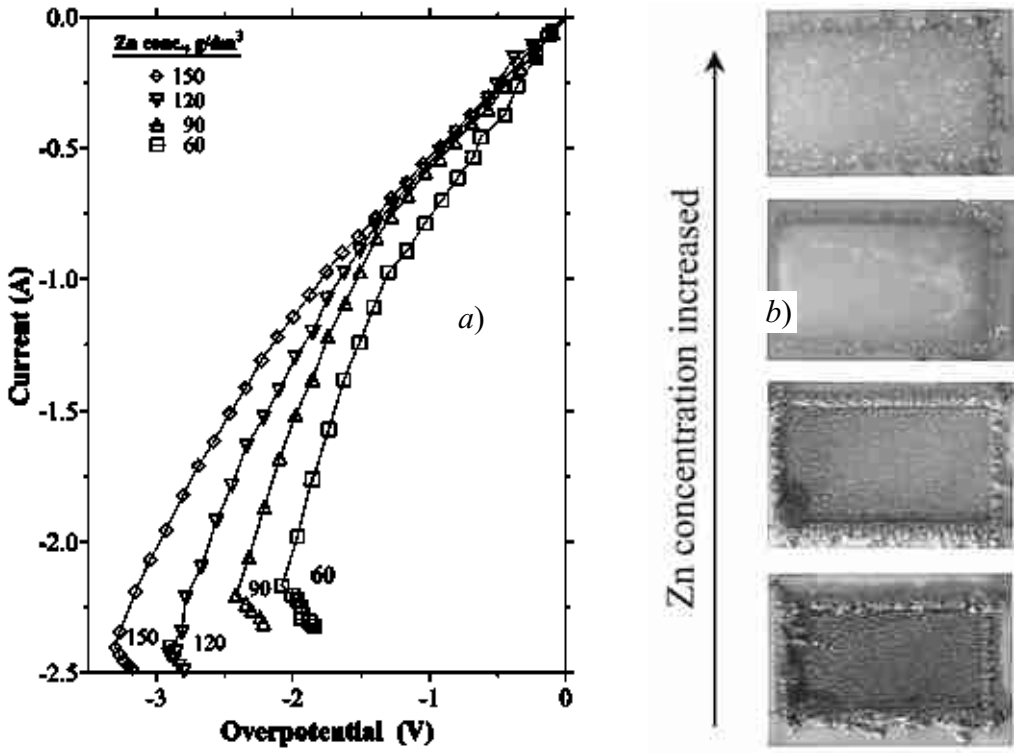

Fig. 5.10 Polarization curves obtained at different concentrations (a) and the photographs of the obtained final deposits (b) in stationary electrolytes.

The final irregularity in the polarization curves expressed by the reversed tendency in the potential are shorter at higher Zn concentrations, and the obtained currents are of smaller absolute value at the same cathodic overpotentials. This indicates a later and reduced extent of dendrite formation. Similar effect was caused by increasing the agitation intensity at a constant Zn concentration in the electrolyte. If the stirring speed is further increased, the final irregularity is eliminated from the polarization curves, and the dendrites almost disappear from the cathode. The deposits were thicker at the edges, and a few less developed dendrites appeared sporadically at the bottom edge.

5.2.3. The effect of Fe impurity on Zn deposition from chloride media

A) High additional Fe concentrations

Theoretically, the preferential Zn electrodeposition from electrolytes contaminated with transition metals is considered anomalous co-deposition. The deposition tendency is governed by the type and the concentration of the ion, as described by the well-known Nernst equation. This may allow a pure recovery of Zn from the preliminary purified SPL, since the concentrations of Fe and other potential contaminants (Ni, Co or Mn) can be depressed to very low (mg/dm^3) levels by the anion-exchanged procedure introduced in Chapter 4, or by other methods of similar

nature [11]. Nevertheless, it is important to clarify the effects of the major practical impurities, which would dictate the degree of the required preliminary purification of the SPL before the treated solution can be applied for Zn electrodeposition.

At first, visual observation of deposits was carried out in the potentiodynamic experiments run on electrolytes contaminated with different levels of iron. The surface images of the final deposits can be seen in Fig. 5.11. The growth pattern of the deposits is the same as in the previous series where the iron-free solutions were tested. However, the dendrite formation decreases and hydrogen evolution increases with the presence of Fe. Initially, the deposition was hindered by the growing hydrogen bubbles, fully covering the cathode surface. Effective deposition may occur after more bubbles are released, which dominantly happens at the area near the edges. Adding iron promotes H_2 evolution due to the lower overpotential of hydrogen on Fe sites.

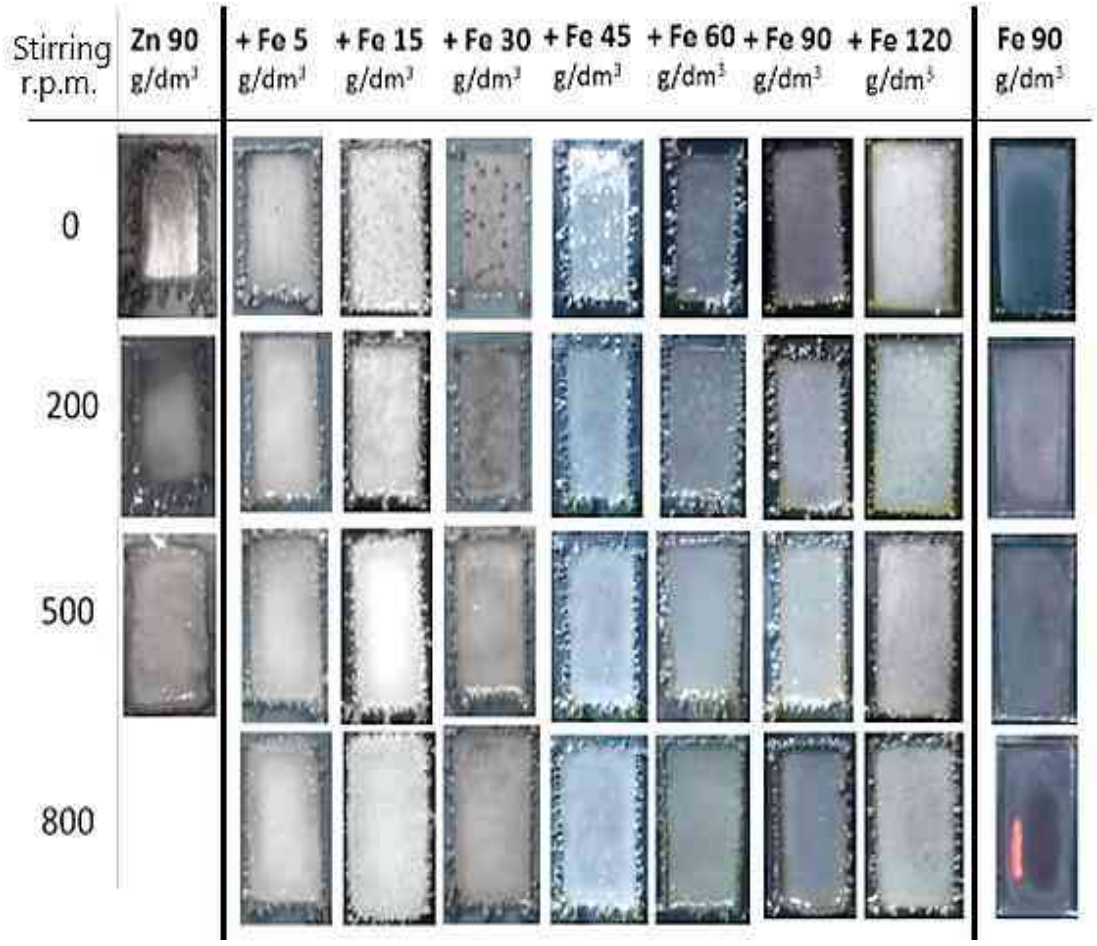

Fig. 5.11 The final structure of the cathodes obtained from the potentiodynamic experiments with different Fe(III) concentrations in the $ZnCl_2$ solution. (1 min runs at 40 mV/s).

Stirring still positively affects the process. The obtained structure tends to be denser with increasing agitation. Stirring enhances the transport toward the cathode surface

and can also remove the bubbles. Nonetheless, hydrogen reduction is still dominant in the Zn-Fe chloride solution. As a result, porous metal deposits occur even at the highest stirring speeds. Analysis of the final deposit is also needed to confirm the ratio of the two metal in the deposition process.

Applying a pure iron chloride solution showed powdery deposition where the deposited iron could be easily removed from the cathode surface, probably related to the concurrent H_2 evolution. The electrolyte solutions got darker because of the dispersion of the detached iron powder. The iron deposit appears darker than that of zinc. The obtained deposit surfaces can be seen closer in Fig. 5.12.

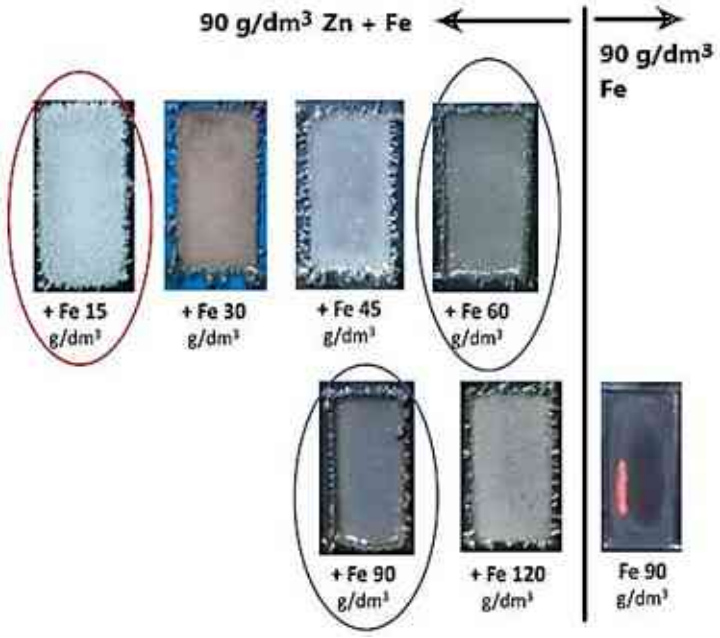

Fig. 5.12 The closer look of the final deposits obtained in the potentiodynamic experiments with 90 g/dm^3 Zn contaminated with different iron concentrations and with 90 g/dm^3 Fe solution, respectively (stirring: 800 r.p.m.). (1 min runs at 40 mV/s).

Further potentiodynamic experiments were carried out same Zn-Fe solutions with copper substrates as starting cathodes of carefully measured masses. The starting and the produced cathodes were weighed. Careful rinsing and drying. After the weighing, the deposit was completely dissolved in 1 M HCl from the copper substrate, and finally, the iron mass was calculated from the analysed concentration. The amount of deposited zinc was determined by subtracting the calculated iron mass from the total mass of the deposit. The highest ratio of zinc was obtained in the range of 45 to 60 g/dm^3 Fe in the solution. The acceleration of Zn electrodeposition by the Fe concentration is shown by the results in Fig. 5.13.

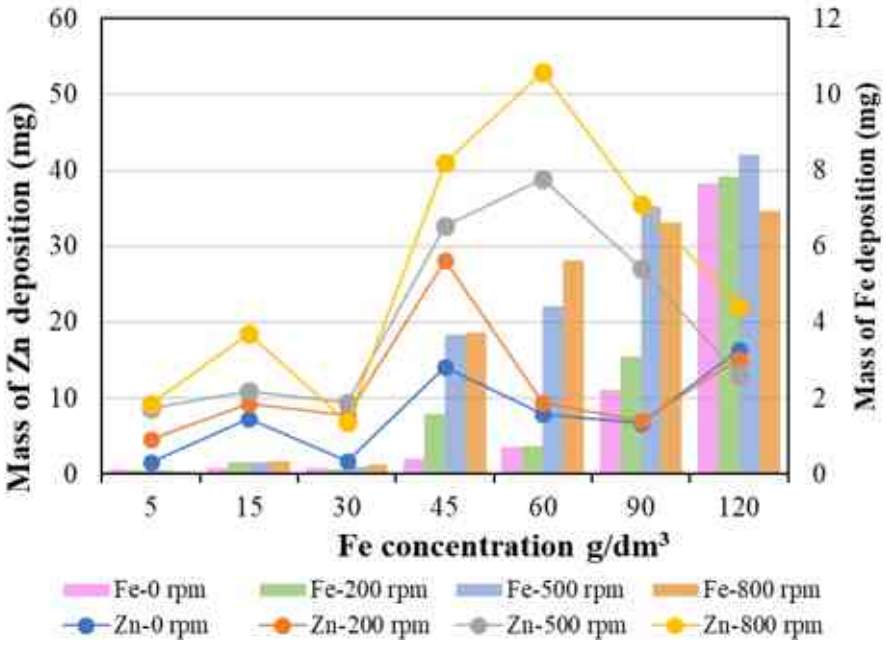

Fig. 5.13 Deposit (Zn – curves, Fe - bars) composition obtained from solutions of 90 g/dm^3 Zn with various concentrations of Fe added (1 min runs at 40 mV/s).

As the bars in Fig. 5.13 show, the amount of iron deposited from the mixed solution increases quickly as the Fe concentration increases beyond 30 g/dm^3. However, zinc deposition is concomitantly enhanced. It is also seen in the plotted curves that the stirring intensity strongly affects the rate of zinc deposition. However, stirring at the highest iron concentration seems to lose its relative importance. Comparing the positions of the Zn-curves and the Fe-bars, it is seen that from stirred solutions of 90 g/dm^3 Zn, the purest Zn deposit can be obtained at the lowest iron concentrations. If, however, the solution is stationary and there is little iron in it, the deposit is too small in mass to make accurate measurements.

With increasing contamination of Fe in the electrolyte solution, hydrogen evolution will increase because of its lower overpotential to Fe. The generated gas bubbles give an extra stirring at the cathode surface, enhancing also the transport of zinc ions. It may increase the rate of Zn deposition, as seen in the 30 – 60 g/dm^3 range of iron concentration. With even more iron in the electrolyte, the mechanical effect of hydrogen evolution is outweighed by the chemical effect of the increasing local pH. It may trigger a local formation of hydroxide particles. Thus, an inhibiting layer can be formed, hindering the deposition of the less noble zinc. Therefore, in the 30 – 60 g/dm^3 Fe range, where Zn deposition is enhanced, the increased rate of iron deposition results in more contaminated zinc deposits. This is especially true if the solution is not stirred

intensively. At higher iron concentrations, even more contaminated zinc deposits can be obtained. Therefore, to get pure zinc from the SPL, it is necessary to apply the planned preliminary purification of the solution, removing iron as much as possible. Stirring can detach H_2 bubbles from the surface and by enhancing ion transport, promotes more compact structures.

The hydrogen evolution from the iron solution was seen as more intensive than from the Zn solutions. As shown in Fig. 5.14.*a* for Zn and 5.14.*b* for iron, no limiting currents are identified in the polarisation curves of either 90 g/dm^3 Zn or 90 g/dm^3 Fe pure solutions. This means that hydrogen evolution was also present from the early stages. The Zn graph is steeper and shows a significant change at a point, implying that less polarization may induce higher currents. This condition is attributable to a looser deposit of higher specific surface. At the end of the curve, the unusual backdrop of the potential with further increasing current is caused by the rapidly growing actual surface of formed dendrites, arising in the pure zinc solution but not in that of iron.

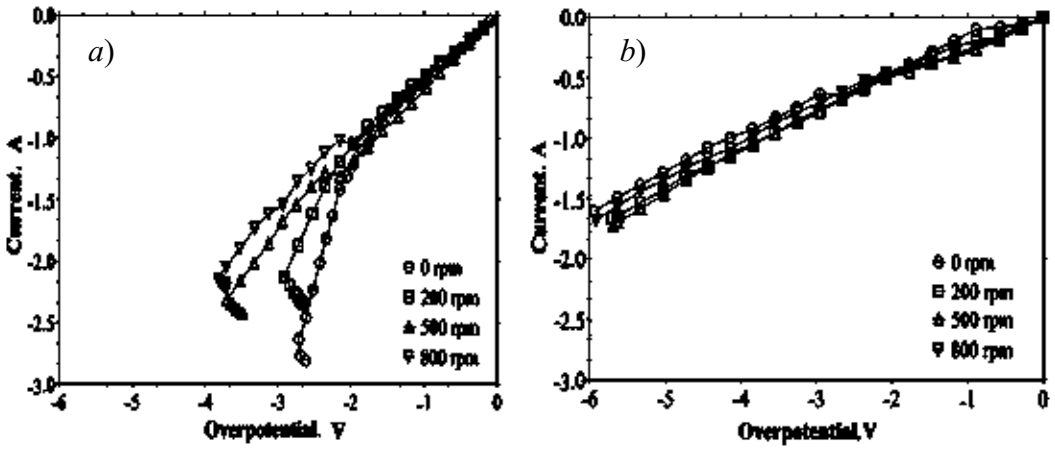

Fig. 5.14 The effect of stirring speed on zinc (a) and iron (b) deposition from 90 g/dm^3 solutions, respectively.

In the case of Zn, stirring can eliminate the accumulation of the hydrogen bubbles and promotes denser deposits, which can become easily removed at intensive levels of agitation. These effects are reflected in the slightly lower maximum currents at the highest speed of agitation. However, the deposition of iron from the pure solution was hardly affected by the applied stirring, and according to the visual observations, the active surface remained quite constant. It indicated that the competition of hydrogen reduction was strong, and even it could become dominant. Similar differences can be observed if iron is added to the basically Zn chloride solution, as shown in Fig. 5.15.

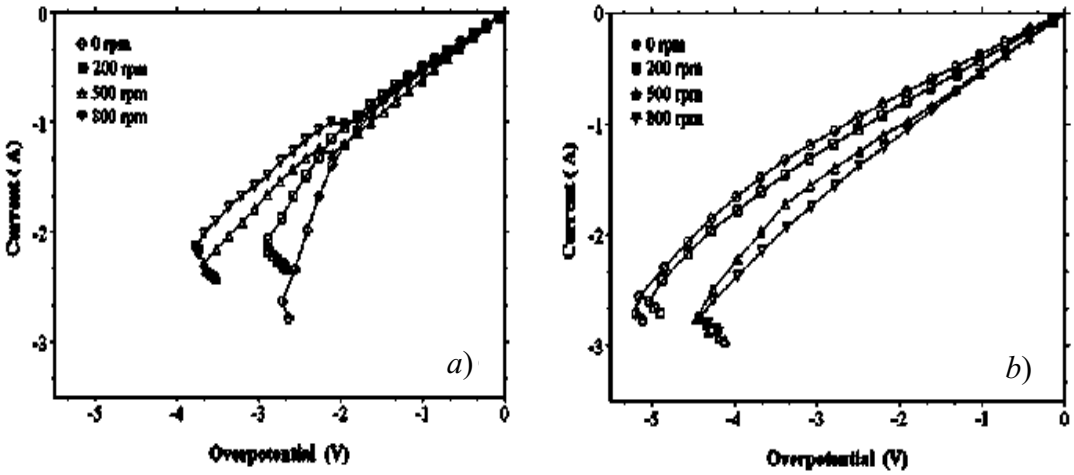

Fig. 5.15 The effect of stirring speed on the deposition of Zn from solutions of 90 g/dm^3 Zn containing (a) 0 g/dm^3 or (b) 30 g/dm^3 Fe.

The stirring in the pure Zn electrolyte depressed the irregular growth at the cathode. It can be inferred from the gentler the slopes at higher stirring speeds, confirmed by the photographs in Fig. 5.12. In the case of solution containing also iron, H_2 evolution is more intensive, and the denser structure of lower specific surface requires higher overpotentials to reach the same currents. Stirring in this case definitely increases the total current, promoting also metal deposition as it detaches the evolved H_2 bubbles from the cathode surface. This tendency is continued with further increased Fe concentrations in the Zn chloride electrolyte, as shown in Fig. 5.16.

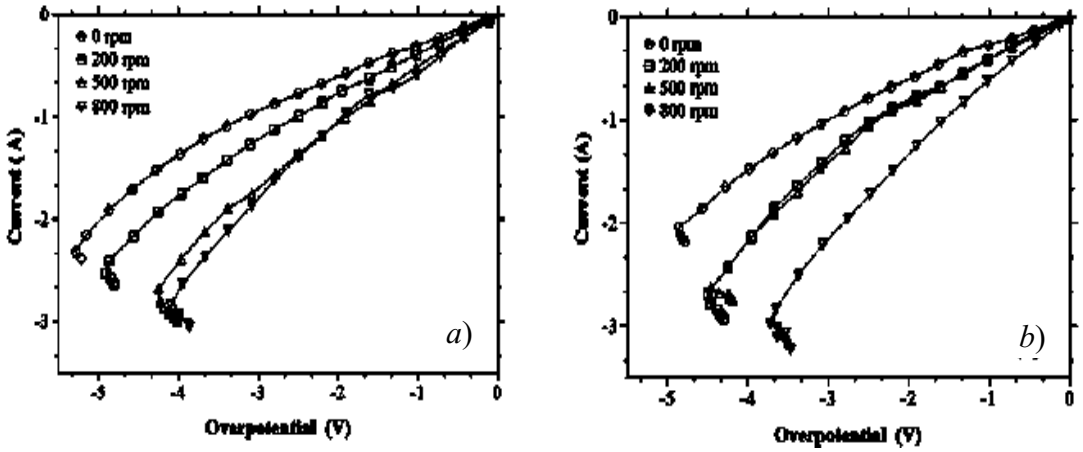

Fig. 5. 16 The effect of stirring speed on zinc deposition from solutions of 90 g/dm^3 Zn containing (a) 45 g/dm^3, (b) 90 g/dm^3 iron.

Introducing the iron concentration to the stationary solution caused a stronger decrease in the obtained current, as also seen in Figs. 5.15 and 5.16. Hydrogen bubbles were slowly and just periodically released, hindering metal deposition. With approximately 2.5 V cathode potential in the stationary and iron free solution 2.7 A current could be

attained, while with the same settings but with 30 – 90 g/dm^3 Fe in the solution, about 1 A was reached. At the extremely high (120 g/dm^3) iron concentrations, mostly powdery iron deposits are produced under any conditions, and the metal particles are easily detached, therefore the surfaces are smoother but the solution becomes turbid with the dark iron powder mixed in. The backdrop potentials were also shifted to more negative values, confirming that less metal could be deposited at lower polarizations without agitation because of the hydrogen blocking. It also proves that iron in the solution promotes hydrogen evolution at the cathode. If iron is added to the solution, the slope virtually remained constant. This is contrary to the that suggested by the Buttler-Volmer-Erdey relationship [64]. Again, this can be explained by the blocking effect of the evolved hydrogen bubbles adhering for some considerable time to the cathode surface. Thus the more constant the slope of the polarization curve is the more dominant the hydrogen reduction can be. It can be seen in the case of the highest concentrations of iron in the electrolyte.

B) Low additional Fe concentrations

The principle changes caused by the addition of large amounts of iron to the zinc chloride electrolyte could reveal the nature of the effects. However, much lower Fe concentrations may refer to the practical case of the purified SPL. It can be seen in Fig 5.17 that Fe contamination in the <1 g/dm^3 range may still have a significant – and here quite monotonous - effect on the cathodic deposition during the potentiodynamic runs of 75 s time with the 400 mV/s polarization speed. In this low range of the iron concentration, H_2 evolution was relatively lower and the rate of Zn deposition was higher as compared to that of previous experiments with much higher Fe concentrations in the Zn electrolyte. Nevertheless, increasing the Fe-concentration from 0 to 1 g/dm^3 can decrease the mass of deposited Zn by half. Enhancing the ion transport by stirring does not cause a significant difference for the Zn deposition, but it has an effect on the deposition of iron, depending in strength on the Fe concentration.

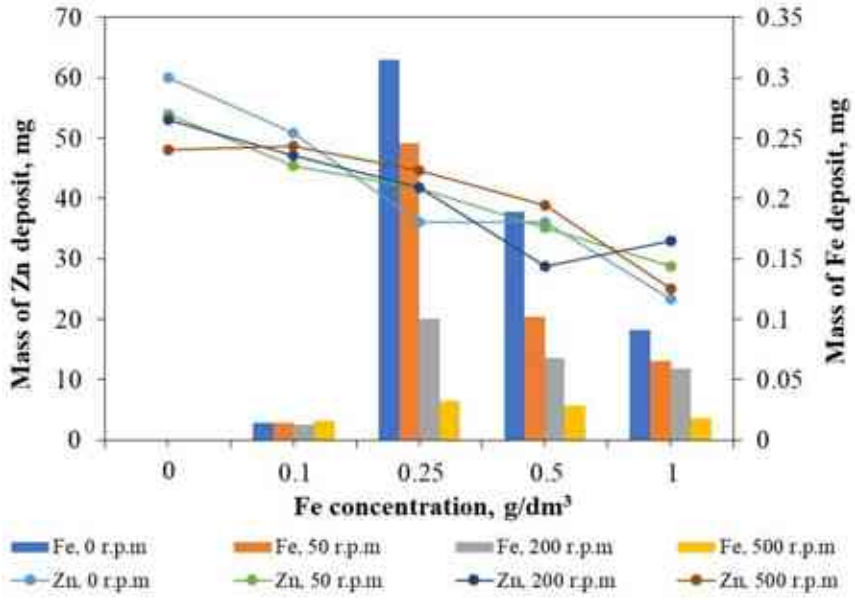

Fig. 5. 17 Deposited masses from solutions of 90 g/dm³ Zn with various concentrations of Fe (pH 1.8, 75 s, 40 mV/s cathodic polarization speed).

The lowest (0.1 g/dm^3) concentration of Fe in the $ZnCl_2$ electrolyte was found to cause little contamination (~ 0,02/50, that is 0.04 %) in the cathode, as the availability of Fe ions near the cathode surface was limited. The highest level of contamination occurred with the 0,25 g/dm^3 Fe addition (~0,7 % in the stationary electrolyte and 0,07 % with 500 r.p.m. stirring applied). It shows the importance of the transfer for the Zinc species to the cathode surface. It is however surprising that with increasing agitation, the ratio of iron deposition decreases at a given Fe concentration in the solution, while agitation had relatively slight effect on the rate of Fe deposition from pure or highly concentrated iron chloride solutions, as shown above. It infers that the side-reaction at the sites of deposited Fe atoms, mostly the H^+ reduction is intensified with agitation. By further increasing the Fe concentration in this low range, the intensity of H_2 evolution is higher, thus the Fe deposition is effectively supressed.

The observed currents result from both metal deposition and hydrogen evolution. In general, it is clearly seen that the agitation increases the current. The set of curves in the agitated solutions show almost no back-turn pattern, indicating that fewer dendrites are formed on the edges of the cathode.

According to Fig. 5.17, increasing the Fe concentration depresses the rate of zinc deposition during the set potentiodynamic run in the low (< 1 g/dm^3) range. Thus more current in the pertaining polarization curves should be related to hydrogen reduction. The evolution of the gas also changes the morphology of the –basically – zinc deposit.

It is seen in Fig. 5.18 that with more Fe added to the solution less dendrites are growing.

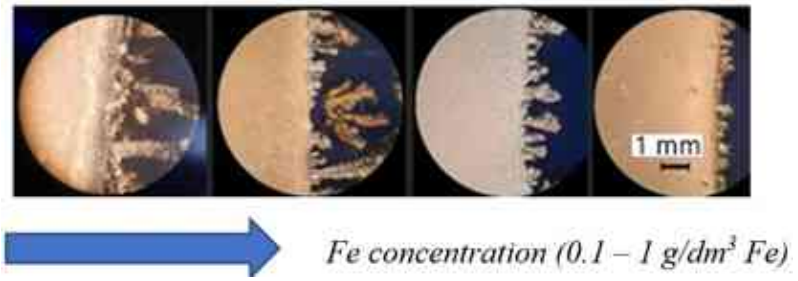

Fig. 5.18 Microphotographs of Zn deposits obtained from zinc chloride solutions (90 g/dm³ Zn) of varied Fe concentrations.

As the iron contamination is increased in this low range, the dendrites observed at the edges of the cathode are getting not just fewer but also shorter. It is related to the effect of iron enhancing hydrogen evolution by the lower hydrogen overpotential. The evolved hydrogen stirs the solution layer adjacent to the cathode surface and promotes the Zn-ion supply, while developing H_2 bubbles are faster released. Some bubbles can still be trapped which is are, however, efficiently released by more vigorous mechanical (magnetic) agitation. This is shown in Fig. 5.19.

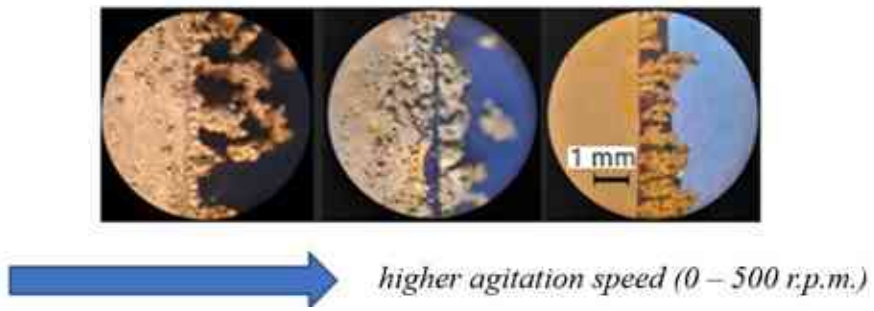

Fig. 5.19 Microphotograph of Zn deposits obtained from zinc chloride solutions (90 g/dm³ Zn) at varied agitation speeds.

In stationary electrolytes more pits occur on the cathode surface, especially close to the cathode edge. These pits/craters in the deposit are the results of trapped hydrogen bubbles, which were not big enough to be released prior to the metal deposition surrounding them.

5.2.4. The effect of Ni impurity on Zn deposition from chloride media

The processes at the Zn cathode depend on the main electrolysis parameters and the composition of the electrolyte. It has been shown that the major impurity, iron also has a strong influence on the main characteristics. Although the preliminary purification

of the SPL by the devised anion-exchange procedure may provide a pure $ZnCl_2$ solution, the economical aspects may set a goal of less perfect purification. Even small residual concentrations of the main impurity, Fe, has been seen to impact the performance of the Zn electrodeposition heavily. Another practical impurity, although at a lower concentration, may be Ni, whose behaviour and effects may be also considered. As it was with iron, the high-Ni solutions should be studied at first.

Nickel electrodeposition from chloride media containing 90 g/dm^3 Ni started with the generation of hydrogen bubbles, entirely blocking the cathode surface. As shown in Fig. 5.20, there is just a slight current development observed until the polarization potential ~ -0.8 V. Magnification of the scale also showed that the polarization curve fluctuated initially, indicating the periodical evolution of H_2 bubbles. In acidic electrolytes the deposition of fresh nickel crystals is always followed by subsequent reduction of H^+ to H_{ads}, which firmly adheres to the electrode surface until it forms recombined hydrogen molecules which are then released as bubbles [106]. After the bubbles get detached, further metal deposition can take place at the same site. At higher overpotentials the hydrogen reduction is accelerated so much that it covers the entire cathode surface.

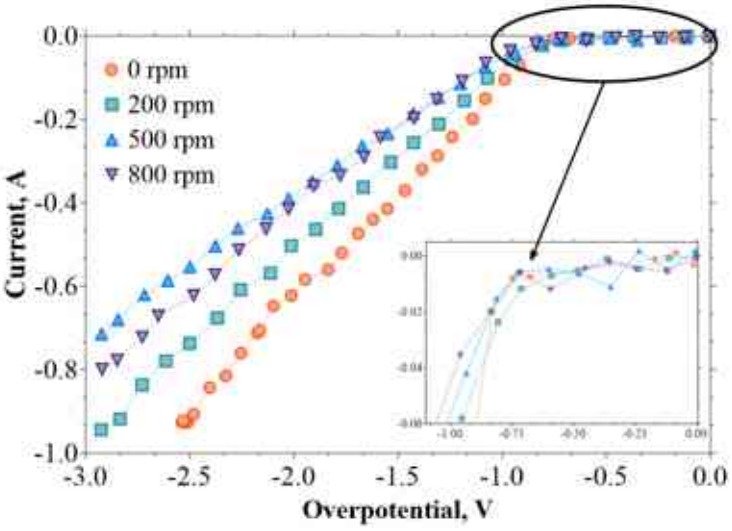

Fig. 5.20 Polarization curves obtained with agitated electrolytes of 90 g/dm^3 Ni.

Instead of increasing, agitation depressed the slopes. It is most likely caused by the refinement of the Ni crystals deposited, resulting in a smoother cathode surfaces and higher actual current densities with the same currents. The required overpotential is proportional to the actual current density. The excessive production of hydrogen bubbles during the deposition of the metal also results in flaky deposits easily detached

from the cathode surface. It is also observed that during the electrodeposition, the solution pH is increased from 4 to 13.5 corresponding to an excessive reduction of hydrogen ions.

With a blank pH 4.3 solution, there was almost no current observed even at higher cathodic polarizations. With 1 g/dm^3 Ni added to the solution, slight cathodic currents occurred, indicating that at this pH Ni deposition can be the initial process and hydrogen evolution can develop when the nickel coverage is almost complete, as seen in Fig. 5.19 referring to high-Ni electrolyte solutions The enhancement of H_2 evolution indicates how nickel deposition may contribute to the loss of useful current in the process of Zn electrodeposition.

Hydrogen evolution and metal deposition was studied in comparison with chloride solutions containing 90 g/dm^3 Zn, 90 g/dm^3 Ni, 90 g/dm^3 Zn + 1 g/dm^3 Ni, and only 1 g/dm^3 Ni. These results are shown together in Fig. 5.21. In the mixed solution, the initial small bubbles accumulated at the cathode surface more than in the pure Zn solution. The bubbles formed contribute to the total current on the one hand, but on the other, they may partly block the active sites as they accumulate.

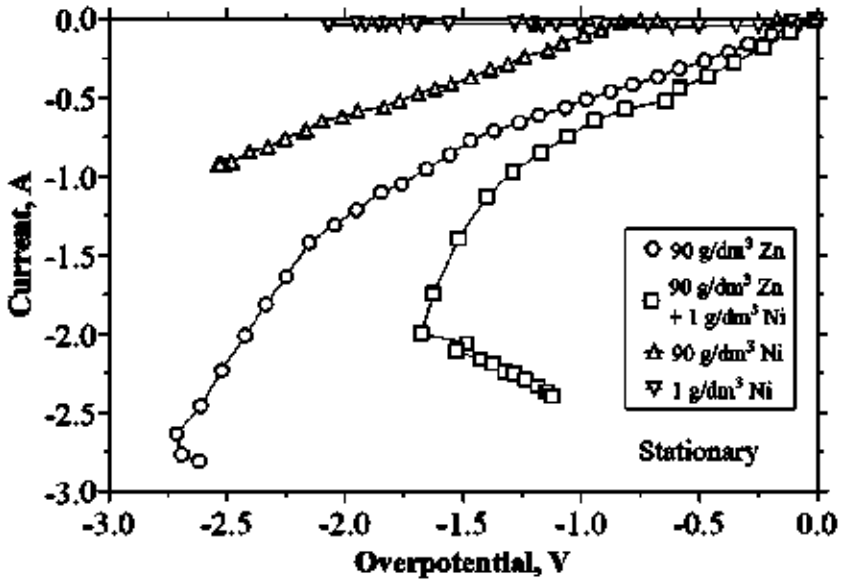

Fig. 5.21 Cathodic polarization curves of Zn, Ni and mixed solutions of pH 4.3 (1 min runs at 40 mV/s polarization speed).

According to the findings presented in Fig. 5.21, no appreciable deposition of any species was observed on the prepared copper cathode surface from the 1 g/dm^3 Ni – pH 4.3 electrolyte. With the concentrated (90 g/dm^3) nickel solution, some nickel initially deposited on the copper cathode, followed by excessive hydrogen reduction

beyond approx. –1 V polarization. It could be observed at the initial stage that the cathode surface was entirely covered with hydrogen bubbles. As the deposition occurs, it continuously grows with a uniform pattern, implying the co-deposition of nickel and hydrogen. At the end of the polarization cycle, some dendrites were observed in the 90 g/dm^3 nickel electrolyte. The fine outgrowths were formed at the edges of the active cathode surface where a better nickel ion supply could be produced. Dendrite formation also occurs from the zinc solution of high (90 g/dm^3) concentration, but nickel dendrites tend to grow with more extended tips, reaching further into the solution and appearing in a relatively uniform pattern at the cathode edge. However, Zn dendrites develop more branches and side-arms, as demonstrated by the first two photos in Fig. 5.22.

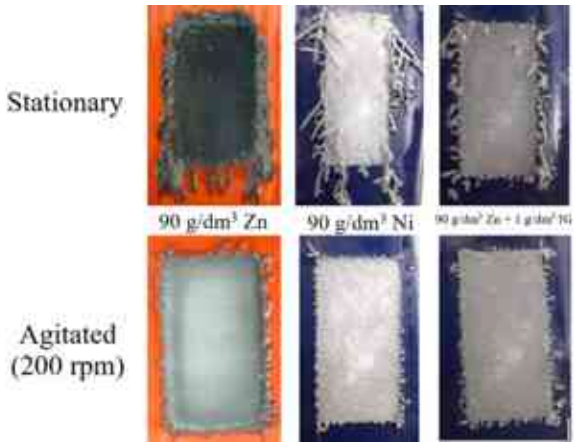

Fig. 5.22. The final potentiodynamic deposits from the 90 g/dm^3 zinc, 90 g/dm^3 nickel and from the mixed 90 g/dm^3 zinc + 1 g/dm^3 nickel solutions.

This dendrite formation is the reason for the back-turns (hooks) at the relevant polarization curves especially seen in the concentrated stationary solutions. However, stirring the electrolyte enhances the supply of ions over the entire cathode surface, thus fewer and smaller dendrites can develop. In this way more polarisation can be reached. Beside the ion transfer, it helps the hydrogen bubble removal.

In the mixed solution, 1 g/dm^3 nickel addition to the 90 g/dm^3 Zn exerts an inhibiting effect of metal deposition, by enhancing the evolution of hydrogen. This is supported also by the visual observations. The current increases while less deposit formation can be observed visually. Since the hydrogen reduction on the cathode surface was unavoidable, some loose powdery deposition was also observed. Stirring of the electrolytes generally helped reach higher cathodic polarizations with less hydrogen evolved. The slopes of the polarization curves are decreased as the dendrite formation

is strongly depressed. However, intensive stirring techniques are difficult to put into practice in the conventional electrolytic cell arrangements.

Although in the actual application of the electrowinning process, an inert anode is used, for the latter experiments the laboratory cell was set up with a zinc anode, to compensate for the larger amounts of zinc deposited from the electrolyte and to avoid excessive gas evolution. Figure 5.23 shows the polarization curve development tendencies as the anode material was fundamentally changed.

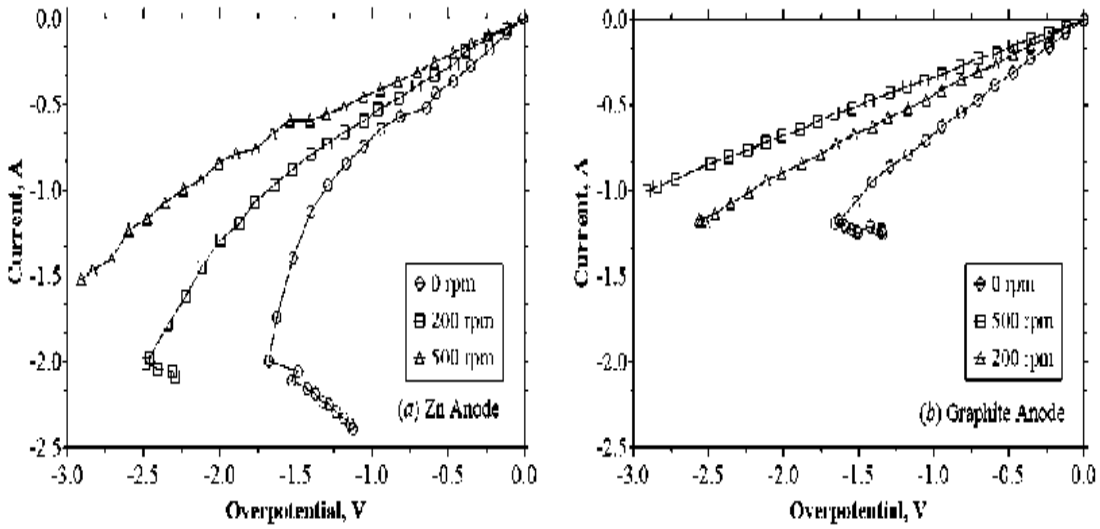

Fig. 5.23 Polarization curves of the mixed model solution (90 g/dm^3 Zn + 1 g/dm^3 Ni) with soluble (a) and inert (b) anode materials.

With the soluble Zn anode, the current reached during the experiment tends to be higher than that of graphite anode. However, the difference is not caused by the relatively negligible amount of the dissolved zinc supplied by the anodic process to the very high (90 g/dm^3) Zn concentration in the basic electrolyte. Rather the physical conditions are changed in the electrolyte when the soluble and the indifferent anodes are exchanged. This remarkable change in the polarization characteristics is caused by the introduction of the strong agitating effect of the gas stream generated at the anode. It is an efficient contribution to the mechanical stirring. Therefore, significantly denser and smoother cathodic deposits are produced with a strongly enhanced supply of metal ions. Hydrogen evolution was also mitigated. This helped produce denser cathodes resulting in generally lower cathodic currents with the inert anode, and weaker effects of increased stirring rate. Whereas in the case of the soluble anode, the agitating effect of the gas stream evolved at the anode is missing. In the stationary or mildly agitated electrolyte, the surface of the cathode developed rougher structures under this

condition, therefore less polarization was necessary for generating higher currents. The hook appearing at the end of the polarization curves indicates even severe dendrite formation. As the rate of stirring was increased the total cathodic current dropped and the polarization curves became shallower. This is the result of the finer crystal structure and the smoother surface assured by the better ion supply.

Nickel has been found to affect Zn electrodeposition from chloride solutions rather remarkably and detrimentally. Fortunately, nickel can be present in real SPL at a relatively low (not higher than 0.8 g/dm^3) level [11], and it can be definitely even lower after solution purification. Therefore, after having studied the major effects on the cathodic process above, further experiments needed to be carried out with less than 1 g/dm^3 Ni concentration in the 90 g/dm^3 Zn chloride solution. These results are summarized in Fig. 5.24.

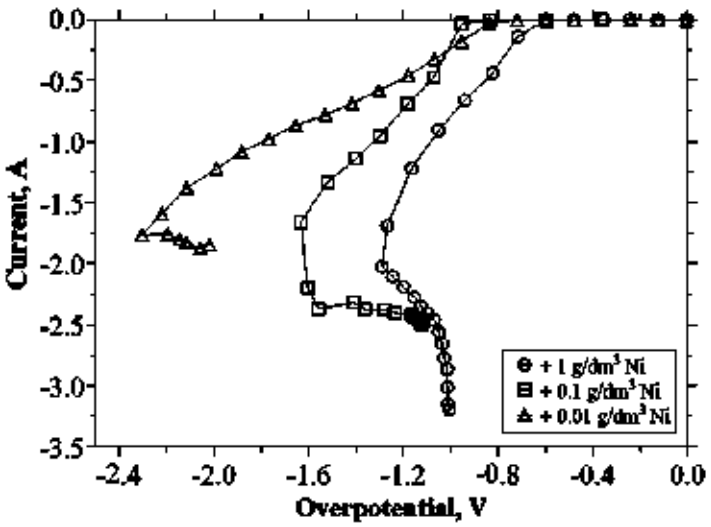

Fig. 5.24 Polarization curves in stationary solutions of 90 g/dm^3 Zn with slightly increased Ni concentrations.

Nickel addition made the polarization curves steeper. The increased current, however, mostly reflect stronger hydrogen evolution. However, as another possible effect, the sharp hooks at the ends of the polarization curves indicate some drastic – even dendritic – roughening of the deposit. It also contributes to the development of higher total currents because of the decreasing actual current densities. The relative importance of the two detrimental effects can be assessed by measuring the deposited mass, as demonstrated below. When agitation of the electrolyte was introduced, the cathodic current got strongly depressed, indicating a better supply of the metal ions,

thereby depressing the evolution of hydrogen and producing smoother deposit structures. The deposition of metals on the cathode surface can be seen in Fig. 5.25.

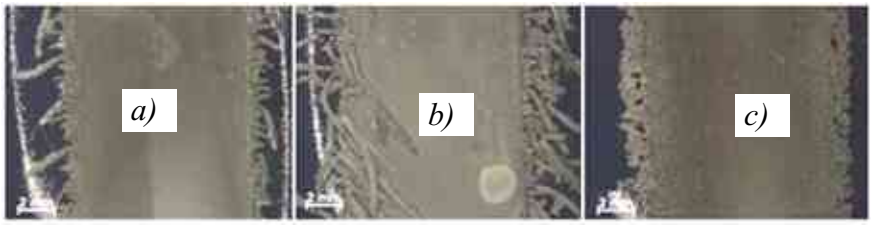

Fig. 5.25 The final deposits of mixed solutions with a) 0.009 g/dm^3 ; b) 0.09 g/dm^3 ; c) 0.9 g/dm^3 Ni in the 90 g/dm^3 Zn solutions of pH 4.3.

Nickel addition of 0.9 g/dm^3 could eliminate the excessive dendrites from the final deposit surface during the potentiodynamic runs under the applied conditions. In contrast, the other two solutions of lower Ni concentration showed more dendrites at the final deposit, but their brighter colours (characteristic of Ni co-deposition) proved the contamination of zinc deposit even with the low Ni concentrations in the electrolyte. With the higher magnification in Fig. 5.26, it is shown that the deposit obtained with the higher Ni concentration in the solution has a looser structure.

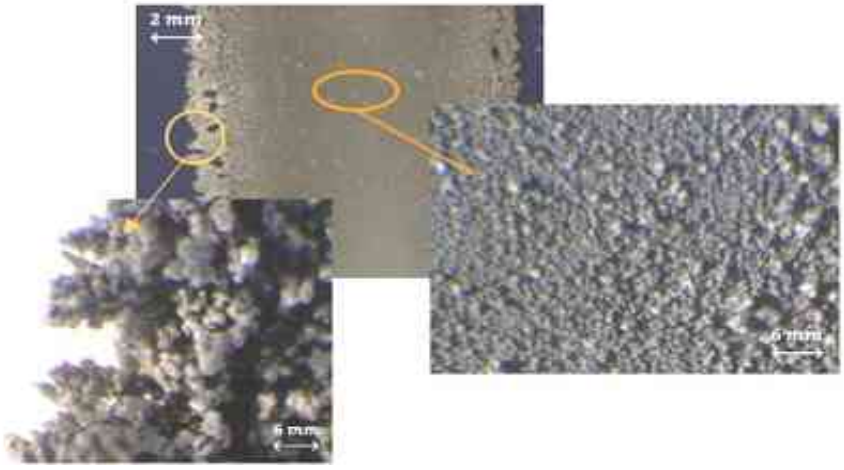

Fig. 5.26 Higher magnification of surface segments of the final deposit obtained with the solution of 0.9 g/dm^3 Ni in the 90 g/dm^3 Zn (pH 4.3).

The polarization experiments were carried out with copper substrates as starting cathodes of carefully measured masses. The cathodes were weighed after rinsing with distilled water and drying. It was followed by a complete dissolution of the deposit from the copper substrate in 1 M HCl with the addition of a few drops of HNO_3. Finally, the nickel and zinc mass was calculated from the analytical results. Figure 5.27 demonstrates the effect of nickel addition on the purity of Zn deposit obtained from the mixed electrolytes.

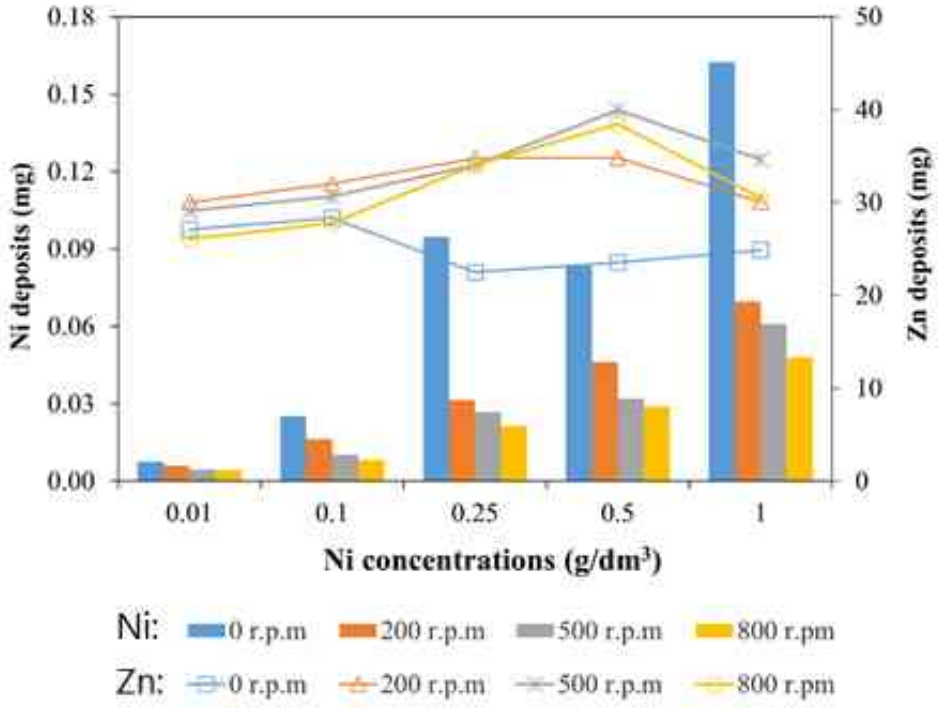

Fig. 5.27 The effect of nickel concentration in the 90 g/dm^3 Zn (pH 4.3) electrolyte on the masses of zinc and nickel deposited in the potentiodynamic runs.

The bars in Fig. 5.27 show that the mass of nickel deposited from the mixed solutions significantly increases as the Ni concentration is increased in the electrolyte, while the masses of deposited zinc (points) are practically unchanged. It means that the purity of the produced Zn is appreciably higher – with respect to Ni – if nickel is efficiently eliminated from the solution before electrowinning. Increasing the stirring intensity beyond 200 r.p.m. did not result in increased efficiencies of Zn deposition. In contrast, the deposited mass of nickel slightly decreases with more vigorous stirring. It is an indirect effect of the smoother Zn deposits produced.

6. Efficient electrowinning of Zn from chloride media

Although the potentiodynamic study has revealed some important characteristics of the cathodic process, actual deposit production by galvanostatic electrowinning experiments were considered necessary to reveal the practical efficiency and morphology characteristics. Galvanostatic studies of Zn electrodeposition was conducted with applied initial current densities ranging from 150 to 4800 mA. Table 6.1 shows the compositions of the electrolytes filled in an electrochemical cell containing 50 cm^3 of starting electrolyte, and the set current densities (c.d.) referring

to the starting geometric surface are of the cathode. The actual current densities may become lower as the deposition of Zn produces irregular outgrowths and rough crystal structures. However, this change in the specific surface area is not known numerically, therefore the geometric current densities are named “apparent”.

Table 6.1 Electrolyte composition and applied parameters of the experiment

Zn Concentration	pH	NaCl Concentration	Current Density
6, 12.5, 25, 50, and 100 g/dm^3	0; 1; 2; 5	0, 1, 2, 4, 6 g/dm^3	~ 150, 300, 600, 1200, 2400 and 4800 A/m^2

The testing setup, shown in Fig. 6.1, was based on the regulated analogue current supplies linked to the electrolysis cell and the multimet0er by alligator clamps. The electrode potential, cell voltage, and pH were monitored during the electrowinning.

Fig. 6.1 Galvanostatic power supplies (a) and the experimental cell (b).

The cathode potential was measured vs. a saturated calomel reference electrode (SCE) connected to the surface of the 1 cm^2 cathode shown in Fig. 6.2. A dimensionally stable anode (DSA) was placed at the opposite side. The cathode mass was measured before and after each experiment to calculate the current efficiency.

In general, the zinc deposit starts to grow in a quasi-uniform pattern on the cathode surface, showing a quasi-homogenous electric field and a uniform current distribution initially. However, the deposition is getting gradually thicker at the edges of the cathode. It is commonly known as the edge effect. The preferred deposition at the protrusions of the edge concentrates also the further metal deposition mostly in these regions. The investigation has also shown the transition from the dendritic crystal growth into the globular bulb development.

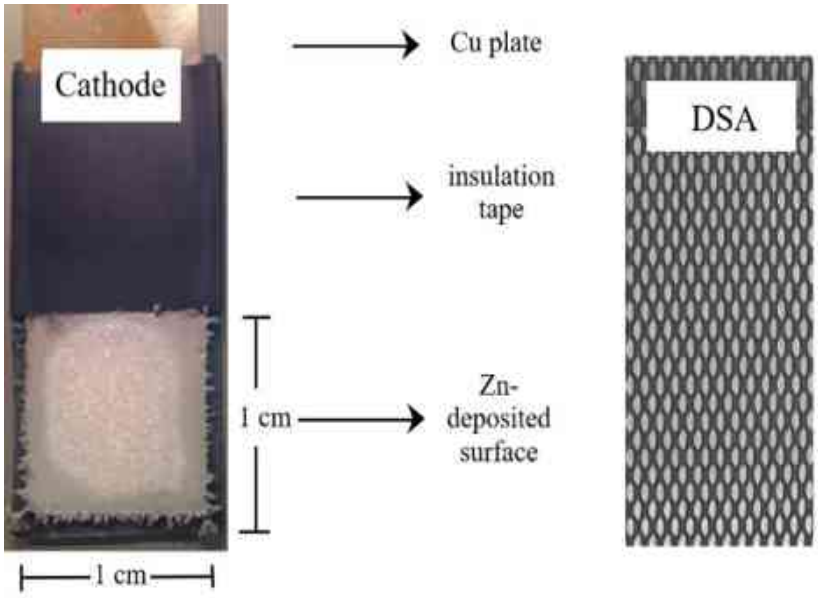

Fig. 6.2 The cathode (left) and the anode (right) used for electrowinning.

Samples of the electrolyte (1 cm^3) were taken from the cell and diluted to evaluate the Zn concentration using atomic absorption spectrophotometry (AAS). The cathode surface was photographed using an optical microscope to examine the changes in the macrostructures of the deposit.

6.1. Efficiency and quality characteristics of the electrowinning process

Primarily, the effects of the initially set pH and the apparent (geometric) current density were targeted in various concentration ranges. The current efficiency was calculated by the expression:

$$c.e. = \frac{n\,\mathbf{F}\,\Delta m}{I\,t\,M_{Zn}} \tag{6.1}$$

where Δm is the change in the cathode mass, n is the valence of the metal deposited, **F** is Faraday's constant, t is the time of electrolysis, and I is the applied current.

As shown by comparing the diagrams in Fig. 6.3, there is a definite dependence of the *c.e.* on the Zn concentration in the stationary electrolyte. So, as to obtain commensurate deposit masses in all the experimental runs, the same amounts of electric charge (864 As) were supplied to the electrolytic cell. For example, the electrolysis time was 2 h with the 300 A/m^2 setting of the geometric (initial) current density (*c.d.*). Due to the irregularly growing crystals, the actual current density value cannot be determined numerically, therefore the "apparent" c.d. values are used.

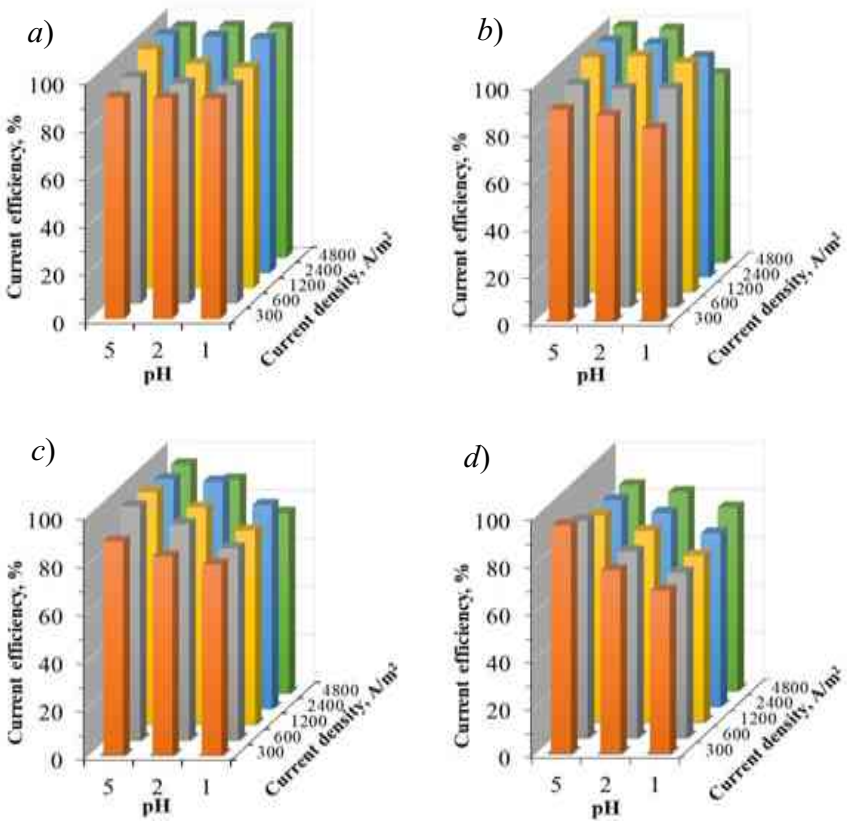

Fig. 6.3 The current efficiency as the function of the initial pH and the apparent current density with a) 100 g/dm^3, b) 50 g/dm^3, c) 25 g/dm^3, d) 12.5 g/dm^3, Zn in the stationary solution. (charge supplied: 864 As).

Decreasing Zn concentration in the examined wide range decreases the current efficiency by allowing the secondary cathode reaction of H_2 evolution. it is clearly seen by comparing the average results in Figs. 6.3.*a* through *d*. Except for the highest Zn concentration (Fig. 6.3.*a*), decreasing the initial pH could also significantly deteriorate the conditions by increasing the ratio of hydrogen evolution in the cathodic current. The electrodeposition from the electrolyte of the highest examined Zn concentration offered an average c.e. of ~ 90%, and the maximum of 99% was reached with pH 5 and 2400 A/m^2 c.d. settings (Fig. 6.3.*a*). On the other hand, at the lowest examined Zn concentration (Fig. 6.3.*d*), the relevant average was about 20 % lower.

As the pH values were found decreasing during the experiments with the starting solution of pH 5, a significant oxygen evolution occurred at the inert anode. In contrast, with the higher initial acid concentration (pH 1), there was an increase in the pH values, inferring a surplus of hydrogen evolution at the cathode. For the balance of the transferred charge, the anode reaction must have included a higher ratio of chlorine evolution in this case. Especially with the high (100 g/dm^3) Zn concentration in the chloride electrolyte, the chlorine evolution from the anodic reaction could be

smelled. Dissolved Cl_2 transported to the cathode may cause corrosion, deteriorating the *c.e.* However, as the *c.e.* values were significantly higher at the highest Zn concentration and increased with higher initial pH settings, the main effect is attributed to the hydrogen evolution. Referring to the results obtained with the highest initial pH setting and sufficiently high Zn concentration, increasing the c.d. can increase the current efficiency by outweighing chemical cathode corrosion. This effect can be clearly noticed in Figs. 6.3.*a* and *b*. The main tendencies continue as the Zn concentration is decreased until 12.5 g/dm^3 (Figs. 6.3. *c-d*). However, if the Zn concentration is further reduced, hydrogen evolution becomes dominant and hardly any appreciable efficiency is obtained. The examined main parameters also affect the morphology of the obtained deposit, as shown in Fig. 6.4.

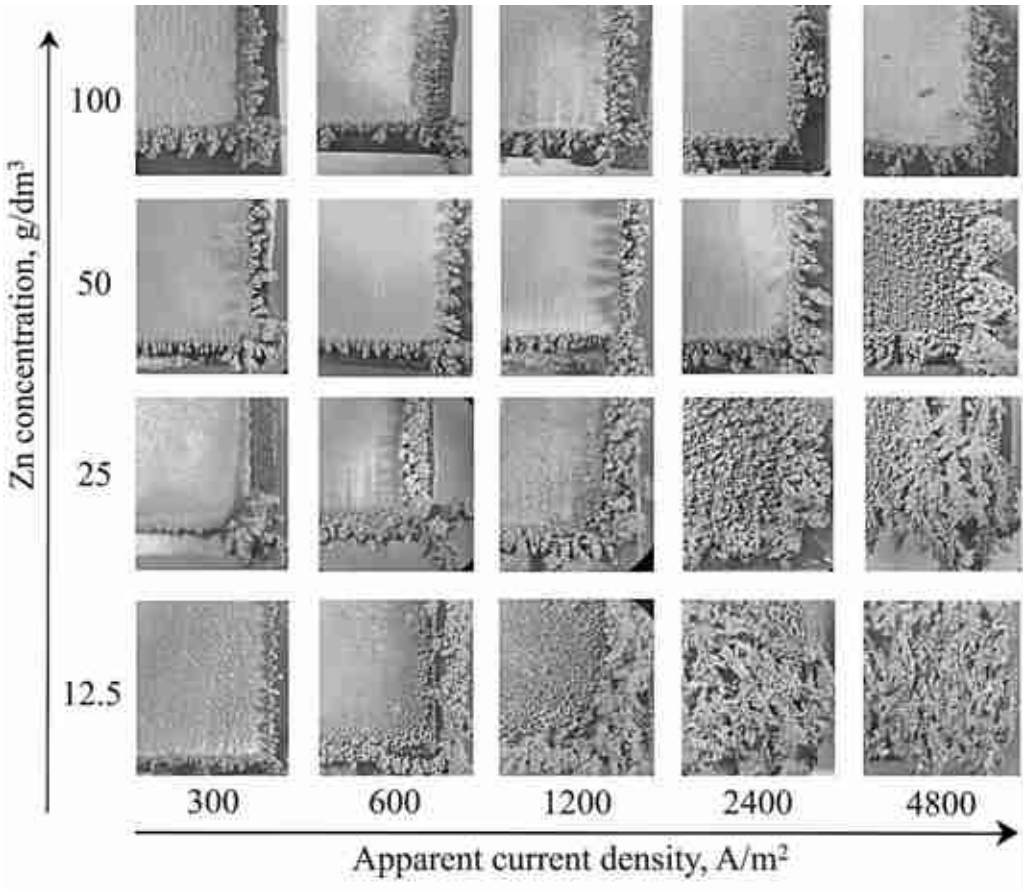

Fig. 6.4 The morphologies of the deposits obtained with different apparent current densities from electrolytes of different Zn concentrations (initial pH 5).

Protrusions of the deposit developed at the edges of the cathodes generally because of the uneven current distribution caused by the uneven electron density in the metal and the preferential ion supply from the surrounding electrolyte. Dendrites could cover the entire surface at lower Zn-concentrations combined with high current densities. Due

to the depletion of the electrolyte in the electroactive Zn species in the vicinity of the cathode, the dendrites tended to grow further out from the base surface in the stationary solution.

The morphology of the cathodic deposit is influenced by the shape of the individual nuclei and the orientation of the developing crystals. The characteristic radii of spherical nuclei formed in a homogeneous nucleation can be approximated as [107]

$$r = 2\frac{\gamma \mathrm{V_m}}{\mathrm{F}\eta_n}, \tag{6.2}$$

where γ is the surface energy, V_m is the molar volume of Zn, F is the Faraday constant, and η_n is the nucleation overpotential. The radius, *r,* is inversely proportional to the overpotential (η), if no diffusion effect is involved. Thus, higher current densities should imply finer crystals, however the shortage of the ion supply causes the development of dendrites growing out from the surface.

The structures obtained with different initial pH settings can be observed in Fig. 6.5. Despite the missing agitation, the tendency of crystal structures with the c.d. can be seen as suggested by Eq. (6.2). However, with the higher pH, the hydroxide precipitation appeared at higher c.d. Due to the reduction of H^+ ions, the local pH may rise, especially at the irregularities, where the white precipitation appears stronger.

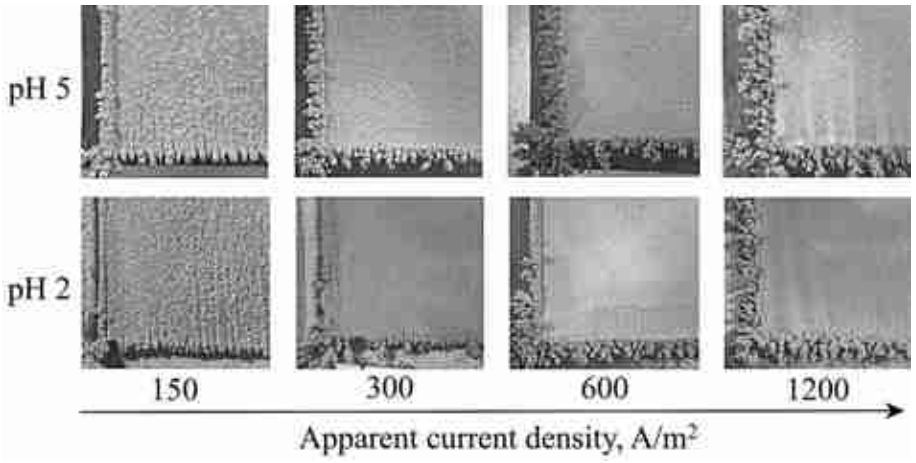

Fig. 6.5 Surface structures observed on the cathodic deposit from 50 g/dm³ Zn chloride electrolytes of pH 2 and pH 5 at various apparent current densities.

The H_2 bubble formation can cause discontinued crystal nucleation, which may develop into pits at the surface. At lower current densities they may get arranged in lines, by the enhancing effect of micro-cavities becoming available as the bubbles get

rising. However, at higher current densities the free streaming of the gas creates more homogeneous conditions.

6.2. The effects of adding NaCl to the electrolyte

It is observed that additional chloride ions affect the amount and the structure of the Zn deposited. Figure 6.6 shows the determined dependence of the c.e. values on the NaCl concentration added to the slightly acidic (pH 3) $ZnCl_2$ solutions of the set Zn concentrations. If rough surfaces were obtained, the c.e. was determined from the analysed difference in the final and the starting Zn concentrations in the solution.

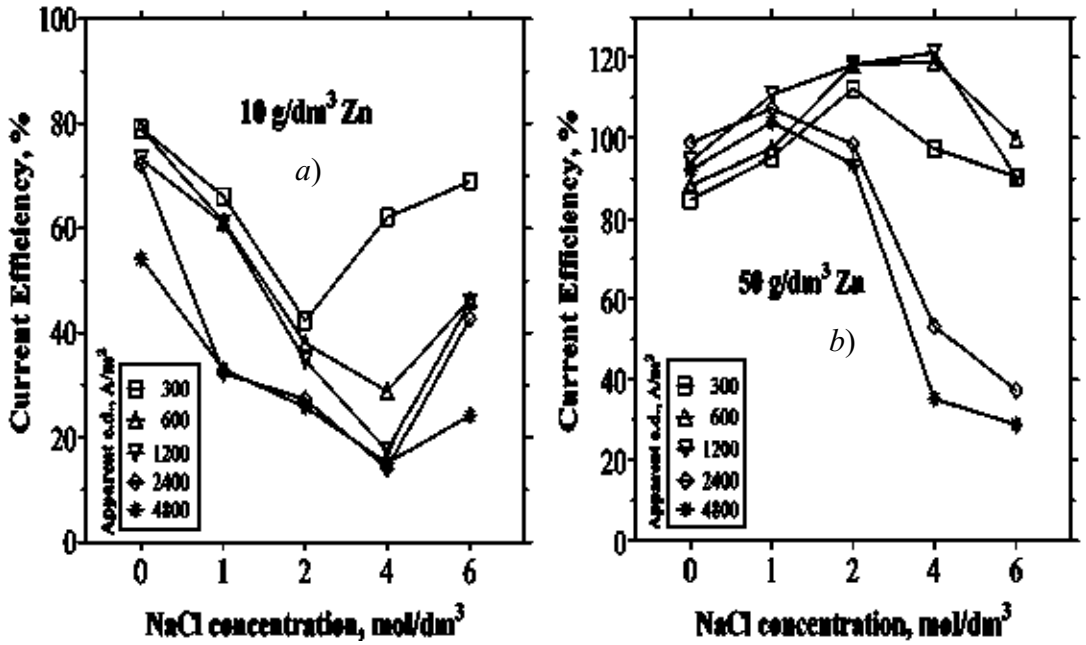

Fig. 6.6 The current efficiencies as functions of the added NaCl concentration at varied current densities in Zn electrolytes of 10 g/dm³ (a) and 50 g/dm³ (b) (pH 3).

In the electrolyte of the lower (10 g/dm^3) Zn concentration (Fig. 6.6.*a*), the c.e. dropped as the Cl^- ion concentration was increased, and this drop was stronger as the c.d. was increased. The lowest value of ~15% resulted with 4M NaCl addition and the highest 2400 – 4800 A/m^2 apparent current densities. The low Zn concentration (10 g/dm^3) of the chloride electrolyte generally provided only loose and spongy deposits, just weakly adhering to the substrate, and the addition of NaCl made the conditions even worse. However, further increasing the NaCl concentration beyond 4 mol/dm^3 resulted in slightly increased current efficiencies, which can be attributed to the rougher crystal structure of higher actual surface area. In general, this low (10 g/dm^3) Zn concentration falls short of practical interest.

On the other hand, in the case of the higher (50 g/dm^3) Zn concentration (Fig. 6.6.*b*), the c.e. value continuously increased with the added NaCl in the lower range. The beneficial effect can be attributed to the Na^+ ions, which are more likely to aggregate at the protrusions, acting as an electrostatic shield, thus minimizing the tip effect of an initial dendrite root [108]. However, the tendency changes at higher NaCl concentrations. The drop of the obtained c.e. occurs from lower NaCl additions if the c.d. is higher. This pattern suggests that the high salt concentration increases the viscosity and decreases the transport of the electroactive species to maintain the required current. The final cathode surfaces obtained in the electrolyte of 50 g/dm^3 Zn concentration are shown in Fig. 6.7 by the array of stereo microscopic photographs of the cathodes referring to different NaCl additions.

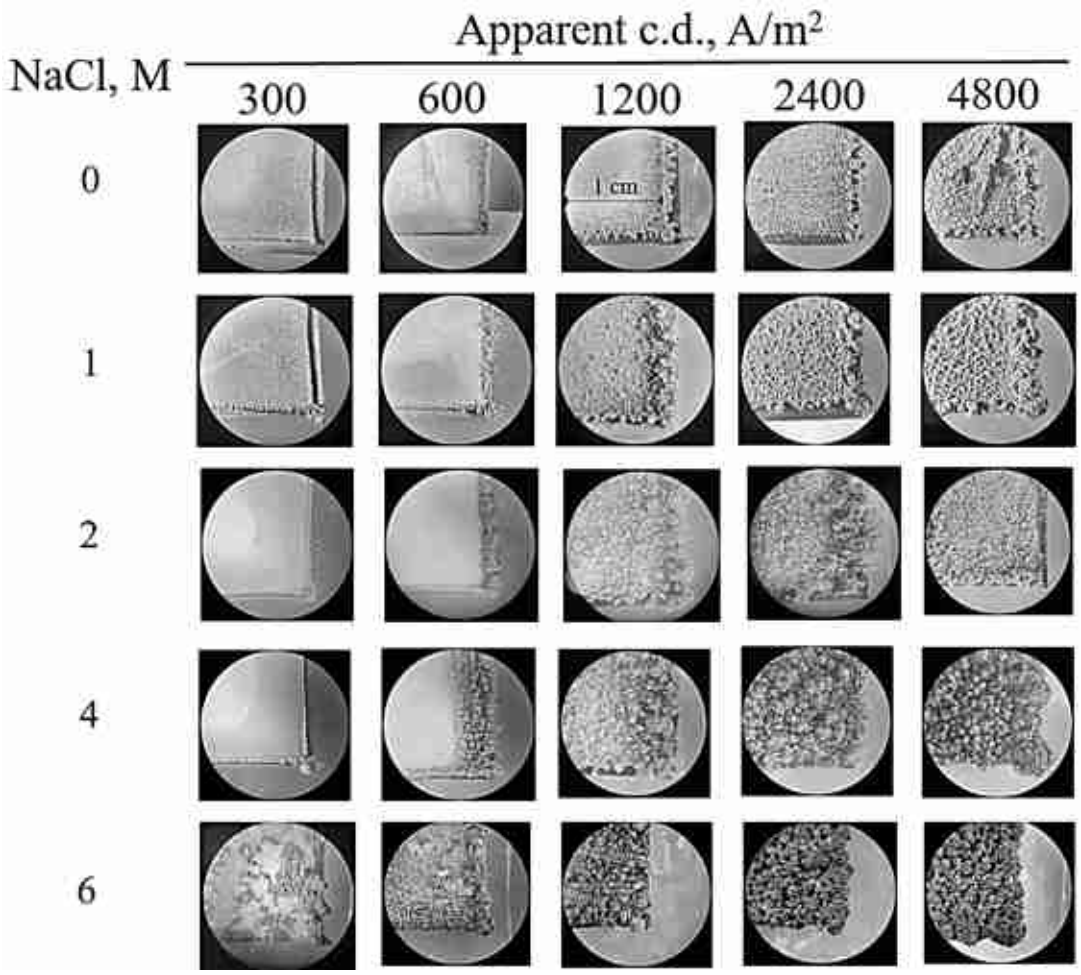

Fig. 6.7 Comparison of the stereo microscopic pictures of the cathodes obtained with different apparent current densities and NaCl concentrations (50 g/dm^3 Zn).

The virtual current efficiency results obtained with the electrolytes of the relatively high (50 g/dm^3) Zn concentration in the higher ranges of (2–4 mol/dm^3) NaCl concentrations and the lower (300–1200 A/m^2) apparent current densities appeared

even surpassing the 100% level. It is associated with the local increase in the pH caused by an intensive reduction of the H^+ ions, causing precipitation. The white coverage of the metallic structure appears at the corresponding surface photographs. The highest (2400 and 4800 A/m^2) apparent current densities combined with the highest (4 and 6 M) NaCl additions have developed loose and spongy deposits easily detached from the surface. The increased resistivity of such deposits was indicated by the increasing cell voltages. Also the evolution of hydrogen is facilitated by this ragged morphology, which is in line with the obtained low current efficiencies (Fig. 6.6.*b*). In these cases, the intensive hydrogen evolution could increase the pH considerably also in the bulk electrolyte. The strongly increasing bulk pH curves in Fig. 6.8 almost exactly mirror the dropping c.e. curves in Fig. 6.6.*b*.

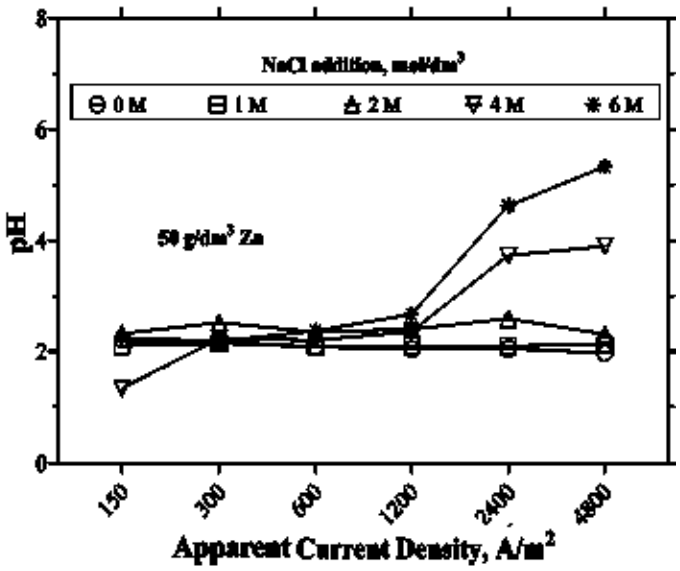

Fig. 6.8 The final pH values measured in the bulk electrolyte (starting pH 3).

The increased pH in the bulk electrolyte indicates that the side reaction at the cathode associated with the reduction of the H^+ ions (H_2 evolution) can surpass the rate of the regular anodic reaction of oxygen evolution. The balance is made up by the evolution of Cl_2. In this case, the transport of dissolved chlorine to the cathode may cause corrosion of the deposited metal, further decreasing the current efficiency.

The comparison of the corresponding surface photographs suggests that a moderate addition (1 – 2 M) of NaCl while setting lower current densities (< 600 A/m^2) enhances a denser Zn deposition and suppresses dendrite formation. However, further increasing the c.d. at high levels of NaCl addition would divert the deposition strongly towards the edges, resulting in extreme edge thickening and surface roughness. For practical

applications, the ranges of higher than 600 A/m^2 c.d. and more than 4 M NaCl concentration should be avoided. Actually, the preliminary anion-exchange purification and electrolyte preparation can offer the required Zn and NaCl concentration of the solution, which corresponds to the model solutions found suitable for the most efficient electrodeposition.

Li et al. [109] concluded that zinc deposition initially takes place in a regularly arranged crystal structure. The hexagonal closed-packed Zn crystals tend to expose the (002) base plane – parallel to the substrate - thereby minimizing the energy associated with atomic migration. However, as shown in the time series of the pictures in Fig. 6.9, a heterogeneous growth pattern is developed gradually. With the mass of the deposit tending to appear in rough globular forms over the entire surface.

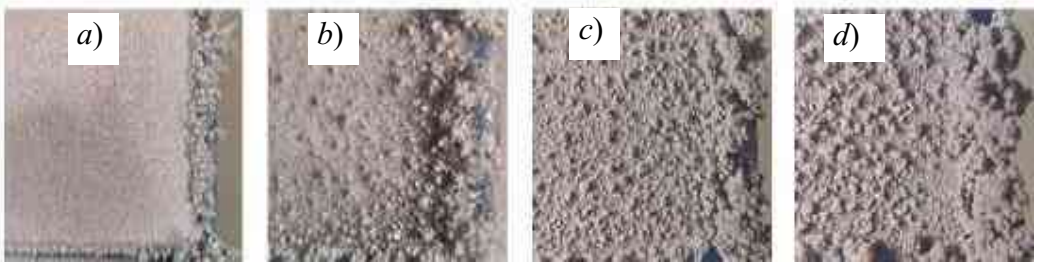

Fig. 6.9 Observed structures of Zn developed after 5 min (a), 15 min (b), 25 min (c), and 30 min (d) of the electrodeposition (pH 3, 1200 A/m2, 50 g/dm3 Zn, 1 M NaCl).

The hexagonally ordered initial growth turns into a non-epitaxial propagation of the crystals, also incurring a subsequent change in the current distribution. Finally, a non-uniform bulbous surface is produced. At the same time, hydrogen bubbles start forming at the roots of the produced crystals. It causes the weak adherence of the deposit observed when applying the examined highest apparent current densities. The side-reaction of H^+ ion reduction can become intensive if high c.d. is applied, in combination with high NaCl concentrations in the high (50 g/dm^3) Zn containing electrolyte, or in the electrolyte of low (10 g/dm^3) Zn concentration even at moderate (>300 A/m^2) apparent current densities. The intensive evolution of hydrogen is also associated with a considerable local increase in the pH and the formation of the $Zn(OH)_2$-type precipitate at the roots of growing crystals may enhance the detachment and re-dissolution of some Zn metal. The hydroxide precipitation can become abundant at the roots and also around the tips of the crystal protrusions. The pictures of the wet and dried precipitates are compared in Fig. 6.10.

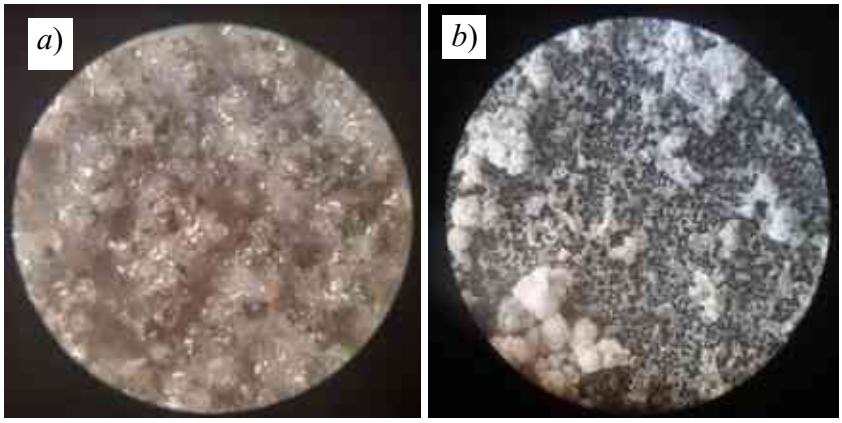

Fig. 6.10 The precipitates formed at 10 g/dm^3 Zn concentrations in wet (a) and dried (b) states (1200 A/m^2, 2 M NaCl, initial pH 3).

While the highest value of pH 6.6 was reached in the bulk electrolyte, the local pH at the surface may have become even higher. According to the Pourbaix-diagram in Fig. 5.1.*b*, the actual compositions of the precipitates formed at the outer tips and at the roots may differ according to the local pH.

Conclusions

A novel method to recover pure Zn from SPL has been devised by combining an efficient anion exchange separation, electrolyte preparation and a suitable electrowinning in a simple open cell. Iron and all the practically important other impurities can be eliminated from the chloride solution containing also NaCl, followed by de efficient electrodeposition of pure Zn.

Recovery of metal from spent pickling liquor coming from the galvanizing industry is widely investigated, but preparing a pure metal from this waste liquor has been out of the conventional topics. The previous research in the Laboratory of Chemical Metallurgy, University of Miskolc was experimenting the recovery of pure iron from SPL without further processing of the Zn fraction. Furthermore, the SPL coming from the stripping bath has not been treated separately. The proposed technique offers minimizing the environmental issue caused by SPL, while adding extra value to the recovered metal. It also fulfils the BAT requirements of SPL regeneration method.

Synopsis

Based on the various tendencies of chloro-complex formation, the metals dissolved in the SPL, a comprehensive purification procedure has been devised. Iron, as the major

impurity, can be removed directly upon the loading and the first rinsing of the chromatographic column holding the strongly basic anion-exchange resin together with the impurities incapable of forming stable anionic chloro-complex species (Al, Mn, Ni and Co). Even though most of the Fe is in the reduced Fe(II) form in the SPL – reacted with the iron surface and the sludge particles – the process still includes a reducing pre-treatment by inducing com-proportionation to assure the uniform ferrous state. Among the practical impurities the separation of only Pb is incomplete, but it can no longer exist in the industrial stream of galvanizing industries in the EU. Although, minor quantities of Cu and Fe may still remain in the final solution, a cementation or pre-deposition technique may eliminate the residues of these more noble contaminants.

The equilibrium studies of the anion-exchange distribution in NaCl solutions showed similar tendencies to those already known in HCl media. The anion-exchange chromatographic separation was devised – with the finer tuning of the parameters – according to the specific equilibrium and kinetic experimental results. The effects influencing the practical breakthrough volumes were also taken into consideration for the optimization of the separation procedure. The best practical loading volume was found close to the gross volume of the resin bed if higher flow rates (3 – 4 BV/h) are to be applied. Besides the extremely high elimination ratios of the important impurities, about 97% of Zn can be obtained in the main eluate by applying the optimized sequence.

To attain a satisfactory cathodic deposition of zinc from the purified chloride solution, it is essential to appropriately adjust the main parameters. The provide a sufficient concentration of Zn, the accurate control of pH, and the selection of the correct range of current density are indispensable requirements in an open cell, while the main impurity, iron can change the conditions by intensifying the evolution of hydrogen even at less than 1 g/dm^3 concentrations. Similar effects of minor Ni contamination were pointed out. The role of these practical parameters and that of the application of electrolyte agitation on the cathodic process could be revealed by the potentiodynamic experiments.

The long-term electrolysis was efficient with Zn concentrations higher than 50 g/dm^3 with relatively high (600 – 1200 A/m^2) apparent (geometric) current densities and ~ pH 3 applied. At as low as 10 g/dm^3 Zn-concentration, no conditions were found

suitable to produce acceptable morphologies of the deposit. At higher apparent current densities than 1000 A/m^2, the reduction of the H^+ ions also resulted in strong increasing pH values leading to considerable hydroxide precipitations. The addition of NaCl could result in complex effects. While the Na^+ ions could mitigate the rough crystal structures, the increasing salt concentration inhibited the transport process and enhanced dendritic crystal growth.

New scientific results

C1. Claims on Zn electrolyte purification by AIEX

C1.1. The replacement of HCl by NaCl provides similar anion-exchange tendencies of zinc and iron, by just slightly decreasing the maximum distribution coefficient of Zn occurring at 2-2.25 M free Cl^- concentration. Any type of strongly basic quaternary amine anion-exchange resin can be used. The new equilibrium distribution functions are presented in the figure below.

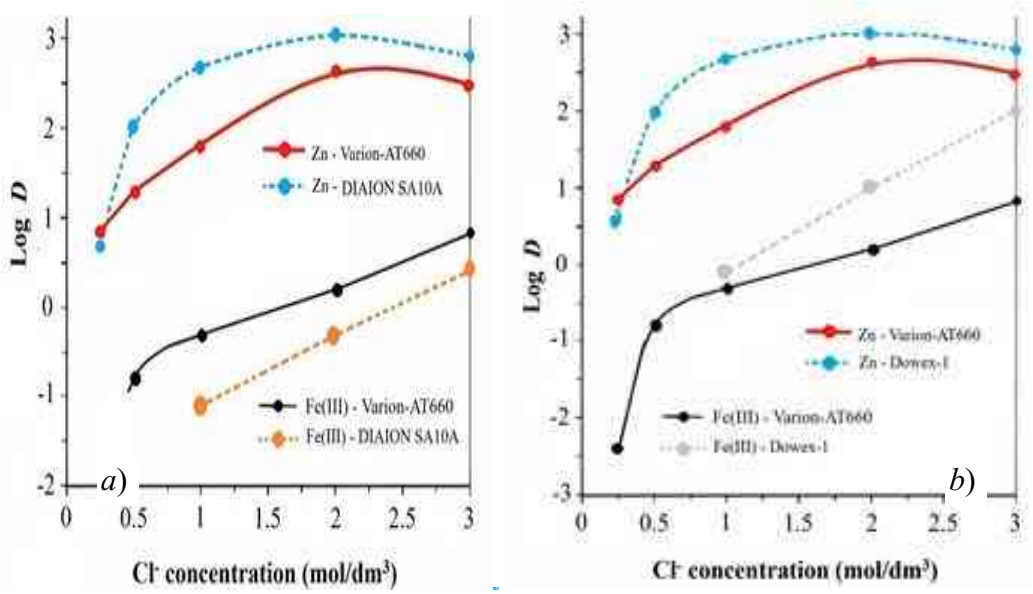

The anion-exchange distribution functions determined for Zn and Fe(III) in NaCl solutions (solid lines) with Varion AT660 resin, and earlier results [60] [97] in HCl solutions with Diaion SA10A (a) and Dowex-1 (b) resins (dashed lines).

C1.2. Iron, as the main impurity, is hard to separate from Zn in the trivalent state. Therefore, the process is effective after reducing the contained Fe(III) to Fe(II) by the com-proportionation reaction, using powdered or granulated iron (mild steel).

After this pre-treatment, any appreciable anion-exchange sorption of iron is avoided at the free Cl^- concentration where Zn is strongly sorbed.

C1.3. The loading of the SPL and the first rinsing step can be carried out with ~ 2 M NaCl solutions, but the elution of Zn should be carried out with a ~ 0.05 M HCl eluent. Further reducing the HCl concentration to 0.001 M can improve the Zn elution and still avoids hydrolytic precipitation, but any Cd impurity is also released from the resin. A 1 - 2 bed volumes/hour (BV/h) flow rate should be generally applied, and lower flow rates can produce better separations.

C1.4. The optimised anion-exchange purification procedure is shown below.

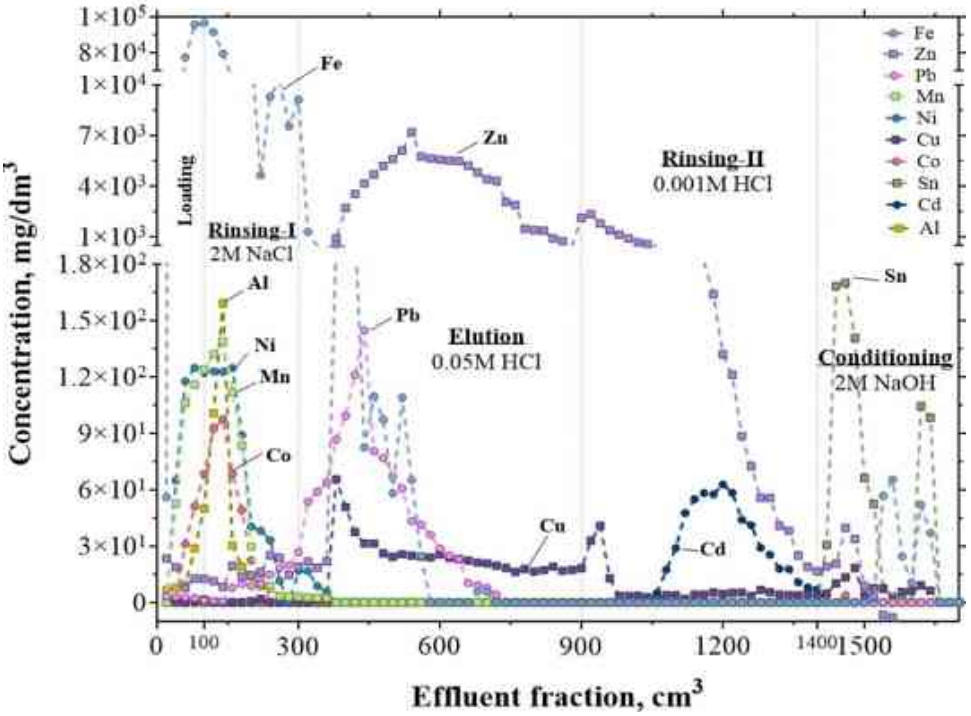

The optimised anion-exchange separation procedure.

This procedure can offer close to 1000 standard purification ratios for Zn in the SPL referring to the main impurities of Fe, Al, Ni, Co, Cd, Mn, and Sn while the yield of Zn is higher than 90 %. The purification ratios of Pb and Cu are however just around 3 – 4. These elements are practically negligible in the SPL, or they can be eliminated by cementation, if required.

C2. Claims on characteristics of Zn electrodeposition from chloride media

C2.1. In the stationary solution corresponding to the purified SPL (~ 50 g/dm^3 Zn, pH~2) cathodic polarization develops first a limiting current plateau around -0.7 - -1 V. The initial rise of the current is dominated by the H^+ reduction. The current plateau is caused by the blocking of the active surface, as the initially formed H_2 bubbles are still attached before growing to the size to be released, it is followed by a more dominant Zn^{2+} reduction induced by the roughening of the deposit. The interlinked phenomena are demonstrated in the figure below.

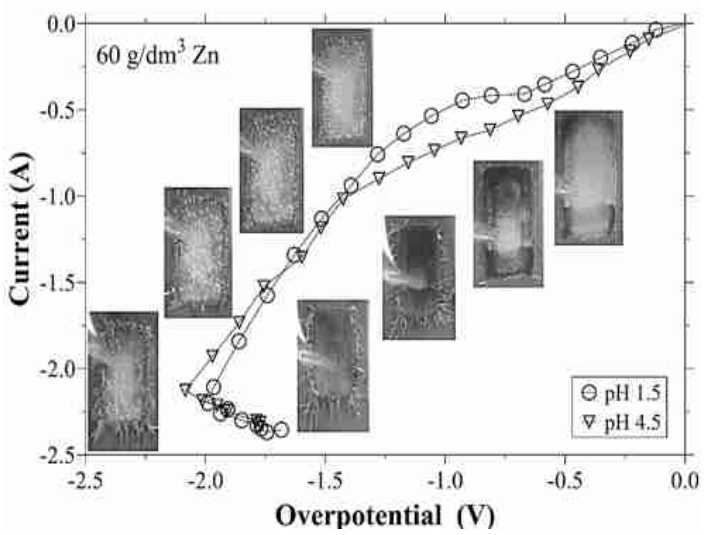

Polarization curves of Zn (60 g/dm^3) electrodeposition from chloride media of different acid concentrations (pH 1.5 and 4.5).

C2.2. Increasing the Zn concentration (even beyond 60 g/dm^3) depresses the H_2 evolution significantly. The electrode surface is less blocked by gas bubbles, thus the effective current density is reduced, while the Zn supply to the surface by the natural diffusion is also increased. This combined effect results in a more uniform zinc deposit and less dendrites grown at the cathode edges. The supply of the electroactive zinc species at the electrode interface plays a decisive role in the deposit macro-morphology.

C2.3. Contaminating the SPL electrolyte with Fe and Ni in the (~ 1 g/dm^3 range), hydrogen evolution will increase because of its lower overpotential to both elements. However, the generated gas bubbles – until released – block the actual site, inhibiting the further preferential deposition and allowing zinc of higher hydrogen overpotential to continue depositing. This kinetic phenomenon is behind

the “anomalous” electrodeposition from a mixed solution. At increased concentrations of these impurities, the dendrites at the edges of the cathode are getting not just fewer but also shorter.

C2.4. In high ranges of Fe concentration (30 – 60 g/dm^3), the intensive generation of hydrogen bubbles agitates the electrolyte solution in the vicinity of the cathode surface. This agitating effect promotes Zn deposition but later it is outweighed by the chemical effect of the increasing local pH. It may trigger a local formation of hydroxide particles, hindering the deposition of the less noble zinc. Iron deposition results in more contaminated zinc deposits.

C3. Claims on the efficiency of Zn electrowinning from purified chloride solution

C3.1. The electrodeposition from the electrolyte of the highest examined Zn concentration (100 g/dm^3) offers an average current efficiency ~ 90% in the pH 1 – 5 and the current density of 300 – 4800 A/m^2 range. The maximum of ~ 99% can be reached with pH 5 and 1200 - 2400 A/m^2 settings. On the other hand, at the lowest examined Zn concentration (12.5 g/dm^3), the corresponding average is about 20 % lower. The reduction of H^+ ions at higher current densities can raise the local pH, especially at the irregularities, where hydroxide precipitation appears. The characteristics are graphically shown below.

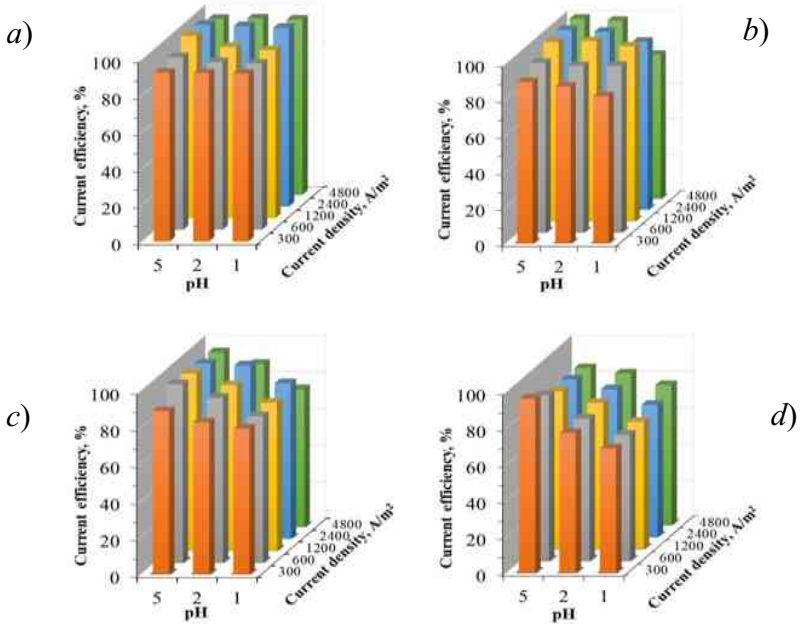

The current efficiency as the function of the initial pH and the apparent current density with a) 100 g/dm^3, b) 50 g/dm^3, c) 25 g/dm^3, d) 12.5 g/dm^3, Zn in the stationary solution. (charge supplied: 864 As).

C3.2. Dendrite formation is promoted by higher current densities and lower Zn-concentrations in the bulk electrolyte. Due to the depletion of electroactive Zn species in the vicinity of the cathode surface, dendrites grow further out from the base surface. The protrusions mostly develop at the edges of the cathode because of the uneven current distribution, due to the skin effect of the electron density in the metal and the preferential ion supply around the edges of the electrode in a stationary solution.

C3.3. Due to the oxygen evolution at the inert anode, the initial pH 5 values decrease in the practically high Zn-containing electrolyte. However, with significant initial acid concentration (pH 1), this tendency is reversed by the surplus of hydrogen evolution at the cathode. In this case the anode reaction includes a sensible ratio of chlorine evolution. This is the second reason why the pH must be controlled.

C3.4. In the practically feasible 50 g/dm^3 Zn – pH3 stationary electrolyte, the current efficiency increases with the additional Cl^- ions in the 0 – 4 M NaCl range, especially with moderate (< ~ 1000 A/m^2) current densities. The beneficial effect is attributed to the Na^+ ions, which are more likely to aggregate around the protrusions. However, this effect is reversed if further NaCl is added, caused by the high salt concentration, which increases the viscosity and decreases the transport of the electroactive species to maintain the required current. The virtual current efficiency may appear beyond 100% in the medium range, which is associated with the local increase in the pH caused by an intensive reduction of the H^+ ions, causing precipitation. On the other hand, in the electrolyte of critically low (~ 10 g/dm^3) Zn concentration, the current efficiency drops sharply as the Cl^- ion concentration is increased. Under these conditions, only loose and spongy deposits, just weakly adhering to the substrate, arise.

References

[1] G. Kong and R. White, “Toward cleaner production of hot dip galvanizing industry in China,” *J. Clean. Prod.,* vol. 18, no. 10-11, pp. 1092-1099, 2010. doi:10.1016/j.jclepro.2010.03.006.

[2] M. Dong, X. Xue, A. Kumar, H. Yang, M. I. Sayyed, S. Liu and E. Bu, “A novel method of utilization of hot dip galvanizing slag using the heat waste from itself for protection from radiation,” *J. Hazard. Mater.,* vol. 344, pp. 602-614, 2017. doi:10.1016/j.jhazmat.2017.10.066.

[3] V. Kuklík and J. Kudláček, “Hot-dip galvanizing and the environment,” in *Hot-dip galvanizing of steel structure*, Oxford, Butterworth-Heinemann is an imprint of Elsevier, 2016. doi:10.1016/B978-0-08-100753-2.00013-6, pp. 199-202.

[4] American Galvanizer Association, “Hot-Dip Galvanized Steel for Power Infrastructure: Hot-Dip Galvanizing (HDG) Process,” American Galvanizer Association, June 2018. [Online]. Available: https://galvanizeit.org/hot-dip-galvanized-steel-for-power-infrastructure/hot-dip-galvanizing-hdg-process. [Accessed 3 January 2019].

[5] Galvanizers Association of Australia, “Galvanizing Process,” Galvanizers Association of Australia, 2020. [Online]. Available: https://gaa.com.au/galvanizing-process/. [Accessed 11 January 2021].

[6] M. Regel-Rosocka, L. Nowak and M. Wisniewski, “Removal of zinc(II) and iron ions from chloride solutions with phosphonium ionic liquids,” *Sep. Purif. Technol.,* vol. 97, pp. 158-163, 2012. doi: 10.1016/j.seppur.2012.01.035.

[7] A. Anderez, F. J. Alguacil and F. A. Lopez, “Acid pickling of carbon steel,” *Rev. de Metal.,* vol. 58, no. 3, pp. 1-11, 2022. doi:10.3989/revmetalm.226.

[8] L. Pietrelli, S. Ferro and M. Vocciante, “Raw materials recovery from spent hydrochloric acid-based galvanizing,” *Chem. Eng. J.,* vol. 341, no. December 2017, pp. 539-546, 2018. doi:10.1016/j.cej.2018.02.041.

[9] V. Kuklik and J. Kudlacek, “Chemical pre-treatment,” in *Hot-Dip Galvanizing of Steel Structures*, Oxford, UK, Butterworth-Heinemann is an imprint of Elsevier, 2016. doi:10.1016/B978-0-08-100753-2.00003-3, pp. 17-27.

[10] Y. Xu, Y. Zhang, Y. Shu, H. Song, X. Shu, Y. Ma, L. Hao, X. Zhang, X. Ren, Z. Wang and X. Zhang, “Composition and leaching toxicity of hydrochloric acid pickling sludge generated from the hot-dip galvanized steel industry,” *ACS Omega,* vol. 7, no. 16, pp. 13826-13840, 2022. doi:10.1021/acsomega.2c00121.

[11] M. Regel-Rosocka, “A review on methods of regeneration of spent pickling solutions from steel processing,” *J. Hazard. Mater.,* vol. 177, no. 1-3, pp. 57-69, 2010. doi:10.1016/j.jhazmat.2009.12.043.

[12] J. Carrillo-Abad, M. Garcia-Gabaldon and V. Perez-Herranz, “Treatment of spent pickling baths coming from hot dip galvanizing by means of an electrochemical membrane reactor,” *Desalination,* vol. 343, pp. 38-47, 2014. doi:10.1016/j.desal.2013.11.040.

[13] A. Argawal and K. Sahu, “An overview of the recovery of acid from spent acidic solutions from steel and electroplating industries,” *J. Hazard. Mater.,* vol. 171, no. 1-3, pp. 61-75, 2009. doi:10.1016/j.jhazmat.2009.06.099.

[14] R. Gueccia, W. Daniel, S. Randazzo, A. Cipollina, J. Koschikowski and G. D. Micale, “An integrated approach for the HCl and metals recovery from waste pickling solutions: pilot plant and design operations,” *Chem. Eng. Res. Des.,* vol. 168, pp. 383-396, 2021. doi:10.1016/j.cherd.2021.02.016.

[15] A. Arguillarena, M. Margallo, A.-F. Axel, J. Pinedo, P. Gomez, I. Ortiz and A. Urtiaga, “Circular economy in hot-dip galvanizing with zinc and iron recovery from spent pickling acids,” *RSC Adv.,* vol. 13, no. 10, pp. 6481-6489, 2023. doi:10.1039/d2ra08195d.

[16] A. Devi, A. Singhal, R. Gupta and P. Panzade, “A study on treatment methods of spent pickling liquor generated by pickling process of steel,” *Clean Technol. Environ. Policy,* vol. 16, no. 8, pp. 1515-1527, 2014. doi:10.1007/s10098-014-0726-7.

[17] G. Leonzio, “Recovery of metal sulphates and hydrochloric acid from spent pickling liquors,” *J. Clean. Prod.,* vol. 129, pp. 417-426, 2016. doi:10.1016/j.jclepro.2016.04.037.

[18] The Europen Parliament and the Council of the European Union, “EUR-Lex Access to European law - Directive (EU) 2018/851 of the European Parliament and of the Council of 30 May 2018

amending Directive 2008/98/EC on waste," Eurpen Union, 30 May 2018. [Online]. Available: https://eur-lex.europa.eu/legal-content/EN/TXT/?uri=CELEX:32018L0851. [Accessed 20 September 2023].

[19] I. Ortiz, E. Bringas, H. Samaniego and M. F. S. Roman, "Membrane processes for the efficient recovery of anionic pollutants," *Desalination,* vol. 193, no. 1-3, pp. 375-380, 2006. doi:10.1016/j.desal.2005.05.034.

[20] M. Kaya, S. Hussaini and S. Kursunoglu, "Critical review on secondary zinc resources and their recycling technologies," *Hydrometallurgy,* vol. 195, no. April, p. 105362, 2020. doi:10.1016/j.hydromet.2020.105362.

[21] Bureau of International Recycling, "Report on the environmental benefits of recycling - 2016 edition," BIR, Brussel, 2016.

[22] Sigma Aldrich, "Material Science Product," Sigma Aldrich, 2018. [Online]. Available: https://www.sigmaaldrich.com/materials-science/material-science-product.html?TablePage=111535999.. [Accessed 11 January 2019].

[23] S. T. Ali, K. S. Rao, C. Laxman, N. R. Muniratham and T. L. Prakash, "Preparation of high pure zinc for electronic applications using selective evaporation under vacuum," *Sep. Purif. Technol.,* vol. 85, pp. 178-182, 2012. doi:10.1016/j.seppur.2011.10.009.

[24] A. Moezzi, A. M. McDonagh and M. B. Cortie, "Zinc oxide particle: Synthesis, properties and applications," *Chem. Eng. J.,* Vols. 185-186, pp. 1-22, 2012. doi:10.1016/j.cej.2012.01.076.

[25] G. Bao , Q. Fan, D. Ge, K. Wang, M. Sun, Z. Zhang, H. Guo, H. Yang, B. He and Y. Zheng, "In vitro and in vivo studies to evaluate the feasibility of Zn-0.1Li and Zn-0.8Mg application in the uterine cavity microenvironment compared to pure zinc," *Acta. Biomater.,* vol. 123, pp. 393-406, 2021. doi:10.1016/j.actbio.2020.12.048.

[26] G. Csicsovszki, T. Kékesi and T. I. Török, "Selective recovery of Zn and Fe from spent pickling solutions by the combination of anion exchange and membrane electrowinning techniques," *Hydrometallurgy,* vol. 77, no. 19-28, pp. 19-28, 2005. doi:10.1016/j.hydromet.2004.10.020.

[27] J. Laso, V. Garcia, E. Bringas, A. M. Urtiaga and I. Ortiz, "Selective Recovery of Zinc over Iron from Spent Pickling Wastes by Different Membrane-based Solvent Extraction Process Configurations," *Ind. Eng. Chem. Res.,* vol. 54, no. 12, pp. 3218-3224, 2015. doi:10.1021/acs.iecr.5b00099.

[28] . M. F. San Román, I. Ortiz Gándara, R. Ibañez and I. Ortiz, "Hybrid membrane process for the recovery of major components (zinc, iron and HCl) from spent pickling effluents," *J. Memb. Sci.,* vol. 415–416, pp. 616-623, 2012. doi:10.1016/j.memsci.2012.05.063.

[29] F. Rogener, M. Sartor, A. Ban, D. Buchloh and T. Reichardt, "Metal recovery from spent stainless steel pickling solutions," *Resour. Conserv. Recycl.,* vol. 60, pp. 72-77, 2012. doi:10.1016/j.resconrec.2011.11.010.

[30] L. Liu, P. Qi and Y. Liu, "A Review on Spent Pickling Liquors Treatment," in *2nd International Conference on Environmental Science and Engineering*, Xiamen, China, 2017. doi:10.12783/dteees/ese2017/14325.

[31] Industrial Emissions Directive 2010/75/EU, "Integrated pollution prevention and control in Best available techniques reference document for the ferrous metals processing industry," EU Science Hub, Seville, Spain, 2022.

[32] D. Bascone, A. Cipollina, M. Morreale, S. Randazzo, F. Santoro and G. Micale, "Simulation of a regeneration plant for spent pickling solutions via spray roasting," *Desalin. Water Treat.,* vol. 57, no. 48-49, pp. 23405-23419, 2016.

[33] D. S. Baik and D. J. Fray, "Electrodeposition of zinc from high acid zinc chloride solutions," *J. App. Electrochem.,* vol. 31, no. 10, pp. 1141-1147, 2001. doi:10.1023/A:1012290132379.

[34] A. Arguillarena, M. Margallo, A. Arruti-Fernandez, J. Pinedo, P. Gomez and A. Urtiaga, "Scale-up of membrane-based zinc recovery from spent pickling acids of hot-dip galvanizing," *Membranes,* vol. 10, no. 12, pp. 1-14, 2020. doi:10.3390/membranes10120444.

[35] T. Kekesi and M. Isshiki, "The purification of base transition metal," in *Purification Process and Characterization of Ultra High Purity Metals*, Berlin-Heidelberg, Springer, 2002.

[36] O. N. Kononova, N. V. Mikhaylova, A. M. Melnikov and Y. S. Kononov, "Ion exchange recovery of zinc from chloride and chloride-sulfate solutions," *Desalination,* vol. 274, no. 1-3, pp. 150-155, 2011. doi:10.1016/j.desal.2011.02.005.

[37] H. Zakiyya and T. Kékesi, “Anion exchange separations to produce a suitable electrolyte for the electrodeposition of pure zinc,” *Multidiscip. Sci.,* vol. 12, no. 3, pp. 127-138, 2022. doi:10.35925/j.multi.2022.3.12.

[38] J. Carrillo-Abad, M. Gracia-Gabaldon and V. Perez-Herranz, “Electrochemical recovery of zinc from the spent pickling solutions coming from hot dip galvanizing industries. Galvanostatic operation,” *Int. J. Electrochem. Sci.,* vol. 7, no. 6, pp. 5442-5456, 2012.

[39] M. Garcia-Gabaldon, J. Carrillo-Abad, E. Ortega-Navarro and V. Perez-Herranz, “Electrochemical study of a simulated spent pickling solution,” *Int. J. Electrochem. Sci.,* vol. 6, no. 2, pp. 506-519, 2011.

[40] J. Carrillo-Abad, M. Garcia-Gabaldon and V. Perez-Herranz, “pH effect on zinc recovery from the spent pickling baths of hot dip galvanizing industries,” *Sep. Purif. Technol.,* vol. 177, pp. 21-28, 2017. doi:10.1016/j.seppur.2016.12.034.

[41] J. Carrillo-Abad, M. Garcia-Gabaldon, I. Ortiz-Gandara, E. Bringas, A. M. Urtiaga, I. Ortiz and V. Perez-Herranz, “Selective recovery of zinc from spent pickling baths by the combination of membrane-based solvent extraction and electrowinning technologies,” *Sep. Purif. Technol.,* vol. 151, pp. 232-242, 2015. doi:10.1016/j.seppur.2015.07.051.

[42] H. Zakiyya and T. Kékesi, “Preliminary study of pure zinc recovery freom spent pickling liquors by combining anion exchange and electrodeposition,” *Hung. Maters. Chem. Sci. Engg.,* vol. 47, no. 1, pp. 88-99, 2023. doi:10.32974/mse.2022.009.

[43] T. Kekesi and M. Isshiki, “Principles of metal purification and purity evaluation,” in *Purrification Process and Charachterization of Ultra High Purity Metals*, Berlin Heidelberg, Springer-Verlag, 2002, pp. 39-69.

[44] A. Devi, A. Singhal and R. Gupta, “A review on spent pickling liquor,” *Ipublishing.Co.in,* vol. 4, no. 3, pp. 284-295, 2013. doi:10.6088/ijes.2013040300007.

[45] K. Shah, K. Gupta and B. Sengupta , “Selective separation of copper and zinc from spent chloride brass pickle liquors using solvent extraction and metal recovery by precipitation-stripping,” *J. Environ. Chem. Eng.,* vol. 5, no. 5, pp. 5260-5269, 2017. doi:10.1016/j.jece.2017.09.061.

[46] M. Wisniewski and M. Regel-Rosocka, “Selective removal of zinc(II) from spent pickling solutions in the presence of iron ions with phosphonium ionic liquid Cyphos IL 101,” *Hydrometallurgy,* vol. 110, no. 1-4, pp. 85-90, 2011.

[47] S. B. Zueva, F. Ferella, V. Innocenzi, I. D. Michelis, V. Corradini, N. M. Ippolito and F. Veglio, “Recovery of zinc from treatment of spent acid solutions from the pickling stage of galvanizing plants,” *Sustainability,* vol. 13, no. 1, pp. 1-8, 2021. doi:10.3390/su13010407.

[48] M. Regel-Rosocka and M. Wisniewski, “Selective removal of zinc(II) from spent pickling solutions in the presence of iron ions with phosphonium ionic liquid Cyphos IL 101,” *Hydrometallurgy,* vol. 110, pp. 85-90, 2011.

[49] J. Carrillo-Abad, M. Garcia-Gabaldon, E. Ortega and V. Perez-Herranz, “Electrochemical recovery of zinc from the spent pickling baths coming from the hot dip galvanizing industry. Potentiostatic operation,” *Separation and Purification Technology,* vol. 81, pp. 200-207, 2011.

[50] A. Pathak, A. Roy and M. Manna, “Recovery of zinc from industrial waste pickling liquor,” *Hydrometallurgy,* vol. 163, pp. 161-166, 2016. doi:10.1016/j.hydromet.2016.04.006.

[51] M. Tomaszewska, M. Gryta and A. W. Morawski, “Recovery of hydrochloric acid from metal pickling solutions by membrane distillation,” *Sep. Purif. Technol.,* Vols. 22-23, pp. 591-600, 2001. doi:10.1016/S1383-5866(00)00164-7.

[52] M. Tomaszewska, M. Gryta and A. W. Morawski, “Mass transfer of HCl and H2O across the hydrophobic membrane during membrane distillation,” *J. Memb. Sci.,* vol. 166, pp. 149-157, 2000. doi:10.1016/S0376-7388(99)00263-X.

[53] M. Tomaszewska, M. Gryta and A. W. Morawski, “The influence of salt in solutions on hydrocholric acid recovery by membrane distillation,” *Sep. Purif. Technol.,* vol. 14, pp. 183-188, 1998. doi:10.1016/S1383-5866(98)00073-2.

[54] M. F. San Roman, I. Ortiz-Gandara, E. Bringas, R. Ibanez and I. Ortiz, “Membrane selective recovery of HCl, zinc and iron from simulated mining effluents,” *Desalination,* vol. 440, no. September 2017, pp. 78-87, 2018. doi:10.1016/j.desal.2018.02.005.

[55] M. Kumar, S. Pramanik, S. Kumar, L. Bahadur, M. Kumar and B. Dhar, "Development of an efficient process for the recovery of zinc and iron as value added products from the waste chloride solution," *Sep. Purif. Technol.,* vol. 167, pp. 37-44, 2016. doi:10.1016/j.seppur.2016.04.049.

[56] T. Kekesi, "Gallium extraction from synthetic Bayer liquors using Kelex 100-kerosene, the effect of loading and stripping conditions on selectivity," *Hydrometallurgy,* vol. 88, no. 7, pp. 170-179, 2007.

[57] M. K. Sinha, S. K. Sahu, P. Meshram and B. D. Pandey, "Solvent extraction and separation of zinc and iron from spent pickle liquor," *Hydrometallurgy,* Vols. 147-148, pp. 103-111, 2014. doi:10.1016/j.hydromet.2014.05.006.

[58] S. Neumann, "Technically speaking: Ion exchange resins in the electroplating industry," *Metal Finishing,* pp. 22-26, March 2012. doi:10.1016/S0026-0576(13)70111-9.

[59] T. Kekesi and M. Isshiki, "Anion Exchange for Ultra-High Purification of Transition Metals," *ERZMETALL,* vol. 56, no. 2, pp. 59-67, 2003.

[60] T. Kekesi, K. Mimura and M. Isshiki, "Ultra-high purification of iron by anion exchange in hydrochloric acid solutions," *Hydrometallurgy,* vol. 63, no. 1, pp. 1-13, 2002. doi:10.1016/S0304-386X(01)00208-0.

[61] T. Kekesi and M. Isshiki, "Anion Exchange Behavior of Copper and Some Metallic Impurities in HCl Solutions," *Mater. Trans. Jim,* vol. 35, no. 6, pp. 406-413, 1994. https://doi.org/10.2320/matertrans1989.35.406.

[62] K. Takahashi, T. Kékesi, Y. Aoki and M. Isshiki, " Preparation of High Purity Zinc by Anion Exchange," in *Lead. Zinc & Lead '95. International Symp. Extraction and Applications of Zinc and Lead, May 22-24.*, Sendai, Japan, pp.321-329, 1995.

[63] G. Csicsovszki, T. Kékesi and T. I. Török, "A clean method applying anion-exchange separation and membrane-electrolysis to regenerate Fe-Zn-HCl spent pickling liquors," in *TMS Annual Meeting*, San Antonio, Texas, USA, pp. 427-436, 2006.

[64] T. Kekesi, "MEMOOC: The fundamentals of chemical metallurgy," 2018. [Online]. Available: https://memooc.uni-miskolc.hu/nyilt/: Miskolci Egyetem.. [Accessed September 2019].

[65] T. Kulcsar, G. B. Toth and T. Kekesi, "Complex evaluation and development of electrolytic tin refining in acidic chloride media for processing tin-based scrap from lead-free soldering," *Transactions of the Institutions of Mining and Metallurgy, Section C: Mineral Processing and Extractive Metallurgy,* vol. 125, no. 4, pp. 228-237, 2016. doi:10.1080/03719553.2016.1206693.

[66] T. S. Lee, "Hydrogen Overpotential on Zinc Alloys in Alkaline Solution," *J. Electrochem. Soc,* vol. 122, no. 2, pp. 171-173, 1975.

[67] T. S. Lee, "Hydrogen Overpotential on Zinc Containing Small Amount of Impurities in Concentrated Alkaline Solution," *J. Elechrochem. Soc,* vol. 120, no. 6, pp. 707-709, 1973.

[68] J. H. Lindsay, "Polarization and Hydrogen Overvoltage," *Plating and Surface Finishing,* pp. 12-14, may 2000.

[69] X. G. Zhang, Corrosion and Electrochemistry of Zinc, Ontario, Canada: Springer Science+Business Media, LLC, 1996.

[70] L. Hong, L.-Y. Wang, Y. Wang, X. Wu, W. Huang, Y. Zhou, K.-X. Wang and J.-S. Chen, "Toward Hydrogen-Free and Dendrite-Free Aqueous Zinc Batteries: Formation of Zincophilic Protective Layer on Zn Anodes," *Adv. Sci.,* vol. 9, no. 6, pp. 1-10, 2022.

[71] H. Zakiyya and T. Kékesi, "Potentiodynamic characteristics of zinc electrodeposition from chloride solutions," MultiScience - XXXIII. microCAD International Multidisciplinary Scientific Conference, Miskolc, 23-24 May, 2019, 2019.

[72] D. J. Mackinnon, J. M. Brannen and R. M. Morrison, "Zinc electrowinning from aqueous chloride electrolytes," *J. App. Electrochem.,* vol. 13, no. 1, pp. 39-53, 1983. doi:10.1007/BF00615886.

[73] K. Kashida, S. Oue and H. Nakano, "Effect of chloride ions in electrowinning solutions on zinc deposition behavior and crystal texture," *Matter. Trans.,* vol. 58, no. 10, pp. 1418-1426, 2017. doi:10.2320/matertrans.M-M2017827.

[74] M. Yasuda, I. Ohno and S. Haruyama, "Role of chloride ion on nickel plating," *J. Surf. Finish. Soc.,* vol. 41, pp. 312-317, 1990.

[75] M. Nicol, C. Akilan, V. Tjandrawan and J. A. Gonzalez, “The effects of halides in the electrowinning of zinc. I. Oxidation of chloride on lead-silver anodes,” *Hydrometallurgy,* vol. 173, no. August, pp. 125-133, 2017.

[76] M. Delgosha, S. Salehi, L. U. Borijeni and S. Sharifi, “AFM Studies of the Effect of Chloride Ion on the Morphology of the Copper Electroplating Surface,” Optics,” *Optics,* vol. 3, no. 2, pp. 15-18, 2014.

[77] B. K. Thomas and D. J. Fray, “The conductivity of aqueous zinc chloride solutions,” *J. App. Electrochem.,* vol. 12, no. 1, pp. 1-5, 1982. doi:10.1007/BF01112058.

[78] B. K. Thomas and D. J. Fray, “The effect of additives on the morphology of zinc electrodeposited from a zinc chloride electrolyte at high current densities,” *J. App. Electrochem.,* vol. 11, no. 6, pp. 677-683, 1981. doi:10.1007/BF00615170.

[79] J. M. West, Electrodeposition and corrosion processes, London, New York: Van Nostrand Reinhold, 1970.

[80] H. Fukushima, T. Akiyama, M. Yano, T. Ishikawa and K. Roland, “Electrode position Behavior of Zn-lron-grou Sulf ate and Chloride Baths p Metal Alloys from sulfate and chloride bath,” *ISIJ International,* vol. 33, no. 9, pp. 1009-1015, 1993.

[81] Z. Nagy, J. Blaudeau, C. N. Hung, L. A. Curtiss and D. J. Zurawski, “Chloride Ion catalysis of the copper deposition reaction,” *J. Electrochem. Soc,* vol. 142, no. 6, pp. L87-L89, 1995.

[82] I. B. Illes and T. Kekesi, “The relative efficiency of electrowinning indium from chloride electrolytes,” *J. App. Electrochem.,* vol. 53, no. 2, pp. 271-284, 2023. doi:10.1007/s10800-022-01779-7.

[83] T. Hurlen and K. P. Fischer, “Kinetic of Zn/Zn(II) reaction in acidified solutionof potasium chloride,” *Electroanal. Chem. Interfac. Electrochem.,* vol. 61, pp. 165-173, 1975.

[84] J. Newman, “Mass transport and potential distribution in the geometries of localized corrosion,” Lawrence Berkeley Laboratory, University of California, California, 1990.

[85] J. T. Kim and J. Jorne, “The Kinetics and Mass Transfer of Zinc Electrode in Acidic Zinc-Chloride Solution,” *J. Electrochem. Soc.,* vol. 127, no. 1, pp. 8-15, 1980. doi:10.1149/1.2129646.

[86] D. J. Mackinnon and J. M. Brannen, “Zinc deposit structures obtain from synthetic zinc chloride electrolyte,” *J. App. Electrochem.,* vol. 9, pp. 603-613, 1979. doi:10.1007/bf00610948.

[87] G. Csicsovszki, T. Kékesi and T. Torok, “Electrodeposition of iron from spent hydrochloric pickling solutions containing Fe(Electrodeposition of iron from spent hydrochloric pickling solutions containing Fe(II) and Zn(II),” in *205th ECS meeting*, San Antonio, 2005.

[88] J. Carrillo-Abad, M. Garcia-Gabaldon and V. Perez-Herranz, “Study of the zinc recovery from spent pickling baths by means of an electrochemical membrane reactor using a cation-exchange membrane under galvanostatic control,” *Sep. Purif. Technol.,* vol. 132, pp. 479-486, 2014. doi:10.1016/j.seppur.2014.05.052.

[89] G. Csicsovszki, T. Kékesi and T. I. Török, “Ion-Exchange Membrane Techniques for the Regeneration of Industrial Process Solutions,” *Acta Metallurgica Slovaca,* vol. 10, pp. 51-59, 2004.

[90] U. Kerney, “Treatment of spent pickling acid from hot dip galvanizing,” *Resour. Conserv. Recycl.,* vol. 10, pp. 145-151, 1994. doi:10.1016/0921-3449(94)90047-7.

[91] G. Roventi, R. Fratesi, R. A. Della Guardia and G. Barucca, “Normal and anomalous codeposition of Zn-Ni alloys from chloride bath,” *J. App. Electrochem.,* vol. 30, no. July, pp. 173-179, 2000. doi:10.1023/A:1003820423207.

[92] M. J. Nicol and H. I. Philip, “Underpotential deposition and its relation to the anomalous deposition of metals in alloys,” *Journal of elecoanalytical chemistry,* vol. 70, pp. 233-237, 1976.

[93] E. Gómez, E. Pelaez and E. Vallésa, “Electrodeposition of zinc+iron alloys: I. Analysis of the initial stages of the anomalous codeposition,” *Journal of Electroanalytical Chemistry,* vol. 469, no. 2, pp. 139-149, 1999.

[94] B. Tang, W. Su, J. Wang, F. Fu, G. Yu and J. Zhang, “Minimizing the creation of spent pickling liquors in a pickling process with high-concentration hydrochloric acid solutions: Mechanism and evaluation method,” *Journal of Environmental Management,* vol. 98, no. 1, pp. 147-154, 2012.

[95] G. Díaz, D. Martín, C. Frías and F. Sánchez, “Emerging applications of ZINCEX and PLACID technologies,” *J. of Metals,* no. 12, pp. 30-31, 12 2001.

[96] J. Mackinnon and D. J. Brannen, “Evaluating of Organic Additives as Levelling Agents for Zinc Electrowinning from Chloride Electrolytes,” *J. App. Electrochem.,* vol. 12, pp. 21-31, 1982.

[97] T. Kekesi and M. Isshiki, “Anion Exchange for Ultra-High Purification of Transition Metals,” *ERZMETALL,* vol. 56, no. 2, pp. 59-67, 2003.

[98] Join Research Center Directorate B - Growth and Innovation Circular Economy and Industrial Leadership Unit European IPPC Bureau, “JRC Science for Policy Report of Best Available Technique (BAT) Reference Document for the Ferrous Metals Processing Industry,” European Commission, Seville, Spain, October 2021.

[99] E. Maranon, Y. Fernandez, F. J Suarez, F. J Alonso and H. Sastre, “Treatment of acid pickling bath by means of anionic resins,” *Industrial & Engineering Chemistry Research,* vol. 39, pp. 3370-3376, 2000.

[100] L. G. SiIlen and A. E. Martell, Stability constants of metal-ion complexes. Special Publ. No. 17., London: The Chemical Society, 1964.

[101] J. F Zaemaitis, D. M Clark, M. Rafal and N. C Scrivner, Handbook of aqueous electrolyte thermodynamics, New York: Wiley, 1986.

[102] T. Kékesi, A novel method of copper purification by anion-exchange in chloride media, Tohoku University, Sendai, Japan: PhD thesis., 1994.

[103] N. D. Nikolić, “A Review: Influence of the exchange current density and overpotential for hydrogen evolution reaction on the shape of electrolytically produced disperse forms,” *J. Electrochem. Sci. Eng.,* vol. 10, no. 2, pp. 111-126, 2020.

[104] K. Keisuke, S. Oue and H. Nakano, “Effect of chloride ions in electrowinning solutions on zinc deposition behavior and crystal texture,” *Mater. Trans.,* vol. 58, no. 10, pp. 1418-1426, 2017.

[105] M. Nicol, C. Akilan, V. Tjandrawan and J. A. Gonzalez, “The effect of halides in the electrowinning of zinc . II . Corrosion of lead-silver anodes,” *Hydrometallurgy,* vol. 173, no. May, pp. 178-191, 2017.

[106] M. Sider and D. L. Piron, “The effects of metallic impurities and 2-butyne-1,4-diol on zinc electrowinning from chloride solutions,” *Journal of Applied Electrochemistry,* vol. 18, pp. 54-61, 1988.

[107] F. Yang, J. A. Yuwono, J. Hao, J. Long, L. Yuan, Y. Wang, S. Liu, Y. Fan, S. Zhao, K. Davey and Z. Guo, “Understanding H2 Evolution Electrochemistry to Minimize Solvated Water Impact on Zinc-Anode Performance,” *Adv. Mater.,* vol. 34, no. 2206754, pp. 1-12, 2022.

[108] F. Wan, L. Zhang, X. Dai, X. Wang , Z. Niu and J. Chen, “Aqueous rechargeable zinc/sodium vanadate batteries with enhanced performance from simultaneous insertion of dual carriers,” *Nature Communications,* vol. 9, no. 1, pp. 1-11, 2018.

[109] Z. Li and A. W. Robertson, “Electrolyte engineering strategies for regulation of the Zn metal anode in aqueous Zn-ion batteries,” *Battery Energy,* vol. 2, no. 1, pp. 1-30, 2022.

List of publications

Journal Articles

1. H. Zakiyya, I. B. Illés and T. Kékesi, "*Interpreting the main effects on the efficiency and morphology for establishing a procedure of electrodepositing Zn from purified chloride SPL solutions*," *Springer Nature, App. Sci*. 2024 (under-revision)
2. H. Zakiyya and T. Kékesi, "*Potentiodynamic study of the effects of nickel on the electrodeposition of zinc from chloride media*," *Int. J. Eng. Manage. Sci.*, vol. 8, no. 2, pp. 15-22, 2023. doi:10.21791/IJEMS.2023.2.2
3. H. Zakiyya and T. Kékesi, "*Preliminary study of pure zinc from spent pickling liquor by combining anion exchange and electrodeposition*," Hungarian Materials Science and Engineering*,* vol. 47, no. 1, pp. 88-99, 2023
4. H. Zakiyya and T. Kékesi, "Anion exchange separations to produce a suitable electrolyte for the electrodeposition of pure zinc," *Multidisciplinary Sciences* vol. 12, no.3, pp. 127-138, 2022. doi:10.35925/j.multi.2022.3.12

Conference Proceedings

1. H. Zakiyya and T. Kékesi, "Potentiodynamic characteristic of zinc electrodeposition from chloride solution," *MultiScience – XXXIII. MicroCAD Multidisciplinary Scientific Conference,* University of Miskolc, 23-24 May, 2019. ISBN 978-963-358-177-3
2. H. Zakiyya and T. Kékesi, "Spent pickling liquor as industrial waste recover opportunities" LIMBRA Ed. Bartha et al.: *Entrepreneurship in the raw materials sector* –ISBN: 978-1-032-19596-4
3. H. Zakiyya and T. Kékesi, "The effect of Fe impurity on the electrodeposition of Zn from spent pickling liquor" ISDM-TU Bergakademie Freiberg

Periodical Articles

1. H. Zakiyya, I. B. Illés and T. Kékesi, "Determination of optimum chromatographic parameters for the anion-exchange separation process to prepare a Zn electrolyte from the spent pickling liquor" *Almanach-of PhD*

Students, Faculty of Materials and Chemical Engineering, University of Miskolc, vol.1, pp. 41-48, 2023. ISSN 2939-7294

2. H. Zakiyya and T. Kékesi, "The effect of main parameters on the electrodeposition of Zn from HCl solutions" *Almanach of PhD Students*, Faculty of Materials and Chemical Engineering, University of Miskolc, vol.1, pp. 76-81, 2022. ISSN 2939-7294

Oral Presentations

1. H. Zakiyya and T. Kékesi, "*Potentiodynamic characteristic of zinc electrodeposition from chloride solution*," MultiScience – XXXIII. MicroCAD Multidisciplinary Scientific Conference, University of Miskolc, 23-24 May, 2019. ISBN 978-963-358-177-3
2. H. Zakiyya and T. Kékesi, "*The importance of preliminary purification process of spent pickling liquor*" 16th Miklos Ivanyi International PhD-DLA Symposium- 26-27 October 2021, Pecs, Hungary
3. H. Zakiyya and T. Kékesi, "*Spent pickling liquor as industrial waste recover opportunities*," LIMBRA: International scientific conference on entrepreneurship in the raw materials sector – 24 November 2021, University of Miskolc, Hungary
4. H. Zakiyya and T. Kékesi, "*The potential processes to recover metals from spent pickling liquor"* International Jubilee Interdisciplinary doctoral student conference (IDK2021) – 12 November 2021, University of Pecs, Hungary
5. H. Zakiyya and T. Kékesi, "*Anion exchange separations to produce a suitable electrolyte for the electrodeposition of pure zinc*" MultiScience – XXXV. microCAD International Multidisciplinary Scientific Conference, 13-14 October 2022, University of Miskolc, Hungary
6. H. Zakiyya and T. Kékesi, "*The recovery of Zn from SPL by combining anion-exchange separation and electrodeposition in chloride solutions*" MTA Committee of Metallurgy, Hungary, 13 December 2022, NAGEV CINK Kft. Ócsa, Hungary
7. H. Zakiyya and T. Kékesi, "*The recovery of pure Zn from SPL by combining electrowinning and aqueous separation process*" Hungarian Science Day, 10 November 2022, Miskolc, Hungary

8. H. Zakiyya and T. Kékesi, "*The potentiodynamic characteristic of iron in the Zn electrodeposition from chloride media*" Digital presentation – 242nd Electrochemical Society Meeting, 9-13 October 2022, Atlanta Hilton, Georgia, USA.
9. H. Zakiyya and T. Kékesi, "*Optimization of anion-exchange separation to produce pure Zn electrolyte from spent pickling liquors*" 224th Electrochemical Society Meeting, 10 October 2023, Gothenburg, Sweden.
10. H. Zakiyya and T. Kékesi, "*Optimization of anion-exchange separation to produce pure Zn electrolyte from spent pickling liquors*" [elevation pitch] 224th Electrochemical Society Meeting, 9 October 2023, Gothenburg, Sweden.
11. H. Zakiyya and T. Kékesi, "*The effect of Fe impurity on the electrodeposition of Zn from spent pickling liquo*r" International Student Day of Metallurgy, 11 April 2024, TU Bergakademie Freiberg, Germany.